Lrp-dependent phenotypic variation of pathogenesis and mutualism in the bacterium *Xenorhabdus nematophila*

By

Mengyi Cao

A dissertation submitted in partial fulfillment of the requirements for the degree of

Doctor of Philosophy

(Microbiology Doctoral Training Program)

at the

UNIVERSITY OF WISCONSIN-MADISON

2017

Date of final oral examination: 5/10/2017

The dissertation needs to be approved by the following members of the Final Oral Committee:

Dr. Heidi Goodrich-Blair (Advisor), Professor, Bacteriology

Dr. Rodney A. Welch, Professor, Medical Microbiology and Immunology

Dr. Michael G. Thomas, Professor, Bacteriology

Dr. Jue D. Wang, Professor, Bacteriology

Dr. Kalin Vetsigian, Assistant Professor, Bacteriology

Abstract

Many bacteria undergo phenotypic variation, a process by which individual cells within a population express distinct phenotypes that confer an adaptive advantage to the whole population in fluctuating environments. In many pathogenic bacteria, phenotypic variation is thought to facilitate the transition between free-living and host-associated states. My thesis project has focused on a phenotypic variation phenomenon, termed VMO (virulence modulation) that impacts host interaction phenotypes in *Xenorhabdus nematophila*, a pathogen of insects and a mutualistic symbiont of nematodes. In VMO, individual cells of a *X. nematophila* population spontaneously and reversibly switch between two distinct states. In one, the cells are virulent in insects, but defective in mutualism with nematodes. In the other, the cells are attenuated for virulence in insects, but engage in normal mutualism with nematodes. Varying levels of the global transcription factor Lrp (leucine responsive regulatory protein) control the VMO switch: High Lrp levels result in virulence attenuation but normal mutualism, while low Lrp levels cause a virulent phenotype but defective mutualism. The findings presented in this thesis show that VMO in *X. nematophila* as a pathogenesis-to-mutualism switch by which a symbiotic bacterium interacts and adapts to alternating host environments. Analysis of mutualism-to-pathogenesis switch also suggests the possibility of predictive adaptation behavior of bacterium which could contribute to the fitness of the bacteria-nematode symbiotic pairs.

Acknowledgements

First I would like to thank my thesis advisor Dr. Heidi Goodrich-Blair. It has been my privilege to learn and grow as a scientist under her mentorship. I would not have been able to complete my thesis without Heidi. I would also like to thank previous and current lab members who supported me and accompanied me for the past six years.

Secondly I would like to thank my collaborators who contributed significantly to my thesis work: Matthew Stilwell (graduate student in Biophysics) and Dr. Douglas B. Weibel. I want to also thank my previous and current committee members: Dr. Rodney A. Welch, Dr. Michael G. Thomas, Dr. Jue D. Wang, Dr. Kalin Vetsigian, and Dr. Edward G Ruby.

I would like to thank other mentors and role models that significantly influenced me in my career development as a scientist. I want to thank my middle school biology teacher, Ms. Junqin Liu and Chemistry teacher Ms. Xiaomin Song, who encouraged me to participlate in science activities. I would also like to thank my high school English teacher, Ms. Yongzheng Wang, whose personal experience inspired me to start my journey as an international student. A special thanks to my advisors in college, Dr. Phoebe Lostroh (Biology), Dr. Murphy Brasuel (Chemistry), and Dr. David Brown (Mathematics) for their lectures, mentorship, and encouraging me to go to graduate school. I would not have been able to get this far without them.

These role models also include my parents who taught me about resilience and commitment to a career. I want to thank them for supporting their only child to travel half across the world to pursue my dream for the past ten years.

Finally, my husband Grischa Chen has been the closest friend and company during my graduate school career. As a graduate student himself, Grischa understands the tears and sweat in science. We have been sharing each other's excitements and pains in research. His love, support, and company, which includes cooking at home and critiques in science, have been crucial for me during my graduate school years.

Table of Contents

Abstract ..... **i**

Acknowledgements ..... **ii**

Table of Contents ..... **iii**

A List of Figures ..... **vi**

A List of Tables ..... **ix**

Chapter 1 ..... **1**

Introduction **1**

Abstract 2

Microbial Symbiont Adaptive Responses to Changing Host Environments 2

Adaptive responses in *Xenorhabdus* bacteria symbionts of *Steinernema* nematodes 7

From the IJ to the insect: 7

From virulence to feeding 9

From the spent cadaver to the IJ 9

Persistence in the IJ 11

Phenotypic variation in *X. nematophila* 13

Thesis Outline 14

References 15

Figures 23

Chapter 2 ..... **26**

High levels of the *Xenorhabdus nematophila* transcription factor Lrp promote mutualism with *Steinernema carpocapsae* nematode hosts, suggesting that Lrp dictates a phenotypic switch in between pathogenesis and mutualism **26**

Abstract 27

Introduction 29

Results 33

Discussion 39

Conclusions 44

Materials and Methods 45

Acknowledgements 53

References 54

Tables and Figures 62

Chapter 3 81

Nutritional conditions influence *Xenorhabdus nematophila* Lrp-dependent phenotypic variation 81

Abstract 82

Introduction 83

Results 88

Discussion 100

Materials and Methods 104

Acknowledgements 106

References 107

Figures 111

Chapter 4: 131

The symbiotic bacterium *Xenorhabdus nematophila* shifts from a mutualistic to a pathogenic population when associated with the transmission stage of the nematode *Steinernema carpocapsae* 131

Abstract 132

Introduction 133

Results 136

Discussion 141

Materials and Methods 143

Acknowledgements 148

References 149

Tables and Figures 153

Chapter 5: 167

Studying the symbiotic bacterium *Xenorhabdus nematophila* in individual, living *Steinernema carpocapsae* nematodes using microfluidic systems 167

Abstract 168

Introduction 170

Results 174

Discussion 181

Materials and Methods 184

Acknowledgements 188

References 189

Tables and Figures 192

Chapter 6: 205

Summary and future directions 205

Abstract 206

I. From IJ to insect 206

II. From virulence to feeding 207

III. From spent cadaver to IJ 208

IV. Persistence in the IJ 210

Lrp-dependent phenotypic variation in *X. nematophila:* a model to study anticipatory behavior in naturally occurring microbial symbiosis? 211

References 213

Tables and Figures 215

A List of Figures

Figure 1.1. Responsive and Anticipatory Adaptations Resulting from Random and Ordered Environmental Exposures. 23

Figure 1.2. Series of *Steinernema* host intestinal environments encountered by *Xenorhabdus*. 24

Figure 2.1. The tripartite life cycle and mutualistic symbiosis among *Xenorhabdus* bacteria and *Steinernema* nematodes. 64

Figure 2.2. Lrp expression levels and virulence of bacteria with no-*lrp,* low-*rp,* and high-*lrp* in-genome fixed strains. 66

Figure 2.3. Biofilm formation of bacterial strains expressing fixed levels of Lrp. 68

Figure 2.4. Mutualistic symbiosis phenotypes in vitro and in vivo. 70

Figure 2.5. Total nematodes per insect. 72

Figure 2.6. Nematode fecundity in *Galleria* insects shown as emerged IJs, non-emerged nematodes, and total nematodes. 74

Figure 2.7. Comparison of experimental and theoretical numbers of emerged IJs, non-emerged nematodes, and total nematodes. 76

Figure 2.8. In vivo mutualism phenotypes. 77

Figure 2.9. Mutualistic interactions measurements in the natural infection of insects with colonized IJs. 79

Figure 3.1. Lrp-dependent fluorescence reporters reveal colony heterogeneity among *X. nematophila* wild type populations. 111

Figure 3.2. Semi-quantitative immunoblotting of Lrp expression levels in the engineered control strains and wild type *X. nematophila* isolates with *PfliC-gfp/Plac-rfp* reporter. 113

Figure 3.3. Heterogeneous populations are more virulent than homogeneously high-Lrp populations in *Manduca sexta* larvae. 114

Figure 3.4. *PfliC-gfp/Plac-rfp* reporter and single-cell FACS analysis revealed three viable subpopulations in *Xenorhabdus nematophila* Lrp expression. 116

Figure 3.5: Quantitative analysis of colony compositions. 118

Figure 3.6. Low-Lrp colonies arise in wild type *X. nematophila* population under nutrient-limiting conditions. 120

Figure 3.7. The effects of casamino acids and glucose on Lrp-dependent population heterogeneity in wild type bacteria under nutrient-limiting conditions. 122

Figure 3.8 The correlation of Lrp heterogeneity with the bacterial growth yield in glucose. 124

Figure 3.9. Current model for Lrp-dependent phenotypic switch in *X. nematophila* life cycle. 126

Figure S3.1: selected examples of diverse phenotypes of wild type *X. nematophila* colonies based on *PfliC-gfp/Plac-rfp* reporter. 128

Figure S3.2: Lrp-dependent reporters showing the number of low-Lrp sectors per colony on minimal medium supplemented with casamino acids agar plate over time. 129

Figure 4.1: Life cycle of bacterium *Xenorhabdus nematophila* and developmental stages of *Steinernema carpocapsae* in a species-specific manner. 154

Figure 4.2. *X. nematophila* expressing fixed high levels of Lrp has a high colonization frequency relative to fixed low-Lrp expressers with early stages of nematode development including AIC, PIV, and immature IJ colonization initiation. 156

Figure 4.3. *X. nematophila* expressing fixed high and fixed low levels of Lrp show similar growth rate in the immature nematode receptacle. 157

Figure 4.4. Lrp-dependent colonization in mature IJs on varying days of emergence. 159

Figure 4.5. Lrp-dependent colonization in cumulative mature IJs. 161

Figure 4.6. Comparison of *X. nematophila* population switch to low-Lrp expressing subpopulations in vitro and in vivo. 163

Figure 4.7. Current model of VMO switch in *X. nematophila* life cycle. 165

Figure 5.1. The mutualistic relationship between *Xenorhabdus nematophila* bacteria and *Steinernema carpocapsae* nematodes. 193

Figure 5.2. Schematic of microfluidic device for *S. carpocapsae* nematode isolation and maintenance. 195

Figure 5.3. Nematode survival and maintenance in the microfluidic device. 197

Figure 5.4. Qualitative and quantitative analysis of bacterial populations in individual, living IJ nematodes. 199

Figure 5.5. Comparison of traditional grinding experiments to microfluidic device experiments for quantification of *X. nematophila* bacterial population dynamics in *S. carpocapsae* nematodes. 201

Figure 5.6. Confocal micrographs of a bacterial population in a receptacle over the course of 3 weeks. 203

Figure 6.1: A working model of Lrp-dependent adaptive prediction as it may occur for *Xenorhabdus* bacteria based on our current data, which encounter predictable stages of host interactions. 216

A List of Tables

Table 2.1. Bacterial strains used in Chapter 2. 62

Table 2.2. Comparison of experimental and theoretical trends 63

Table 4.1. Bacterial strains used in Chapter 4. 153

Table 5.1. Parameter values in design of microfluidic devices. 192

Table 6.1. A summary of Lrp-dependent VMO switch in the life cyle of *X. nematophila.* 215

Chapter 1

Introduction

This Chapter has been partially adapted from manuscript '**Mengyi Cao and Heidi Goodrich-Blair;** Ready or Not: Microbial Adaptive Responses in Dynamic Symbiosis Environments. *Journal of Bacteriology,* special issue conference proceedings.'

Mengyi Cao**:** Outlined, wrote, and revised the manuscript. Arts for Figures.

Heidi Goodrich-Blair**:** Edited and revised the manuscript. Arts for Figures.

Abstract

In mutually beneficial and pathogenic symbiotic associations, microbes must adapt to the host environment for optimal fitness. Both within an individual host and during transmission between hosts, microbes are exposed to temporal and spatial variation in environmental conditions. The environments experienced by a symbiotic microbe during its life history can be erratic or predictable, each of which can impact the evolution of adaptive responses. The phenomenon of phenotypic variation, in which different subpopulations of cells express distinctive and potentially adaptive characteristics, can contribute to microbial success in a lifestyle that includes rapidly changing environments. Also, the predictability of a rhythmic or cyclical series of environments may promote the evolution of signal transduction cascades that allow pre-adaptive responses to environments that are likely to be encountered in the future, a phenomenon known as adaptive prediction. In this chapter, we summarize environmental variations known to occur in some well-studied models of symbiosis, and how these may contribute to the evolution of microbial population heterogeneity and anticipatory behavior. We provide details about the symbiosis between *Xenorhabdus* bacteria and *Steinernema* nematodes as a model to investigate the concept of environmental adaptation and adaptive prediction in a microbial symbiosis.

Microbial Symbiont Adaptive Responses to Changing Host Environments

Microbial symbiotic associations, which are pervasive, can be beneficial (mutualistic), neutral (commensal), or harmful (pathogenic) to the host animal. Within symbioses, microbes can exploit the host for space and nutrients, or as a vector for dissemination to other environments. Both within and between hosts, microbes experience changing environmental conditions to which they must adapt for optimal fitness and to maintain symbiotic associations. For instance, mutualistic and pathogenic symbionts that are acquired by their hosts each new generation (horizontally transmitted) experience transitions between host-associated and free-living states or among varied hosts (e.g. mammals) and the vectors that transmit them (e.g.

insects). These transitions can be associated with changes in key environmental parameters such as temperature, pH, and host immune factors. Similarly, an individual microbe that exclusively resides within a single host, or is passed directly to progeny through the parent (vertical transmission), can encounter dramatic shifts in environmental conditions (e.g. nutrient availability, ion concentrations, osmotic and oxidative stress) in response to host diet or hormonal shifts. For example, the mammalian gastrointestinal tract comprises numerous niches with variations in sugars, pH and metals.

To a microbe of a few microns, these variations over millimeter or centimeter scales can represent drastic environmental changes. Further, transitions among these niches can follow a predetermined pattern. For example, the process of enteropathogen infection has sequentially ordered steps: loose association with the host mucosal surface, induction of virulence factors and toxins, intimate attachment, and invasion [reviewed in (1)]. Mutualistic symbionts also undergo regimented infection processes during transmission to new hosts. In several well-described examples of horizontal transmission, such as that between the bacterium *Xenorhabdus nematophila* and its mutualistic host *Steinernema carpocapsae*, transmission is initiated by attachment to particular tissues, followed by a selective colonization bottle-neck, and movement of the selected symbiont to a specialized host niche (2–4).

Spatial and temporal environmental shifts within symbioses can be roughly categorized into two types: erratic and predictable (Fig. 1.1). In the former, the symbiont, while it is regularly exposed to a finite number of different environments, does not encounter these environments in any predictable order (Fig. 1.1A) (5, 6). In predictable shifts, the environments experienced by a microbe during its life history fluctuate in a temporally ordered manner (Fig. 1.1B) (7, 8) . Microbes might experience such life histories when they are obligately transmitted by a vector between primary hosts (9), or within a single host due to the host's temporal rhythms, which can be entrained (circadian/circannual) or induced (diel) by light-dark periods (10).

In either predictable or erratic environmental life histories, many microbes have evolved an adaptive behavior known as phenotypic variation, a process by which individual cells within a population express distinct phenotypes that each can confer an adaptive advantage in a particular environment. The presence of more than one phenotype and the ability of microbes to switch among them provides better fitness for the microbial population as a whole. The process of phenotypic variation can be stochastic, occurring randomly within a subpopulation, or induced, in which an environmental condition triggers the switching among variant phenotypes. Also, phenotypic variants that are adapted to the prevailing environment can be induced or selected by that environment (11).

In many pathogenic bacteria, phenotypic variation is thought to facilitate the transition between free-living and host-associated states. Erratic environmental fluctuations (Fig. 1.1A) may select for symbionts with phenotypes that switch stochastically among potential states, such that at any given time, a subpopulation of bacteria may be expressing adaptive traits appropriate to that environment, either in or out of the host. At the same time, a subset of the population may be expressing traits that would be advantageous in some future, unpredictable environment (12). Thus, in rapidly changing environments a population already exists that is pre-adapted to the new environment. For example, *Vibrio cholerae* frequently, but unpredictably transit between two environments: the mammalian host and the aquatic environment, which may include biofilm formation on the surfaces of invertebrates, such as copepods. Attachment to mammalian host mucosal surfaces during infection requires low levels of c-di-GMP that are necessary for virulence gene expression (13). In contrast, bacterial persistence in the aquatic environment requires high levels of c-di-GMP to ensure biofilm formation, but would inversely regulate virulence genes (14). *V. cholerae* exhibits population heterogeneity with respect to these traits during a transient period after release from mammalian host, called the ‘short-term persistence’ stage. During this period in particular, the upcoming environment is erratic, since the next host or condition is unpredictable. ToxT, the master regulator of virulence controls

population heterogeneity which results in a small subpopulation of bacteria expressing virulence genes that provide an adaptive benefit if the next environment is a new mammalian host. Concurrently, the majority virulence-OFF subpopulation is proposed to better adapt to biofilm formation and long-term persistence in the aquatic environment (15, 16) .

Microbes that have evolved under a predictable fluctuation life history (Fig. 1.1B) may have the capacity to interpret prevailing conditions to anticipate an upcoming environment. Such anticipation would allow the microbe to regulate genes in a temporal order to pre-induce gene profiles that are optimal for success in the predicted future environment. Experimental support for this adaptive prediction theory has been presented for *E. coli* that occupy the mammalian gastrointestinal tract, which may provide opportunities for microbes to predict and pre-adapt to the future host niches based on the current environmental stimuli (7, 8). For example, while passing through the GI tract *E. coli* reproducibly are exposed first to lactose (Signal 1, or S1) then to maltose (Signal 2, or S2). In laboratory experiments, the authors of one study showed that when exposed to lactose (S1), *E. coli* induces a lactose gene promoter (Response 1, or R1) and to a lesser extent a maltose gene promoter (Response 2, or R2), prior to exposure to maltose (S2). This response provides an adaptive benefit for growth on maltose (S2) (7). The data indicated that the regulatory network is specifically anticipatory, such that the first signal can induce a response to an upcoming environment, but not the other way around. More importantly, the authors showed that evolution in the absence of the lactose/maltose temporal link led to a weakening of this asymmetric regulation. This study suggests that predictable temporal changes in the host environments can select for anticipatory behaviors in symbiotic microbes.

Microbes may experience predictable changes in environment, even if they occupy a single host niche, due to predictable rhythmic oscillations (e.g. diel, circadian, seasonal). Even though animal rhythmicity has been investigated for decades as a mechanism for anticipatory behavior, how rhythmic changes in the host environments impact the host-associated microbial

community has attracted attention only recently (For detailed examples of circadian rhythms in both mutualistic and pathogenic associations, see the review by (10)). Daily (circadian/diel) or seasonal alterations of animal physiology cause predictable changes to the microenvironments experienced by host-associated symbionts. For example, immunity within species as diverse as fruit fly to humans is subject to circadian control, and the outcome of infection can depend on the time of day (17, 18).

Host rhythms could also cause a predictable pattern in nutrient availability for the symbiotic microbes. For instance, the light organ of the *Euprymna scolopes* squid, which houses the light-producing bacterial symbiont *Vibrio fischeri*, undergoes diel rhythmic morphological and physiological changes that have direct impacts on symbionts. At dawn, the adult squid expels the contents of the light organ, including the bulk of the symbiont population (19), and the light organ epithelium undergoes morphological changes that alter local environment (20, 21). Such host environmental changes are synchronized with symbiotic bacterial transcription profiles to express glycerol metabolism genes that support symbiont growth on host-derived glycerol substrates during the day (22). Based on transcriptomic and other data, it appears that bacterial growth in turn initiates chemical dialog between host and microbe that allows each to adapt in anticipation of nightfall. First, the growing bacterial population induces quorum sensing and bioluminescence production a few hours before dusk, prior to the need for light emission. In the meantime, the colonization of symbionts causes host hemocyte migration into the crypts of the light organ, where they lyse and release chitin for chitin catabolism among the bacterial symbionts (23). Chitin metabolism acidifies the host tissue and further induces bacterial acid tolerance response and intensifies the bacterial luminescence production right after dusk, facilitating the host nocturnal predation (24). The symbiont microbial associated molecular patterns (MAMPs) and luminescence also ensure the expression of host cryptochrome protein in the light organ, which is proposed to regulate host circadian behavior (25).

The examples described above indicate that host-symbiont interactions are intimately entwined with rhythmic behaviors. An open question remains as to whether evolution of symbionts in a predictable environmental regime, such as that caused by rhythmicity has led to bacterial adaptive prediction in any of these systems. The symbiosis between *Xenorhabdus* bacteria and their invertebrate hosts, *Steinernema* nematodes and insects, may offer a particularly amenable system to investigate this question, since it is experimentally tractable and as described in more detail below, the temporal order of host environments encountered by *Xenorhabdus* is predictable.

Adaptive responses in *Xenorhabdus* bacteria symbionts of *Steinernema* nematodes

Xenorhabdus is an insect pathogen transmitted between hosts by virtue of its ability to colonize the intestine of soil-dwelling entomopathogenic *Steinernema* nematodes. The infective juvenile (IJ) stage nematode carries and releases bacteria into the body cavity (hemocoel) of insects, and this infection results in rapid insect death. As part of their mutually beneficial relationship, the bacteria and nematodes both use the insect cadaver as the nutrient source to support reproduction. Once these nutrients are depleted, *Xenorhabdus* bacteria colonize the IJ transmission stage of the nematode, which migrates to the soil to repeat the life cycle. The general stages of the *Xenorhabdus* life cycle, insect infection, reproduction within the cadaver, and colonization of the IJ for transmission to another insect host (26), represent a predictable series of host environments encountered during *Xenorhabdus* life history (Fig. 1.1C). The evolutionary success of *Xenorhabdus* depends on its adaptive responses to these environments, through expression of genes that encode pathogenic (towards insects) and mutualistic (towards nematodes) activities, and to the different tissues and host responses encountered (26, 44). We describe these temporally ordered environments in more detail below.

From the IJ to the insect:

Tens to hundreds of *Xenorhabdus* bacterial cells colonize and persist for months in the relatively nutrient poor intestinal receptacle of soil-dwelling IJ nematodes (Fig. 1.2D) (28–32). IJs can persist in the soil for many months (33–36) and in the IJ receptacle, *Xenorhabdus* likely expresses traits that support its long-term stationary phase survival. IJ infection of an insect (Fig.1.2A) is an obligate step in the reproductive fitness of both the nematode and bacterium, and therefore is predictable in their integrated evolutionary life histories. When an IJ infects an insect, it gains entry into the insect hemocoel, into which it releases its *Xenorhabdus* symbiont (37–39). The hemocoel cavity is bathed in hemolymph, a relatively nutrient rich fluid (40). IJ ingestion of insect hemolymph is always the first step leading to bacterial release into the insect hemocoel, similar to the blood meals of a mosquito or a flea before the transmission of vector-borne pathogens. In *Yersinia pestis,* the temperature of and nutrients in mammalian blood during the flea feeding induce phenotypic variation and changes in bacterial virulence gene expression prior to introduction of the bacteria to the host itself (41–43). Similarly, *X. nematophila* exposure to hemolymph prior to their release into insect hemocoel may lead to pre-induction of virulence genes, perhaps through sensing of its high concentrations of sugars (trehalose and glucose) (44–46).

The transition of *Xenorhabdus* from the aging IJ receptacle to the hemocoel of an insect represents a dramatic shift in selective environment. The hemocoel is relatively nutrient rich, but is a primary site for host surveillance and induction of immune responses. Insect cellular immunity involves hemocytes that engulf bacteria and help clear bacteria through melanin production. Humoral immune responses include the production of antimicrobial peptides that can lyse bacteria (47). In the insect hemocoel, bacterial survival depends on rapidly countering immunity and killing the host, and indeed *X. nematophila* can suppress insect immunity and produces virulence factors that contribute to insect host death (26, 48). Pre-adaptive responses that prime *Xenorhabdus* expression of immuno-suppressive activities and toxins while still within the IJ receptacle could provide a selective advantage.

From virulence to feeding

A second predictable change in environment occurs upon death of the insect (arrow between panel 2A and 2B). The insect cadaver serves as a nutrient source for bacterial growth and nematode reproduction, and *Xenorhabdus* are key players in the liberation of the nutrients (carbohydrates, lipids, and amino acids) contained within the insect biomass (26). Events that may precede and indicate impending insect death, and that therefore may serve as signals for pre-adaptive responses, are the release of nutrients from dying hemocytes (49), the growth of competing microorganisms (50), or changes in the insect intestinal barrier (39).

Xenorhabdus bacteria are not necessarily only living freely within the insect cadaver. Recent discoveries revealed that during the insect-degradation phase of the symbiotic life cycle, *X. nematophila* cells colonize the intestinal epithelium of all stages of the developing nematode host. In adult and juvenile stages of nematode, multiple *Xenorhabdus* cells attach to the epithelial surface of the anterior intestinal caecum (AIC) (Fig. 1.2B) (51). The consequences of this colonization for either *Xenorhabdus* or *Steinernema* have not been elucidated, but these observations remind us that the insect cadaver does not represent a single homogenous environment, but rather that different *X. nematophila* cells within the population may be encountering varied challenges and nutritional content, depending on if they are free-living in the liquefied insect cadaver, associated with insect tissues, attaching to the nematode AIC region, or passing through the nematode intestinal lumen while the nematode is actively digesting. Despite its complexity in the spatial distribution of nutrients, the local environments in the insect cadaver could play a similar role as those in mammalian GI tract, driving phenotypic heterogeneity and pre-adaptive responses in symbiotic bacteria.

From the spent cadaver to the IJ

The depletion of nutrients and high population densities prompts *Xenorhabdus* colonization of the developing IJ receptacle. This process has not been observed yet within an individual nematode, but population-wide studies suggest that it, like the other stages of the *Xenorhabdus* life cycle, consists of a temporally ordered series of events. The pre-IJ is characterized by a collapsing intestinal tract, and during this stage, *Xenorhabdus* bacteria are no longer observed at the AIC, but rather individual cells colonize the pharyngeal-intestinal valve (PIV), in a pocket formed by nematode tissues (Fig. 1.2C). As pre-IJ nematodes undergo further morphological changes and develop into a non-feeding stage of IJ nematodes, the receptacle (intestinal pocket) is formed in a completely closed intestine, and individual bacterial cells are observed in this location, rather than at the pharyngeal intestinal valve (51) (Fig. 1.2D). During this IJ colonization initiation phase, few *Xenorhabdus* bacterial cells localize in the newly formed receptacle. These subsequently grow very slowly into a clonal, or near clonal population (52) that persists until they are introduced a new insect host. The serial events during the process of *Xenorhabdus* bacteria transitioning from insect cadaver to associating with IJ nematodes features predictable nutrient change of local environments, which could cause adaptive changes in gene expression. What signals occur within the insect cadaver that might trigger pre-adaptive modulation of gene expression optimal for colonization? The receptacle of *Steinernema* IJ nematodes contains a wheat-germ-agglutinin-reactive mucus-like substance, which perhaps is utilized by *X. nematophila* as a nutrient source within this environment (53). Pre-adaptive responses to this substance may be triggered by similar glycans expressed on the AIC surface of developing nematodes, or by other sugars present in the insect cadaver. Other potential candidate signaling molecules could be derived from the insect cadaver. This idea is supported by evidence that nematodes better associate with bacterial symbionts when grown in the insect compared to those reared *in vitro* on nutrient agar bacterial lawns (29, 30). This suggests that metabolites specifically derived from the insect tissues (via either nematode or bacterial metabolism) may be important for symbiont transmission and nutrient adaptation.

Nematodes also may be a source of pre-adaptive signals for colonization. For instance, *Steinernema* spp. and other nematodes secrete a variety of ascarosides, signaling pheromones that can regulate social behaviors such as mating, development, and dispersal (54–56). In the nematode *Caenorhabditis elegans* the accumulation of specific ascarosides at high population densities triggers juvenile nematodes to enter dauer stage, a non-feeding larval stage similar to the *Steinernema* IJ (55). In addition, particular ascaroside molecules produced in the *Steinernema* IJs signals nematode dispersal behavior that leads to their emergence from insect cadaver into the soil (54). Since the timing of ascaroside accumulation may synchronize or precede the process of bacterial colonization during IJ formation, they are excellent candidates as signals for pre-adaptive responses. Finally, molecules produced by *Xenorhabdus* themselves may be pre-adaptive signals. *Xenorhabdus* secondary metabolites are produced during the reproductive phase of the life cycle and can antagonize invading microbial species to protect the insect cadaver (50, 57). Changes in the local concentrations of these metabolites could be indicative of conditions that warrant IJ development and emergence.

As mentioned above, the insect cadaver is spatially heterogeneous and may present distinctive signals that promote specialized adaptive responses. Future research on the identification and quantification of metabolites (both spatially and temporally) derived from insect tissues, nematodes, and bacteria in the insect cadaver will help elucidating the particular environmental changes during the host-switching events and the mechanisms in bacterial (pre)-adaptive responses.

Persistence in the IJ

Once few bacterial cells colonize the IJ receptacle, they grow slowly into a population that persists in the host for up to months until the nematode enters a new insect host (30, 52). The IJ receptacle has some spatial and temporal nutrient complexity that could help trigger adaptive gene expression as IJs age. The closed mouth and collapsed intestine in the non-

feeding IJs (28) makes the receptacle a relatively closed environment, restricting nutrient exchange with the outside. The receptacle is the lumen between two anterior intestinal cells that are morphologically distinct from the rest of the intestinal cells (53). Also, in some *Steinernema* nematodes, *Xenorhabdus* symbionts are enclosed in a cellophane-like envelope membrane, termed the vesicle (58). The receptacle (or the vesicle in those nematodes) contains an intra-vesicular structure (IVS) that is a cluster of anucleate particles surrounded by mucus-like material (Fig. 1.2D). This may indicate spatial distribution of nutrients, which could create heterogeneous local environments for the symbionts. Indeed, within the receptacle, *Xenorhabdus* bacteria can be observed attached to the IVS surface, tightly packed with other bacterial cells, or individually as unattached and free-floating in the receptacle space (53). Nutrient availability in the IJ receptacle is likely to vary temporally during IJ host persistence in the soil, and such changes could contribute to pre-adaptive responses to the following insect host environment. Although the IJ does not itself receive fresh influx of nutrients, it may contribute varying nutrients to its symbiont as it ages. Indeed, *X. nematophila* does have access to certain essential amino acids in the receptacle, since auxotrophs for those amino acids are able to colonize and grow there (32). Finally, IJs colonized by symbionts showed reduced life-span in comparison to aposymbiotic IJs (59), suggesting bacteria may continuously exploit the host nutrients during IJ aging process. During this non-feeding stage, IJs store and utilize energy from lipid droplets that contain triglycerols, sterol esters, phospholipids, and proteins (60, 61). In *Steinernema* species, glycogen and trehalose reserves are continuously synthesized and significantly consumed during IJ aging process (62, 63). It is not known yet if and how nematode transfer metabolites into the receptacle. Neither is it known if temporal changes in the nematode physiology (i.e. IJ maturation, movements, and aging, etc.) affect the nutrients provided to symbionts. Regardless, spatial complexity and temporal dynamics of nutrient composition in aging IJ receptacles may be signals that cause colonizing *Xenorhabdus* pre-adapt to the next phase of the life cycle: the insect host.

Phenotypic variation in X. nematophila

The sequential environments encountered by *X. nematophila* described above set the stage for the evolution of adaptive regulatory pathways. One of these pathways is controlled by the global transcription factor, Lrp. Lrp homologs are small (~19 kDa) DNA binding proteins that are widely conserved among bacteria and archaea (64, 65). They are members of a larger conserved family of transcriptional regulators known as the feast/famine regulatory proteins. These regulators contribute to nutrient adaptation by sensing various environmental signals and eliciting an adaptive global change in gene expression (66). In *X. nematophila,* Lrp is a global regulator that controls numerous genes with predicted roles in host interactions, motility, nutrient adaptation, and the production of small molecules (67, 68). An *lrp* mutant has defects in each stage of *X. nematophila* host interactions: it is defective in immune suppression and killing of *M. sexta* insects, supporting reproduction of and colonizing nematodes, and transitioning between nutrient-limiting and nutrient-rich media (67, 69).

A more complicated role for Lrp in the *X. nematophila* life cycle was recently reported, based on the discovery that it controls a phenotypic variation phenomenon known as virulence modulation (VMO) (68, 70). This phenomenon is marked by the spontaneous and reversible switch between virulent and virulence-attenuated phenotypes (as assessed by the ability to kill *Manduca sexta* insects upon injection) (68, 70). A role for Lrp in VMO was initially suggested by the finding that Lrp protein levels vary from cell-to-cell in wild type populations and that these levels correlate with immuno-suppressive and virulence phenotypes after injection into insects. Surprisingly this correlation is inverse: *X. nematophila* cells expressing high levels of Lrp exhibit attenuated immune suppression and virulence, while those expressing low levels of Lrp are immunosuppressive and virulent (68) (Fig. 1.2E). The link between Lrp levels and virulence phenotypes has been substantiated using *X. nematophila* engineered to constitutively express high or low levels of Lrp. These cells exhibit attenuated and virulent phenotypes respectively (68). More recent studies have explored the biological role of the virulence-attenuated high Lrp

cell type, revealing that high-Lrp expressers are significantly better than low-expressers in supporting nematode reproduction, and are slightly better at initiating colonization of IJs (Fig. 1.2FG, see details in Chapter 2). In contrast, bacteria expressing constitutively low levels of Lrp are virulent but defective in supporting nematode reproduction and colonization (Fig. 1.2F) (68). Overall these data suggest that an individual *X. nematophila* cell expresses one of two symbiotic gene expression profiles, optimal for virulence or mutualism, depending on if it has low or high cellular levels of Lrp, respectively. Further, the high- or low-Lrp expresser state is heritable and reversible, suggesting a phenotypic variation phenomenon controls the switch between high and low states (and therefore between mutualistic and virulent phenotypes) (68, 70, 71).

In this thesis, I will present and discuss my research work investigating Lrp-dependent virulence modulation in laboratory medium and in host environment. This work contributes to our understanding of phenotypic variation in the naturally occurring system and basic mechanisms underlying fundamental questions in microbial symbiosis.

Thesis Outline

Chapter 1: Introduction

Chapter 2: High levels of *Xenorhabdus nematophila* transcriptional factor Lrp promotes bacteria-nematode mutualism, suggesting that Lrp dictates a phenotypic switch in between pathogenesis and mutualism

Chapter 3: Nutritional conditions in vitro drives Lrp-dependent VMO switch and population heterogeneity in *X. nematophila*

Chapter 4: Lrp-dependent phenotypic switching occurs in IJ nematodes

Chapter 5: Studying the symbiotic bacterium *Xenorhabdus nematophila* in individual, living *Steinernema carpocapsae* nematodes using microfluidic systems

Chapter 6: Summary and future directions

References

1. **Wales AD**, **Woodward MJ**, **Pearson GR**. 2005. Attaching-effacing bacteria in animals. J Comp Pathol **132**:1–26.
2. **Sachs JL**, **Skophammer RG**, **Regus JU**. 2011. Evolutionary transitions in bacterial symbiosis. Proc Natl Acad Sci U S A **108 Suppl**:10800–10807.
3. **Douglas AE**. 2010. The symbiotic habit. Princeton University Press, Princeton, New Jersey; Woodstock, Oxfordshire.
4. **Chaston J**, **Goodrich-Blair H**. 2010. Common trends in mutualism revealed by model associations between invertebrates and bacteria. FEMS Microbiol Rev **34**:41–58.
5. **Acar M**, **Mettetal JT**, **van Oudenaarden A**. 2008. Stochastic switching as a survival strategy in fluctuating environments. Nat Genet **40**:471–475.
6. **Balaban NQ**, **Merrin J**, **Chait R**, **Kowalik L**, **Leibler S**. 2004. Bacterial persistence as a phenotypic switch. Science **305**:1622–1625.
7. **Mitchell A**, **Romano GH**, **Groisman B**, **Yona A**, **Dekel E**, **Kupiec M**, **Dahan O**, **Pilpel Y**. 2009. Adaptive prediction of environmental changes by microorganisms. Nature **460**:220–224.
8. **Tagkopoulos I**, **Liu Y-C**, **Tavazoie S**. 2008. Predictive Behavior Within Microbial Genetic Networks. Science **320**:1313–1317.
9. **Keim PS**, **Wagner DM**. 2009. Humans and evolutionary and ecological forces shaped the phylogeography of recently emerged diseases. Nat Rev Microbiol **7**:813–821.
10. **Heath-Heckman EAC**. 2016. The Metronome of Symbiosis: Interactions Between Microbes and the Host Circadian Clock. Integr Comp Biol **56**:776–783.
11. **Van Der Woude MW**. 2011. Phase variation : how to create and coordinate population diversity. Curr Opin Microbiol **14**:205–211.
12. **Kussell E**, **Leibler S**. 2005. Phenotypic Diversity, Population Growth, and Information in Fluctuating Environments. Science **309**:2075–2078.

13. **Tischler AD**, **Camilli A**. 2005. Cyclic diguanylate regulates *Vibrio cholerae* virulence gene expression. Infect Immun **73**:5873–5882.

14. **Tischler AD**, **Camilli A**. 2004. Cyclic diguanylate (c-di-GMP) regulates *Vibrio cholerae* biofilm formation. Mol Microbiol **53**:857–869.

15. **Schild S**, **Tamayo R**, **Nelson EJ**, **Qadri F**, **Calderwood SB**, **Camilli A**. 2007. Genes Induced Late in Infection Increase Fitness of *Vibrio cholerae* after Release into the Environment. Cell Host Microbe **2**:264–277.

16. **Nielsen AT**, **Dolganov NA**, **Rasmussen T**, **Otto G**, **Miller MC**, **Felt SA**, **Torreilles S**, **Schoolnik GK**. 2010. A bistable switch and anatomical site control *Vibrio cholerae* virulence gene expression in the intestine. PLoS Pathog **6**:e1001102.

17. **Tsoumtsa LL**, **Torre C**, **Ghigo E**. 2016. Circadian Control of Antibacterial Immunity: Findings from Animal Models. Front Cell Infect Microbiol **6**:54.

18. **Man K**, **Loudon A**, **Chawla A**. 2016. Immunity around the clock. Science **354**:999–1003.

19. **Nyholm S V.**, **McFall-Ngai MJ**. 1998. Sampling the light-organ microenvironment of *Euprymna scolopes*: Description of a population of host cells in association with the bacterial symbiont *Vibrio fischeri*. Biol Bull **195**:89–97.

20. **Lamarcq LH**, **McFall-Ngai MJ**. 1998. Induction of a gradual, reversible morphogenesis of its host's epithelial brush border by *Vibrio fischeri*. Infect Immun **66**:777–785.

21. **Heath-Heckman EAC**, **Foster J**, **Apicella MA**, **Goldman WE**, **McFall-Ngai M**. 2016. Environmental cues and symbiont microbe-associated molecular patterns function in concert to drive the daily remodelling of the crypt-cell brush border of the *Euprymna scolopes* light organ. Cell Microbiol **18**:1642–1652.

22. **Wier AM**, **Nyholm S V**, **Mandel MJ**, **Massengo-Tiassé RP**, **Schaefer AL**, **Koroleva I**, **Splinter-Bondurant S**, **Brown B**, **Manzella L**, **Snir E**, **Almabrazi H**, **Scheetz TE**, **Bonaldo MDF**, **Casavant TL**, **Soares MB**, **Cronan JE**, **Reed JL**, **Ruby EG**, **McFall-Ngai MJ**. 2010. Transcriptional patterns in both host and bacterium underlie a daily rhythm of

anatomical and metabolic change in a beneficial symbiosis. Proc Natl Acad Sci U S A **107**:2259–2264.

23. **Heath-Heckman EAC**, **McFall-Ngai MJ**. 2011. The occurrence of chitin in the hemocytes of invertebrates. Zoology **114**:191–198.
24. **Schwartzman JA**, **Koch E**, **Heath-Heckman EAC**, **Zhou L**, **Kremer N**, **McFall-Ngai MJ**, **Ruby EG**. 2015. The chemistry of negotiation: Rhythmic, glycan-driven acidification in a symbiotic conversation. Proc Natl Acad Sci U S A **112**:556–571.
25. **Heath-Heckman EAC**, **Peyer SM**, **Whistler CA**, **Apicella MA**, **Goldman WE**, **Mcfall-ngai MJ**. 2013. Bacterial bioluminescence regulates expression of a host cryptochrome gene in the squid-Vibrio symbiosis. MBio **4**:1–10.
26. **Richards GR**, **Goodrich-Blair H**. 2009. Masters of conquest and pillage: *Xenorhabdus nematophila* global regulators control transitions from virulence to nutrient acquisition. Cell Microbiol **11**:1025–1033.
27. **Morran LT**, **Penley MJ**, **Byrd VS**, **Meyer AJ**, **O'Sullivan TS**, **Bashey F**, **Goodrich-Blair H**, **Lively CM**. 2016. Nematode-Bacteria Mutualism: Selection Within the Mutualism Supersedes Selection Outside of the Mutualism. Evolution (N Y) **7**:687–695.
28. **Bird AF**, **Akhurst RJ**. 1983. The nature of the intestinal vesicle in nematodes of the family steinernematidae. Int J Parasitol **13**:599–606.
29. **Flores-Lara Y**, **Renneckar D**, **Forst S**, **Goodrich-Blair H**, **Stock P**. 2007. Influence of nematode age and culture conditions on morphological and physiological parameters in the bacterial vesicle of *Steinernema carpocapsae* (Nematoda: Steinernematidae). J Invertebr Pathol **95**:110–118.
30. **Goetsch M**, **Owen H**, **Goldman B**, **Forst S**. 2006. Analysis of the PixA inclusion body protein of *Xenorhabdus nematophila*. J Bacteriol **188**:2706–2710.
31. **Jubelin G**, **Pagès S**, **Lanois A**, **Boyer M-H**, **Gaudriault S**, **Ferdy J-B**, **Givaudan A**. 2011. Studies of the dynamic expression of the *Xenorhabdus* FliAZ regulon reveal

atypical iron-dependent regulation of the flagellin and haemolysin genes during insect infection. Environ Microbiol **13**:1271–1284.

32. **Martens EC**, **Russell FM**, **Goodrich-Blair H**. 2005. Analysis of *Xenorhabdus nematophila* metabolic mutants yields insight into stages of *Steinernema carpocapsae* nematode intestinal colonization. Mol Microbiol **58**:28–45.

33. **Ishibashi N**, **Kondo E**. 1986. *Steinernema feltiae* (DD-136) and *S. glaseri*: Persistence in Soil and Bark Compost and Their Influence on Native Nematodes. J Nematol **18**:310–6.

34. **Kung S-P**, **Gaugler R**, **Kaya HK**. 1991. Effects of soil temperature, moisture, and relative humidity on entomopathogenic nematode persistence. J Invertebr Pathol **57**:242–249.

35. **Kung SP**, **Gaugler R**, **Kaya HK**. 1990. Influence of Soil pH and Oxygen on Persistence of *Steinernema* spp. J Nematol **22**:440–5.

36. **Kung S-P**, **Gaugler R**, **Kaya HK**. 1990. Soil type and entomopathogenic nematode persistence. J Invertebr Pathol **55**:401–406.

37. **Poinar GO**, **Thomas GM**. 1967. The nature of *Achromobacter nematophilus* as an insect pathogen. J Invertebr Pathol **9**:510–514.

38. **Snyder H**, **Stock SP**, **Kim S-KK**, **Flores-Lara Y**, **Forst S**. 2007. New insights into the colonization and release processes of *Xenorhabdus nematophila* and the morphology and ultrastructure of the bacterial receptacle of its nematode host, *Steinernema carpocapsae*. Appl Environ Microbiol **73**:5338–5346.

39. **Sicard M**, **Brugirard-ricaud K**, **Page S**, **Lanois A**, **Boemare NE**, **Brehe M**, **Givaudan A**, **Gpia L**. 2004. Stages of Infection during the Tripartite Interaction between *Xenorhabdus nematophila* , Its Nematode Vector , and Insect Hosts. Appl Environ Microbiol **70**:6473–6480.

40. **Phalaraksh C**, **Lenz EM**, **Lindon JC**, **Nicholson JK**, **Farrant RD**, **Reynolds SE**, **Wilson ID**, **Osborn D**, **Weeks JM**. 1999. NMR spectroscopic studies on the haemolymph of the tobacco hornworm, *Manduca sexta*: assignment of ^{1}H and ^{13}C NMR spectra. Insect

Biochem Mol Biol **29**:795–805.

41. **Vadyvaloo V**, **Jarrett C**, **Sturdevant DE**, **Sebbane F**, **Hinnebusch BJ**. 2010. Transit through the flea vector induces a pretransmission innate immunity resistance phenotype in *Yersinia pestis*. PLoS Pathog **6**:e1000783.

42. **Hinnebusch BJ**, **Rudolph AE**, **Cherepanov P**, **Dixon JE**, **Schwan TG**, **Forsberg A**. 2002. Role of Yersinia murine toxin in survival of *Yersinia pestis* in the midgut of the flea vector. Science **296**:733–5.

43. **Rebeil R**, **Jarrett CO**, **Driver JD**, **Ernst RK**, **Oyston PCF**, **Hinnebusch BJ**. 2013. Induction of the *Yersinia pestis* PhoP-PhoQ regulatory system in the flea and its role in producing a transmissible infection. J Bacteriol **195**:1920–1930.

44. **Rodaki A**, **Bohovych IM**, **Enjalbert B**, **Young T**, **Odds FC**, **Gow NAR**, **Brown AJP**. 2009. Glucose promotes stress resistance in the fungal pathogen *Candida albicans*. Mol Biol Cell **20**:4845–55.

45. **Kalscheuer R**, **Koliwer-Brandl H**. 2014. Genetics of Mycobacterial Trehalose Metabolism. Microbiol Spectr **2**.

46. **Elbein AD**, **Pan YT**, **Pastuszak I**, **Carroll D**. 2003. New insights on trehalose: a multifunctional molecule. Glycobiology **13**:17R–27R.

47. **Casanova-Torres ÁM**, **Goodrich-Blair H**. 2013. Immune Signaling and Antimicrobial Peptide Expression in *Lepidoptera*. Insects **4**:320–38.

48. **Herbert EE**, **Goodrich-Blair H**. 2007. Friend and foe: the two faces of *Xenorhabdus nematophila*. Nat Rev Microbiol **5**:634–646.

49. **Cowles KN**, **Goodrich-Blair H**. 2005. Expression and activity of a *Xenorhabdus nematophila* haemolysin required for full virulence towards *Manduca sexta* insects. Cell Microbiol **7**:209–219.

50. **Singh S**, **Orr D**, **Divinagracia E**, **McGraw J**, **Dorff K**, **Forst S**. 2015. Role of secondary metabolites in establishment of the mutualistic partnership between *Xenorhabdus*

nematophila and the entomopathogenic nematode *Steinernema carpocapsae*. Appl Environ Microbiol **81**:754–764.

51. **Chaston JM**, **Murfin KE**, **Heath-Heckman EA**, **Goodrich-Blair H**. 2013. Previously unrecognized stages of species-specific colonization in the mutualism between *Xenorhabdus* bacteria and *Steinernema* nematodes. Cell Microbiol **15**:1545–1559.
52. **Martens EC**, **Heungens K**, **Goodrich-Blair H**. 2003. Early Colonization Events in the Mutualistic Association between *Steinernema carpocapsae* Nematodes and *Xenorhabdus nematophila* Bacteria. J Bacteriol **185**:3147–3154.
53. **Martens EC**, **Goodrich-Blair H**. 2005. The *Steinernema carpocapsae* intestinal vesicle contains a subcellular structure with which *Xenorhabdus nematophila* associates during colonization initiation. Cell Microbiol **7**:1723–1735.
54. **Kaplan F**, **Alborn HT**, **von Reuss SH**, **Ajredini R**, **Ali JG**, **Akyazi F**, **Stelinski LL**, **Edison AS**, **Schroeder FC**, **Teal PE**. 2012. Interspecific nematode signals regulate dispersal behavior. PLoS One **7**:e38735.
55. **Ludewig AH**, **Schroeder FC**. 2013. Ascaroside signaling in *C. elegans*. WormBook 1–22.
56. **Choe A**, **von Reuss SH**, **Kogan D**, **Gasser RB**, **Platzer EG**, **Schroeder FC**, **Sternberg PW**. 2012. Ascaroside Signaling Is Widely Conserved among Nematodes. Curr Biol **22**:772–780.
57. **Park D**, **Forst S**. 2006. Co-regulation of motility, exoenzyme and antibiotic production by the EnvZ-OmpR-FlhDC-FliA pathway in *Xenorhabdus nematophila*. Mol Microbiol **61**:1397–412.
58. **Sugar DR**, **Murfin KE**, **Chaston JM**, **Andersen AW**, **Richards GR**, **DeLéon L**, **Baum JA**, **Clinton WP**, **Forst S**, **Goldman BS**, **Krasomil-Osterfeld KC**, **Slater S**, **Stock SP**, **Goodrich-Blair H**. 2012. Phenotypic variation and host interactions of Xenorhabdus bovienii SS-2004, the entomopathogenic symbiont of Steinernema jollieti nematodes.

Environ Microbiol **14**:924–939.

59. **Mitani DK**, **Kaya HK**, **Goodrich-Blair H**. 2004. Comparative study of the entomopathogenic nematode, *Steinernema carpocapsae*, reared on mutant and wild-type *Xenorhabdus nematophila*. Biol Control **29**:382–391.

60. **Patel MN**, **Stolinski M**, **Wright DJ**. 1997. Neutral lipids and the assessment of infectivity in entomopathogenic nematodes : observations on four *Steinernema* species. Parasitology **114**:489–496.

61. **Bartz R**, **Li W-H**, **Venables B**, **Zehmer JK**, **Roth MR**, **Welti R**, **Anderson RGW**, **Liu P**, **Chapman KD**. 2007. Lipidomics reveals that adiposomes store ether lipids and mediate phospholipid traffic. J Lipid Res **48**:837–47.

62. **Patel MN**, **Wright DJ**. 1997. Glycogen: its importance in the infectivity of aged juveniles of *Steinernema carpocapsae*. Parasitology **114**:591–6.

63. **Qiu L**, **Lacey MJ**, **Bedding RA**. 2000. Using deuterium as an isotopic tracer to study the energy metabolism of infective juveniles of *Steinernema carpocapsae* under aerobic conditions. Comp Biochem Physiol Part B Biochem Mol Biol **127**:279–288.

64. **Platko J V**, **Calvo JM**. 1993. Mutations affecting the ability of *Escherichia coli* Lrp to bind DNA, activate transcription, or respond to leucine. J Bacteriol **175**:1110–1117.

65. **Tani TH**, **Khodursky A**, **Blumenthal RM**, **Brown PO**, **Matthews RG**. 2002. Adaptation to famine: a family of stationary-phase genes revealed by microarray analysis. Proc Natl Acad Sci U S A **99**:13471–13476.

66. **Yokoyama K**, **Ishijima SA**, **Clowney L**, **Koike H**, **Aramaki H**, **Tanaka C**, **Makino K**, **Suzuki M**. 2006. Feast/famine regulatory proteins (FFRPs): *Escherichia coli* Lrp, AsnC and related archaeal transcription factors. FEMS Microbiol Rev **30**:89–108.

67. **Cowles KN**, **Cowles CE**, **Richards GR**, **Martens EC**, **Goodrich-Blair H**. 2007. The global regulator Lrp contributes to mutualism, pathogenesis and phenotypic variation in the bacterium *Xenorhabdus nematophila*. Cell Microbiol **9**:1311–1323.

68. **Hussa EA**, **Casanova-Torres ÁM**, **Goodrich-Blair H**. 2015. The global transcription factor Lrp controls virulence modulation in *Xenorhabdus nematophila*. J Bacteriol **197**:3015–3025.

69. **Heungens K**, **Cowles CE**, **Goodrich-Blair H**. 2002. Identification of *Xenorhabdus nematophila* genes required for mutualistic colonization of *Steinernema carpocapsae* nematodes. Mol Microbiol **45**:1337–1353.

70. **Park Y**, **Herbert EE**, **Cowles CE**, **Cowles KN**, **Menard ML**, **Orchard SS**, **Goodrich-Blair H**. 2007. Clonal variation in *Xenorhabdus nematophila* virulence and suppression of *Manduca sexta* immunity. Cell Microbiol **9**:645–656.

71. **Cao M**, **Patel T**, **Goodrich-Blair H**, **Hussa EA**. 2017. High levels of Xenorhabdus nematophila transcription factor Lrp promote mutualism with *Steinernema carpocapsae* nematode hosts. Appl Environ Microbiol **83**:17.

Figures

Figure 1.1. Responsive and Anticipatory Adaptations Resulting from Random and Ordered Environmental Exposures.

(A) For an organism that encounters the multiple environments (represented by outer lines), but in a random, unpredictable manner, adaptive gene expression (represented by inner shapes) occurs in response to cues, or is selected by conditions encountered within, the current environment (e.g. the outer and inner colors of each symbol match). (B) Temporal progression through a cyclic series of predictable environments (outer line color: orange triangle, blue square, red diamond, and purple circle) can select for the evolution of adaptive prediction, in which the cellular program of gene expression (inner shape color: orange circle, blue triangle, red square, and purple diamond) is pre-adapted for the next environment. Anticipatory or pre-adaptive responses can occur in response to environmental cues. For instance, the orange environment (triangle) triggers a change in gene expression that is adaptive to blue environment (square) or in response to endogenous molecular clocks.

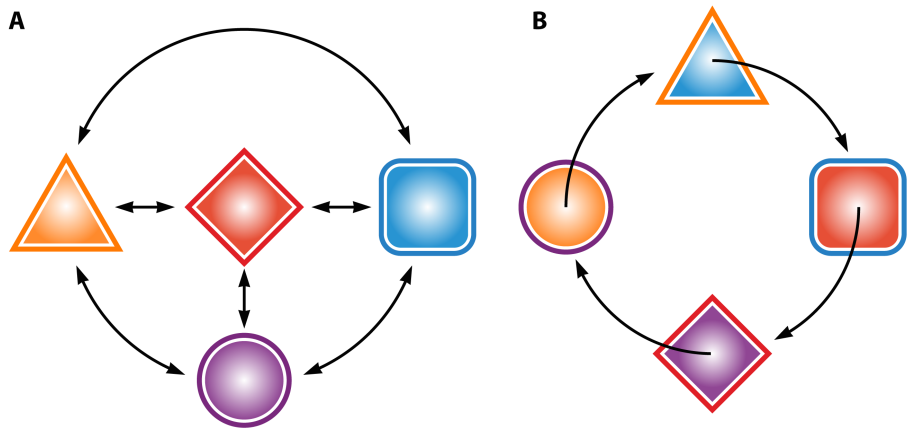

Figure 1.2. Series of *Steinernema* host intestinal environments encountered by *Xenorhabdus*.

(A-D) Simplified intestinal structures of nematodes (not whole organisms) at different stages (IJ, adult and juvenile, and pre-IJ) are schematically represented, with Xenorhabdus bacteria indicated by green ovals. (A) Once an IJ nematode enters the insect hemocoel from the soil, bacteria X. nematophila (green ovals) are released from the widening intestinal lumen (IL) of the recovering IJ into insect hemolymph during infection. (B) Adult and juvenile nematodes in the insect cadaver are colonized by symbiotic bacteria at the anterior intestinal caecum (AIC), a region within the intestine immediately below the pharyngeal intestinal valve (PIV). (C) In a pre-IJ nematode, a few symbiotic bacterial cells are enclosed in pouches within the PIV. (D) In an IJ nematode with a closed intestine, symbiotic bacteria colonize the receptacle. Bacteria are either associated with the intravesicular structure (IVS) or move freely in the receptacle lumen. (E) X. nematophila bacteria expressing low levels of Lrp are more virulent towards insects. (F) X. nematophila bacteria expressing high levels of Lrp better support nematode reproduction in the insect cadaver. (G) X. nematophila bacteria expressing high levels of Lrp show a high colonization frequency in IJ nematodes. bb: basal bulb; IL: intestinal lumen; AIC: anterior intestinal cecum; PIV: pharyngeal intestinal valve; IVS: intravesicular structure.

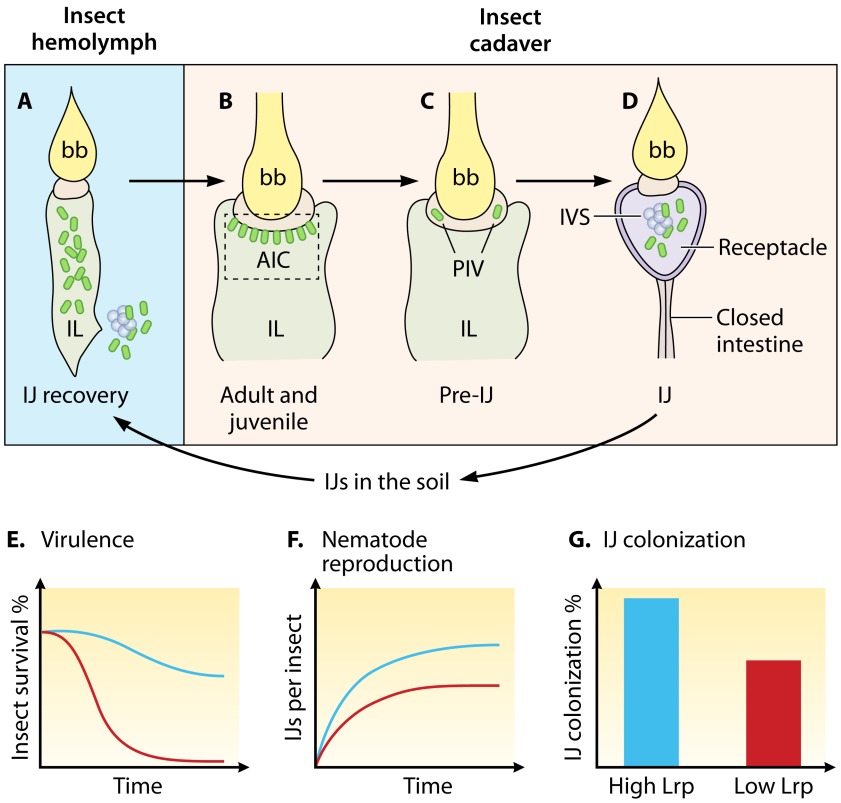
Insect hemolymph
Insect cadaver
A
B
C
D
bb
AIC
IL
PIV
IVS
Receptacle
Closed intestine
IJ recovery
Adult and juvenile
Pre-IJ
IJ
IJs in the soil

E. Virulence
Insect survival %
Time
F. Nematode reproduction
IJs per insect
Time
G. IJ colonization
IJ colonization %
High Lrp
Low Lrp

Chapter 2

High levels of the *Xenorhabdus nematophila* transcription factor Lrp promote mutualism with *Steinernema carpocapsae* nematode hosts, suggesting that Lrp dictates a phenotypic switch in between pathogenesis and mutualism

This Chapter is published: **Cao, M.,** Patel, T., Goodrich-Blair, H., & Hussa, E. A. (2017). High levels of *Xenorhabdus nematophila* transcription factor Lrp promote mutualism with *Steinernema carpocapsae* nematode hosts. *Applied and Environmental Microbiology*, *83*(e00276), 17.'

Mengyi Cao: developed hypotheses, designed and performed experiments, data analysis, math modeling, manuscript writing, arts of figures.

Heidi Goodrich-Blair: manuscript writing and editing.

Abstract:

Xenorhabdus nematophila bacteria are mutualistic symbionts of *Steinernema carpocapsae* nematodes and pathogens of insects. The *X. nematophila* global regulator Lrp controls expression of many genes involved in both mutualism and pathogenic activities, suggesting a role in the transition between the two host organisms. We previously reported that natural populations of *X. nematophila* exhibit variable levels of Lrp expression, and that cells expressing relatively low levels of Lrp are optimized for virulence in the insect *Manduca sexta.* The adaptive advantage of the high-Lrp-expressing state was not established. Here we used strains engineered to express constitutively high or low levels of Lrp to test the model that high-Lrp-expressing cells are adapted for mutualistic activities with the nematode host. We demonstrate that high-Lrp cells form more robust biofilms in laboratory media than do low-Lrp cells, which may reflect adherence to host tissues. Also, our data showed that nematodes cultivated with high-Lrp strains are more frequently colonized relative to those associated with low-Lrp strains. Taken together these data support the idea that high-Lrp cells have an advantage in tissue adherence and colonization initiation. Furthermore, our data show that high-Lrp expressing strains better support nematode reproduction than their low-Lrp counterparts in both in vitro and in vivo conditions. Our data indicate that heterogeneity of Lrp expression in *X. nematophila* populations provides diverse cell populations adapted to both pathogenic (low Lrp) and mutualistic (high Lrp) states.

Importance:

Host associated bacteria experience fluctuating conditions both during residence within an individual host and during transmission between hosts. For bacteria that engage in evolutionarily stable, long-term relationships with particular hosts these fluctuations provide selective pressure for the emergence of adaptive regulatory mechanisms. Here we present

evidence that the bacterium *Xenorhabdus nematophila* uses variable levels of the transcription factor Lrp to optimize its association with its two animal hosts: nematodes and insects, with which it behaves as a mutualist and a pathogen, respectively. Building on our previous finding that relatively low cellular levels of Lrp are optimal for pathogenesis, we demonstrate that conversely, high levels of Lrp promote mutualistic activities with the *Steinernema carpocapsae* nematode host. These data suggest that *X. nematophila* has evolved to utilize phenotypic variation between high and low Lrp expression states to optimize its alternating behaviors as a mutualist and a pathogen.

Introduction

Animals associate with microbes in relationships that can be mutualistic (beneficial), commensal (neutral), or pathogenic (harmful). Within all of these types of relationships, and during transitions between different hosts or natural environments, microbes can experience rapidly changing local conditions, such as fluctuating nutrient availability and dynamic host immune responses. Bacterial fitness is increased by adaptive responses to such changes. One mechanism by which bacteria can adapt to rapid environmental fluctuations is phenotypic variation, in which an isogenic population (derived from the same parental cell) comprises subpopulations exhibiting different phenotypes, each of which confers a selective advantage in a particular environment (1). Phenotypic variation can thereby eliminate the temporal lag associated with sense-and-response mechanisms during fluctuations in environment and/or host conditions.

The life cycle of bacterium *Xenorhabdus nematophila* alternates between a pathogenic phase in multiple types of insects and a mutualistic stage, specifically with the entomopathogenic nematode *Steinernema carpocapsae,* which transmits *X. nematophila* between insect hosts. During the transmission phase of life cycle, *X. nematophila* are carried in the intestine, in a region termed the receptacle, of the nematode's soil-dwelling infective juvenile (IJ) stage (Fig. 2.1). The IJ invades the blood cavity of a host insect, and releases *X. nematophila,* which helps suppress insect immunity and expresses virulence determinants that contribute to insect death. In the insect cadaver, bacteria secrete various enzymatic activities that degrade insect tissues, liberating nutrients that support nematode development and sexual reproduction. Progeny nematodes that experience nutrient depletion and high population densities will develop into IJs, colonized by their bacterial symbionts, and emerge from the insect cadaver into the soil to seek a new host to infect (2).

X. nematophila adaptation to the three general phases of its life cycle (infection, reproduction, and transmission) will directly impact its own fitness and the fitness of its symbiotic partner (Fig. 2.1) (3). Within each phase, *X. nematophila* experiences distinctive environmental conditions and varying growth rates (4, 5). With regard to nutrient composition and concentration, insect blood is rich in glucose and trehalose but limiting for iron (6, 7), the insect cadaver which supports growth of *X. nematophila* to high densities appears to contain utilizable iron, lipids and proteins (3, 7–9), and the IJ nematode receptacle, an environment in which *X. nematophila* experiences limited reproduction, contains growth-supporting levels of some amino acids and vitamins (e.g. serine, histidine, and pantothenate) but not others (threonine, paraminobenzoate, and pyridoxine) (10, 11).

The three different life cycle phases also offer distinctive surfaces and host molecules with which *X. nematophila* may interact. During infection of a living insect, *X. nematophila* encounters both constitutive and inducible immune factors such as melanin and antimicrobial peptides (12–14) and localizes to iron- and collagen-rich connective tissue in the midgut extracellular matrix (15). *X. nematophila,* but not other bacteria adhere to the anterior intestinal region of the developing and reproducing nematodes within the insect cadaver (16, 17) and in emerging IJs, *X. nematophila* cells are physically associated with a host-derived anucleate structure called the IVS (intra-vesicular structure), which is coated with wheat-germ-reactive mucus-like material containing either *N*- acetyl glucosamine or *N*- acetyl neuraminic acid moieties (17). Although biofilm formation has yet to be fully characterized in *X. nematophila*, the species-specific association of *X. nematophila* with distinctive nematode tissues may involve biofilm-mediated attachment, similar to that which occurs in other mutualisms such as between *Vibrio fischeri* bacteria and *Euprymna scolopes* squid during initiation of colonization (18).

To successfully navigate its life cycle and express the appropriate symbiotic activities, *X. nematophila* must sense and adapt to shifts in nutrient and host molecule identities. *X. nematophila* exhibits phenotypic variation that may contribute to this process. Two distinct but overlapping types of phenotypic switching have been observed in *X. nematophila*: variation between a "primary" and "secondary" form cell type, and virulence modulation (VMO). Primary form cells are typically observed in natural populations of *Xenorhabdus* bacteria, but prolonged growth in laboratory conditions leads to the appearance of secondary form cells that no longer express multiple behaviors such as the ability to swim or swarm, bind dye bromothymol blue, agglutinate red blood cells, and produce antibiotics and exoenzymes. Both primary and secondary forms of the bacteria colonize nematode IJs and kill insects and the specific selective advantage of this phenomenon remains unclear (19–21). In VMO, a subpopulation of wild type *X. nematophila* primary form cells exhibits attenuated virulence, measured by direct injection of the bacteria into the insect blood cavity. The VMO switch is spontaneous and reversible among bacterial colonies in laboratory conditions (22, 23). The adaptive benefit of a switch that results in a subpopulation of *X. nematophila* cells that are attenuated for virulence has not been investigated yet, but it may play a role in the reproductive and transmission stages of the *X. nematophila* life cycle.

In *X. nematophila* both primary/secondary form variation and VMO are controlled in part by the Leucine-responsive regulatory protein (Lrp), a global regulatory transcription factor. Lrp homologs are small (~19 kd) regulatory proteins conserved across bacteria and archaea (24, 25). They are members of a larger conserved family of transcriptional regulators known as the feast/famine regulatory proteins, which are involved in nutrient adaptation (26). In *X. nematophila,* Lrp regulates more than 65% of the visible proteome and regulates genes that encode functions involved in pathogenesis, mutualism and nutrient adaptation (27, 28). An *lrp* mutant has defects in suppressing insect immunity, shows reduced abilities to support

nematode reproduction and colonize IJs, and has delayed growth relative to wild type when transiting from nutrient-limiting to nutrient-rich conditions (27, 29). In addition, the *lrp* mutant shares many characteristics with secondary form cells, including the inability to bind bromo-thymol blue dye and reduced expression of exoenzymes such as lipase and protease. These *lrp* mutant phenotypes suggest that Lrp might be involved in the primary to secondary form switch (27).

We recently reported that Lrp expression levels fluctuate among *X. nematophila* primary form wild type isolates and colonies and that this variation is responsible for the distinctive virulent and attenuated virulence phenotypes observed in the VMO switch. When directly injected in the *M. sexta* insect larvae, wild type *X. nematophila* isolates naturally expressing either low or high relative levels of Lrp were virulent and immuno-suppressive or virulence-attenuated and non-immunosuppressive, respectively. When Lrp expression levels were 'fixed' by plasmid-encoded constitutive expression of either low- or high-Lrp levels, we again observed virulent/suppressive and virulence-attenuated/non-suppressive phenotypes respectively, establishing a direct link between Lrp levels and the virulence phenotype. These findings suggest that in wild type *X. nematophila*, variations in Lrp expression levels create heterogeneous subpopulations with respect to virulence phenotypes (23).

A further prediction from our previous study was that the VMO switch may contribute to *X. nematophila* adaptation during its transitions between hosts. The virulence-attenuated, fixed high Lrp-expressing strains consistently exhibited increased antibiotic, protease and lipase activities *in vitro* (23). Since these activities may promote degradation and protection of the insect cadaver (7, 30–32) we hypothesized that high Lrp subpopulations may be adapted for optimal support of the reproductive stage of the symbiosis and that population heterogeneity with respect to Lrp levels contributes to adaptation between host environments. In this study,

we sought to further explore the role of high- versus low-*lrp* expressing populations in mutualism (reproduction, transmission) and mutualism-associated phenotypes (biofilm formation).

Results

Fixed high levels of Lrp confer optimal biofilm formation and mutualistic phenotypes in *X. nematophila*

We hypothesized that, relative to *X. nematophila* low-*lrp*-expressing strains, those strains expressing high levels of Lrp (high-*lrp*) are optimized for mutualistic interactions with the *S. carpocapsae* nematode host. In various mutualistic microbial symbioses biofilm formation is associated with tissue-specific colonization of the host animal (33, 34). To characterize the impact of varying Lrp levels on *X. nematophila* biofilm formation we measured adherence to the surfaces of borosilicate glass tubes, using previously described fixed *lrp* strains of *X. nematophila*: an *lrp-2::kan* mutant carrying control or low-*lrp* or high-*lrp* plasmids (23). After static incubation for 6 d in LB medium, all strains formed adherent populations at the liquid-air interface (Fig. 2.3A). Solubilization and quantification of stained biofilm material revealed that *X. nematophila* expressing high levels of Lrp (high-*lrp*) had significantly more adherent cells than did either the no-*lrp* or low-*lrp* strains (Fig. 2.3B).

We next used as a proxy for *X. nematophila* mutualistic association with the nematode, the number of infective juvenile (IJ) nematodes produced after co-culture on agar lawns of *X. nematophila* expressing plasmid-encoded fixed levels of Lrp (23). IJs that emerged from the bacterial lawns into water traps were counted over time. On day 7 and 10 post water-trap, the high-*lrp* plasmid strain supported significantly higher IJ production than did either the no-*lrp* vector control or the low-*lrp* plasmid strain (Fig. 2.4A), supporting the idea that the high-*lrp*

plasmid strain provided greater mutualistic benefits to the nematode host than did the other strains.

In our previous work, the high-*lrp,* low-*lrp,* and no-*lrp* plasmid strains were used for short term (<100h) virulence assays in *Manduca sexta* insects (23). However, using a plasmid-based method to provide fixed levels of Lrp is not ideal for long experimental times (10-64 d) required to monitor the full spectrum of mutualistic behaviors, since plasmid loss is likely to occur as antibiotic selection decays over time, ultimately masking phenotypes that may be associated with differing fixed levels of Lrp expression. To counter this issue we constructed strains with genome-encoded fixed levels of *lrp*: the low-*lrp* and high-*lrp* constructs were integrated into the genome of the *lrp-2::kan* strain at the *kefA* gene, a locus that does not disrupt bacteria-nematode interactions (4) and the resulting strains were verified to express the expected relative levels of Lrp and virulence (Fig. 2.2) (see Materials and Methods for details).

We monitored the cumulative numbers of IJs emerging over a 55 d time course from agar lawns of in-genome fixed-*lrp* strains (Fig. 2.4B). Over this time period, high-*lrp X. nematophila* supported the production of significantly higher numbers of emerged IJs compared to the no-*lrp* and low-*lrp* strains, indicating similar mutualistic behavior of the plasmid and in-genome *lrp* expression strains. Taken together, these experiments demonstrate that *X. nematophila* expressing high levels of Lrp are optimal for supporting nematode development into the transmission IJ stage.

A fundamental aspect of the *S. carpocapsae-X. nematophila* mutualism is the ability of the bacteria to colonize the IJ stage for transmission to the next insect host. To determine if Lrp expression levels impact this mutualistic trait we monitored the frequency of *X. nematophila* colonization of the receptacles of emerged IJs (Fig. 2.4C). Colonization could be detected using

fluorescence microscopy based on the presence of constitutively expressed red-fluorescence protein encoded in the *kefA* locus inserts (see Materials and Methods). Consistent with previous data (27), *X. nematophila* lacking *lrp* or expressing low levels of *lrp* had reduced colonization levels (~75% and 78%, respectively) relative to those typically observed for wild type (>90%) (4, 10, 35). In contrast, the high-*lrp* strain exhibited a wild-type colonization frequency of 96%, significantly higher than the no-*lrp* and low-*lrp* strains (Fig. 2.4C).

Bacteria expressing high levels of Lrp support high levels of mutualism in vivo.

The experiments presented thus far indicate that in vitro on agar plates, *X. nematophila* expressing high levels of Lrp supports both higher IJ production and higher colonization frequency, relative to strains expressing no or low levels of Lrp. In nature, nematode reproduction occurs within an insect cadaver. Given that Lrp is considered the "feast or famine" transcriptional regulator (26), the distinct nutritional environment of an insect cadaver relative to an agar plate may have an impact on the role of Lrp in supporting mutualistic phenotypes (11, 36). To test this possibility, we measured IJ reproduction and colonization after injection of each *X. nematophila* fixed Lrp strain and aposymbiotic IJ nematodes into individual *G. mellonella* insects (Fig. 2.4D, and 2.4E). We chose *G. mellonella* rather than *M. sexta* (used for virulence assays) as an insect host (23), since the former has a less robust immune response and better supports nematode reproduction than the latter (our unpublished observations). Bacterial strains expressing no-*lrp,* low-*lrp,* and high-*lrp* either on plasmids (Fig. 2.4D) or in the genome (Fig. 2.4E) were used to assess the role of Lrp in IJ production in vivo (i.e. in the insect cadavers). As expected, 100% death was achieved in all insects 36 hours post injection except for control insects injected with PBS (data not shown).

IJ reproduction was measured as the ability to produce IJ progeny from each insect (productive infection, Fig. 2.4D) and the numbers of IJs produced from each infection (Fig. 2.4E). Consistent

with the in vitro experiments described above, insects injected with high-*lrp* strains showed a significantly higher rate of productive infection (Fig. 2.4D) and higher numbers of cumulative progeny IJs (Fig. 2.4E) relative to those injected with either the no-*lrp* or low-*lrp* strains. Similarly, a positively correlated trend was apparent between Lrp levels and colonization frequency (Fig. 2.4F). However, in contrast to the in vitro data, colonization frequencies of IJs emerged from insects did not vary significantly depending on strain, indicating that the nutritional environment of the insect cadaver may ameliorate the negative impact of low Lrp levels on colonization frequency, as we proposed above. Overall, the colonization frequency of each strain was higher in vivo than in vitro, consistent with published observations (11, 36).

The experiments described above relied upon IJ emergence as a proxy for nematode reproduction. To explore more fully the role of Lrp during nematode reproduction and development, *G. mellonella* insects were injected with nematodes and fixed *lrp* expression strains and the resulting insect cadavers were dissected to enumerate nematodes from all developmental stages. When plasmid-based fixed *lrp* expression strains were used, total nematode counts were highly variable among individual insect cadavers, likely due to inconsistent maintenance of the *lrp*-encoding plasmids (Fig. S4A). In spite of this variability, overall the trend showed that the high-*lrp* strain supported higher total nematode counts per insect relative to the no-*lrp* and low-*lrp* strains.

We next monitored emerged, non-emerged, and total (emerged + non-emerged) nematode numbers 23 d after co-injection with genome-encoded fixed *lrp* expression strains (Fig. 2.5B, 2.5C, Fig. 2.6). The high-*lrp* strain supported significantly higher average nematode counts of both emerged IJs and total nematodes. The non-emerged nematodes were not statistically different among bacterial strains. Based on these data, we conclude that *X. nematophila* strains

expressing high levels of Lrp are better able to support nematode progression into the IJ transmission stage relative to strains expressing little or no Lrp.

The number of emerging IJs reflects the success of multiple stages of the nematode life cycle: development through reproductive juvenile and adult stages, fecundity of adults that mate and produce progeny, development of progeny into the IJ transmission stage, and the dispersal of the IJs from the lawn or cadaver (Fig. 2.1). To predict if Lrp affects any of these stages we created a simple mathematical model to simulate theoretical numbers of emerged, non-emerged, and total numbers of nematodes in comparison to experimental data from Fig. 2.6. The model includes four adjustable parameters, each controlling one stage: nematode progeny per reproductive cycle (a), IJ formation (b), dispersal (c), and life cycle progression (d). The theoretical numbers of emerged IJs, non-emerged IJs, and total number of nematodes were simulated in Mathematica to test the following hypotheses:

(i) High Lrp only promotes more progeny per reproductive cycle (parameter a);
(ii) High Lrp only promotes a higher percentage of IJ formation per reproductive cycle (parameter b);
(iii) High Lrp only promotes a higher IJ dispersal or emergence (parameter c);
(iv) High Lrp only promotes faster reproduction and more reproductive cycles (parameter d).

First, we set each of the hypotheses to be true by increasing each parameter individually and continuously in Mathematica. The simulated outputs were compared to the initial condition output, reflecting the theoretical prediction of each hypothesis (Table 2.2). Then, the predicted outcomes from the model were compared to our experimental data to assess if these hypotheses could be true in our biological system (Table 2.2). For instance, we set hypothesis (i) to be true by increasing parameter a. The math model output was recorded as increased

number of emerged IJs, non-emerged nematodes, and total number of nematodes (Table 2.2). Thus the predicted outcome under either hypothesis (i) or the opposite of hypothesis (i) would not match our experimental data, suggesting that hypothesis (i) cannot be the only explanation for the biological system.

Our mathematical model indicates that high levels of Lrp expression are likely to promote both nematode reproduction and nematode dispersal (Table 2.2). To show an example of theoretical prediction under a hypothesis combining (i), (ii), and (iii), specific sets of parameter values (a=3.3, b=0.5, c=0.2, d=5 for the low-*lrp* strain) and (a=4.5, b=0.7, c=0.9, d=5 for the high-*lrp* strain) were chosen to simulate the math model and compared to the experimental data (Fig. 2.7).

S. carpocapsae associated with _X. nematophila_ expressing high levels of Lrp are more fit than those expressing no or low levels of Lrp.

Symbiotic fitness between *S. carpocapsae* and *X. nematophila* depends on the production of colonized IJs from an infected cadaver and the abilities of these emerged IJs to reproduce in the next round of infection. The data described above demonstrate that when measuring individual parameters (percent productive infection (Fig. 2.4D), progeny IJs per infection (Fig. 2.4E and Fig. 2.6) and frequency of IJ colonization (Fig. 2.4D-F), high levels of *X. nematophila* Lrp expression provide greater benefits than either low-Lrp or no-Lrp strains. To obtain a representation of the overall fitness of the mutualistic pair, we first determined the total number of colonized IJs, versus the total number of uncolonized IJs (which are unlikely to be productive in future infections) (Fig. 2.8) (see Materials and Methods). In experiments conducted in vivo, while the frequency of colonization among the total numbers of IJs observed was not significantly different among the three strains (Fig. 2.4F), our calculations revealed that the high-Lrp strain supported the production of significantly higher overall number of colonized IJ progeny than do those injected with either the no-Lrp or low-Lrp strains (Fig. 2.8B). Thus,

reproduction of nematodes in the presence of *X. nematophila* expressing high levels of Lrp are more likely (relative to low- or no-*lrp*) to result in high numbers of IJ progeny capable of transmitting the symbiont to a new infection.

To assess the abilities of such emergent IJ populations to initiate a new round of infection, emerged IJs (from agar plates) were tested using a sand trap assay, which measures successful infection (requiring host-seeking, entry, recovery from the IJ stage, and release of bacteria), reproduction in the insect cadaver, and development into another generation of colonized IJs (37). We infected *G. mellonella* insects with IJs that had emerged from lawns of no-*lrp,* low-*lrp,* and high-*lrp* in-genome bacterial strains (Fig. 2.9). Infections were conducted in a modified sand-trap assay that incorporates the natural infection stages noted above. We did not observe significant differences among bacterial strains in insect survival post infection, indicating the ability to locate, infect, and kill *G. mellonella* was not influenced by the life history of the IJs with respect to bacterial strain (Fig. 2.9A). As before, we used percent productive infections as a measure of nematode reproduction. IJs derived from the high-*lrp* strain exhibited a significantly higher percentage of productive infections relative to the no-*lrp* and low-*lrp* strains (Fig. 2.9B), indicating the overall fitness of the *S. carpocapsae-X. nematophila* association is positively influenced by the expression of high levels of Lrp in the bacterial symbiont.

Discussion

Our previous research provided a clear link between the transcription factor Lrp and the VMO phenomenon, in which a subpopulation of *X. nematophila* cells that express high levels of Lrp are attenuated for virulence and immunosuppression during initial infection of insect hosts (23). Here, we provide evidence that the selective advantage of these high-Lrp expressing strains is to support later stages of the *X. nematophila* life cycle, during which it provides mutualistic activities that support nematode reproduction and the development of the transmission IJ stage.

Further, the high-Lrp cells are adapted for initiating colonization of the developing IJs, and may have an advantage in colonizing host tissues, based on its robust biofilm-forming phenotype.

High Lrp-expressing cells are adapted for mutualism

The high-Lrp-expressing strain supports the production of higher numbers of IJs, relative to strains lacking *lrp* or expressing low levels, emerging from the cultivation assay (from bacterial lawns or from *G. mellonella* insects). In addition, our mathematical model indicates that high levels of Lrp positively influence both nematode reproduction and nematode dispersal from insect cadavers.

In both cases, it is the gene expression profile of the high-Lrp strain that likely is responsible for the observed phenotypes. Indeed, our findings suggest that high and low levels of Lrp result in distinctive gene expression profiles that promote either mutualism or virulence, respectively. As such, characterizing these profiles will facilitate assignment of specific gene products and pathways to their functional roles in one or the other symbiotic association. The *X. nematophila* Lrp regulon has been characterized using microarray analysis to compare gene expression in an *lrp* mutant versus wild type *X. nematophila* that was heterogeneous with respect to Lrp (23, 38, 39). Recent attempts in our lab to compare gene expression profiles of plasmid-encoded fixed high- and low-Lrp strains were inconclusive, likely due to variability in plasmid maintenance (data not shown). Our creation of genome-encoded constitutive Lrp strains, as described here, likely will provide more consistent and interpretable data.

Until such data are available, our knowledge of the Lrp regulon can still provide insights into the possible activities that contribute to the success of the high Lrp strain in promoting mutualistic functions. Lrp regulates expression of the flagellar regulon, which includes genes (*xlpA* and *prtA*) that encode lipase and protease respectively (30). The *xlpA*-encoded lipase promotes

nematode IJ production through an unknown mechanism, and lipase activity is expressed more highly in high-Lrp strains (23, 30, 31). Furthermore, flagellar motility and flagellar regulon-encoded activities appear to be induced during the transition between the virulence and reproduction stages of the *X. nematophila* life cycle (7, 30). Taken together, these findings suggest that high-Lrp strains may express elevated levels of expression of the flagellar regulon, including the *xlpA*-encoded lipase that has a positive effect on emerging IJ population numbers. Nematode dispersal is a chemosensing-based behavior that can be in response to nematode-produced small molecules (40). Lrp may play a role in this behavior by regulating either the sensing or production of small molecule signals derived from the insect tissues (such as ammonia), nematodes (such as pheromones), or bacteria (such as secondary metabolites) (40, 41). *X. nematophila* Lrp controls the production of numerous small molecules, many with unknown biological function (23, 27, 39). An intriguing possibility that awaits further investigation is that one or more *X. nematophila* Lrp-dependent small molecules either trigger or enhance the dispersal behavior of its *S. carpocapsae* nematode host, thereby increasing its own fitness by ensuring transmission to the next insect host.

In addition to supporting production of greater numbers of IJs, the high-Lrp-expressing strain also is optimal for colonizing these IJs, a process that is crucial to *X. nematophila* transmission to the next round of its life cycle (infection of a new insect host). The superior colonization levels of the high-Lrp-expressing strain were more apparent under the in vitro cultivation conditions than in the in vivo cultivation conditions. This might indicate that the *G. mellonella* cadaver environment contains or lacks specific molecules, such as particular amino acids, that influence Lrp-dependent adaptation of *X. nematophila* from the reproduction to the transmission stage of its life cycle. For example, it is possible that within an insect cadaver but not on a spent agar plate there are metabolites that trigger the induction of colonization genes either independent of Lrp, or in conjunction with it such that low-levels of Lrp are sufficient to promote colonization.

The processes of *X. nematophila* colonization of both reproductive stage and IJ stage nematodes have been described (4, 16) and each involves visible bacterial attachment to specific internal nematode surfaces. To directly test the influence of Lrp levels on the general ability of *X. nematophila* to attach to a surface we used a well-established laboratory biofilm formation assay. Consistent with our models that biofilm formation is a component of the *X. nematophila-S. carpocapsae* association, and that high-Lrp strains are best adapted for mutualistic phenotypes, we found that high-Lrp strains form more robust biofilms than do low-Lrp or no-Lrp strains. Whether this biofilm phenotype corresponds specifically to an in vivo adherence phenotype remains to be addressed, a process that will be facilitated by the identification of conditions and Lrp-dependent genes that contribute to biofilm formation. Future detailed genetic and biochemical analysis of these pathways will yield insights into the symbiotic timeline, tissue tropism, and host environmental conditions experienced by *X. nematophila* as it interacts with its two invertebrate hosts.

Lrp-regulated virulence modulation is a switch between pathogenic and mutualistic phenotypes.

The current study, combined with our previous data (23), establishes that Lrp regulates bacterial mutualism in a reciprocal manner relative to virulence: a virulent strain expressing fixed low levels of Lrp has a defect in mutualistic interactions with nematodes, while a virulence-attenuated strain expressing fixed high levels of Lrp establishes optimal mutualism. Thus, *X. nematophila* variation in Lrp levels controls a phenotypic switch between pathogenic and mutualistic behaviors.

In many bacteria, phenotypic variation serves as a mechanism to confer the adaptations under erratic or predictable environmental fluctuations. The fact that *X. nematophila* laboratory-grown

populations are heterogeneous with respect to Lrp levels (and therefore symbiotic behavior) suggests that the switch is stochastic, and that *X. nematophila* may be using a bet-hedging strategy to adapt to the changing host environments (42, 43).

Whether *X. nematophila* has evolved stochastic bet-hedging or other strategies to optimize fitness of itself and its nematode host remains to be tested. Regardless, our data indicate Lrp is a key component of adaptation to host environments and that the overall cellular levels of Lrp dictate the symbiotic phenotype. Switching between a high (mutualistic) and low (virulence) Lrp state by a cell could occur through random or stochastic noise, such as uneven distribution of Lrp proteins in the two daughter cells during cell division. Alternatively, a bimodal or multimodal distribution of Lrp levels could be due to genetic, post-transcriptional or post-translational modifications that modulate the expression or stability of Lrp levels within the cell. Consistent with the latter possibility, our published data demonstrated that *lrp* transcription is negatively auto-regulated, as is true in *E. coli* (23).

In uropathogenic *E. coli* (UPEC), Lrp controls a phenotypic ON/OFF switch of Pap fimbriae, dictated by Lrp binding to the the proximal or distal sites the *pap* promoter (44). Lrp regulatory output in *E. coli* may be modulated by Lrp multimerization, protein modification (e.g. acetylation) and interactions with metabolites and other regulators (45, 46). In turn, each of these control points may be influenced indirectly by host environment and directly by the concentration of Lrp available within the cell. Based on the data we present here, it seems likely that *X. nematophila* senses the nutritional environment of its hosts and responds, through varying Lrp levels, to alter global gene expression. However, mechanistic details of this phenomenon remain to be examined. For example, do mutualistic and pathogenic subpopulations of *X. nematophila* co-exist in a heterogeneous population that is subject to selective pressure from host environments for one phenotype or the other (i.e. the nematode environment selects for cells expressing

mutualistic behaviors while the insect environment selects for those with virulent traits)? Or, does the host environment induce or prime one phenotype over the other, resulting in homogeneous populations expressing either high or low levels of Lrp that are adapted for a particular stage of the life cycle? The answers to these questions will require monitoring and quantification of Lrp and Lrp-dependent gene expression within individual bacterial cells existing in situ.

Conclusions

Xenorhabdus bacteria have a complicated life history in which they alternate between a pathogenic interaction with insects and a mutualistic interaction with *Steinernema* nematodes, and our work has demonstrated that *X. nematophila* adapts to these changes using an Lrp-dependent phenotypic switch. While the concept of host-associated microbes utilizing phenotypic variation to adapt to changing host/environmental conditions is well described, our work establishes that subtle variations in cellular concentrations of a global regulatory protein can dictate the outcome of an individual symbiotic interaction and the overall fitness of symbiosis partners. Further, our work indicates that *X. nematophila* uses Lrp-dependent phenotype variation to inversely coordinate mutualistic and pathogenic behaviors that are both critical to its fitness but are potentially conflicting with each other (47). Similar inverse coordination may be a feature of other systems in which a symbiont, such as a vector-borne pathogen, encounters multiple distinct hosts during their life cycles. For example, *Yersinia pestis* alternates between flea and mammalian hosts in which it expresses host-specific transcriptional profiles (48).The molecular mechanism controlling this global switch in *Y. pestis* has not been elucidated, but may involve a phenotypic variation phenomenon such as the one we have described here.

The *X. nematophila* mutualism-to-pathogenesis phenotypic variation phenomenon appears to be distinct from other well-established examples of phenotypic variation in parasitic symbioses that alternate between ON and OFF states of virulence genes, such as the *fim* switch in pathogenic *E. coli* (49) and the ToxT switch in *V. cholerae* (50). However, it is possible that the "OFF" state in these systems is coordinated with a reciprocal expression of genes that are adapted to other environments encountered by these pathogens. Experimental evolution selecting for commensalism in the nematode pathogen *Pseudomonas aeruginosa* resulted in attenuated virulence through a mutation in a global regulatory protein (51). It will be interesting to explore the function of this protein in the ancestral strain and to determine if it also controls a phenotypic switch between pathogenic and beneficial (or commensal) behaviors.

Materials and Methods

Bacterial growth

The bacterial strains and plasmids used in this study are listed in Table 2.1. Bacteria were grown in lysogeny broth (LB) culture media (52) at either 30°C (for *X. nematophila*) or 37°C (for *E. coli*). The medium was either stored in the dark or supplemented with 0.1% sodium pyruvate (53). *Xenorhabdus* bacteria carrying plasmids were grown in the culture medium supplemented with 7.5 μg/ml of tetracycline in order to maintain plasmids. Other antibiotics were used as indicated at the following concentrations: ampicillin (Amp), 150 μg/ml; chloramphenicol (Cm), 15 μg/ml (*X. nematophila*) and 30 μg/ml (*E. coli*); kanamycin (Kan), 50 μg/ml; and erythromycin (Erm), 200 μg/ml.

Plasmid and strain construction

Construction of the plasmid pEH69 (Tn*7* promoterless-*gfp*/P*lac-rfp)* Turbo *rfp* was digested from pTurbo-RFP-B (Evrogen, Moscow, Russia) with NheI and XhoI, and ligated into

plasmid pEVS107 (54) (digested with SpeI, followed by creation of blunt ends using T4 DNA polymerase (Promega)), generating plasmid pEH39. A *gfp* gene was amplified from pVSV209 (55) using Polymerase Chain Reaction (PCR) with the PrimeSTAR high fidelity polymerase (Clontech Laboratories, Inc., Mountain View, CA) and primers: CATGFP F (5'-AAAGGGCCCGCTTGCTCAATCAATCACCG-3') and CATGFP R (5'-AAAGGGCCCGCCGCATAGTTAAGCCAGC-3'), then introduced into pEH39 (digested with AvrII and filled in), generating the plasmid pEH69.

Construction of plasmid pMYC1 (Tn*7* P*fliC-gfp*/P*lac-rfp*) The *X. nematophila fliC* promoter region was cloned upstream of the promoterless chloramphenicol resistance and *gfp* genes in pEH69 by PCR amplifying a 485-bp fragment containing the region upstream of and 12-bp within the *fliC* gene using primers F2_P_{fliC} AvrII (5'-CCTAGGCTTTTTCAGTTCTTCTGATGCTG-3') and R2_P_{fliC} AvrII (5'-CCTAGGGACTGATGCCATAGTAGAGTTCC-3') (Note: In all primers listed, any engineered restriction enzyme digestion sites are underlined.) (Integrated DNA Technologies, Coralville, IA) and the PrimeSTAR high-fidelity polymerase (Clontech Laboratories, Inc., Mountain View, CA) according to manufacturer's instructions. The PCR-amplified fragment and pEH69 were both digested with AvrII and ligated (New England Biolabs Inc., Ipswich, MA), generating plasmid pMYC1.

Construction of pMYC4 and pMYC5. Plasmids pMYC4 (low-*lrp*) and pMYC5 (high-*lrp*) were constructed by modifying plasmids pEH54 and pEH56 (23). The origins of replication in pEH54 and pEH56 were removed using restriction digestion with ClaI and XmnI according to manufacturer's directions (Promega, Madison, WI). The suicidal origin of replication *oriR6K* was PCR-amplified from plasmid pEVS107 using primers: OriR6K_F1_XmnI (5'-gaatttttttcCCATGTCAGCCGTTAAGTGTTC-3') and OriR6K_R1_ClaI (5'-atcgatGAGGATCTGAAGATCAGCAGTTC-3') (Integrated DNA Technologies, Coralville, IA) and standard PCR techniques with the PrimeSTAR high-fidelity polymerase (Clontech Laboratories,

Inc., Mountain View, CA); then it was introduced into pEH54 and pEH56 to replace the origins of replication using standard restriction digestion (ClaI and XmnI) and ligation (T4 DNA ligase, Promega, Madison, WI), generating pMYC2 (pEH54-*oriR6K*) and pMYC3 (pEH56-*oriR6K*). A fragment of *kefA* gene from *X. nematophila* (ATCC 19061) genome was PCR-amplified using primers: sau_F1_ClaI (5'-atcgatGATCTTGATGATTTGATTTGGGG-3') and sau_R1_ClaI_long (5'-atcgatGATCCAAGGCCATTGGAGG-3'), and introduced to pMYC2 and pMYC3 by standard restriction digestion (ClaI) and ligation, generating pMYC4 and pMYC5.

Creating *X. nematophila* strains expressing low and high levels of Lrp from the genome. To create low and high Lrp expressing *X. nematophila* strains, pMYC4 (low-*lrp* donor plasmid) and pMYC5 (high-*lrp* donor plasmid) were inserted in *kefA* of an *lrp-2::kan* mutant via bi-parental conjugation and homologous recombination, respectively. Plasmid integration at the *kefA* gene locus does not interfere with nematode colonization (4, 16, 56, 57). The Lrp-dependent fluorescence reporter pMYC1 (*PfliC-gfp/Plac-rfp*) was introduced to the attTn7 site of the genomes in both of the low Lrp and high Lrp expressing *X. nematophila* strains described above by tri-parental conjugation and Tn7 transposition (58, 59), creating low-*lrp* in-genome (low-*lrp*/Tn7-*PfliC-gfp/Plac-rfp*) and high-*lrp* in-genome (high-*lrp*/Tn7-*PfliC-gfp/Plac-rfp*) strains. Lrp expression levels in the low-*lrp* and high-*lrp* in-genome strains were initially screened by fluorescence microscopy using Nikon Eclipse TE300 inverted microscope (Nikon, Melville, NY, USA) and confirmed to be positively correlated to GFP expression levels (Table 2.1, (23)). The Lrp expression levels of the in-genome low and high-*lrp* strains were further confirmed by semi-quantitative western blot (Fig. 2.2A) performed using previously published methods (23).

The orientation and sequence accuracy of all introduced regions in the plasmid constructs in this research was verified by sequencing at University of Wisconsin-Madison Biotechnology Center using BigDye version 3.1 (Applied Biosystems, Foster City, CA).

The virulence of the in-genome no-*lrp,* low-*lrp,* and high-*lrp* strains were tested by directly injecting overnight bacterial culture into 4th instar *Manduca sexta* larvae (23, 60).

Consistent with previously published data, the low-*lrp* in-genome fixed strain is more virulent than either of the no-*lrp* or high-*lrp* strains (Fig. 2.2B).

Biofilm Assay

For biofilm experiments bacterial strains were grown overnight in LB from frozen stocks. Overnight cultures were diluted 1:100 in fresh LB media, and grown at room temperature under static incubation for 6 days. Biofilm material was stained for 15 minutes with 1% crystal violet, then drained and dried completely. Quantitative analyses of biofilm material followed, in which 70% ethanol was used to de-stain glass test tubes (with agitation). The resulting solution was quantitated by spectrophotometry at optical density of 590 nm (61).

Nematode maintenance

Conventional nematodes were propagated through *Galleria mellonella* larvae (Grubco, Hamilton, OH) and used for generating aposymbiotic nematodes. A new batch of conventional nematodes was used for each biological replicate. Aposymbiotic nematodes were generated from standard axenic egg preparation from conventional nematodes (62). To generate aposymbiotic IJs, axenic eggs were then reared on *X. nematophila* colonization-deficient *rpoS* mutant lawns and aposymbiotic nematodes were water-trapped, surface-sterilized, and confirmed by grinding and plating on LB agar. Axenic nematodes were surfaced-sterilized right before adding to bacterial lawns in colonization and fecundity assays (8).

In-vitro nematode fecundity assays

X. nematophila overnight culture were grown at 30°C and spread onto lipid agar (15ml per plate), incubated at 25°C for 48 hours to create bacterial lawns. In the experiments using *X. nematophila* engineered strains that carry multicopy plasmids such as HGB 1966 (*lrp-2::kan* plus no-*lrp* vector), 1967(*lrp-2::kan* plus low-*lrp* plasmid) and 1968 (*lrp-2::kan* plus high-*lrp*

plasmid) (23), tetracycline (7.5 μg/ml) was supplemented in lipid agar to maintain plasmids during bacterial growth. In the experiments using *X. nematophila* strains with in-genome insertions no antibiotics were used when growing bacteria. Approximately 5000 aposymtiotic IJs were surface-sterilized and seeded on the bacterial lawns. Before 10 days post-nematode seeding, water traps were set up to collect emerging progeny nematodes. For plasmid-carrying strains expressing no-*lrp,* low-*lrp,* and high-*lrp* (HGB 1966, 1967, and 1968), emerged IJs were counted on day 3, 7, and 10 post water trap. At each time point, 0-60 nematodes were enumerated in each water trap and used for calculating cumulative IJs from each bacterial lawn. Cumulative IJ for each bacterial strain was represented by the average of 3 technical replicates in each of the 5-6 biological replicate. For in-genome construct strains no-*lrp,* low-*lrp,* and high-*lrp* (HGB 2261, 2262, and 2263), emerged IJs were counted on days 1, 2, 3, 5, 10, 28, 30, 33, 51, and 55 post water trap. At each time point, 40-150 IJs were enumerated in each water trap and used for calculating cumulative IJs from each bacterial lawn. Cumulative IJ for each bacterial strain was represented by the average of 5 technical replicates in each of the 3 biological replicate. IJs collected from in-genome construct strains expressing no-*lrp,* low-*lrp,* and high-*lrp* (HGB 2261, 2262, and 2263) were stored for use in sand-trap assay and colonization screen.

In-vivo nematode fecundity assay

Co-injection of bacteria and nematodes. *G. mellonella* larvae (Grubco, Hamilton, OH) were used for bacteria-nematodes co-injections. Overnight cultures of bacteria were serially diluted in phosphate-buffered saline (PBS). Prior to injection, optical density (OD) measurements and CFU counting by dilution plating were done to ensure that equal CFU counts were injected among bacterial strains. Aposymbiotic nematodes were surface sterilized, diluted in PBS, and combined with bacteria to approximately 50 IJs and 10^3 CFU in10 μl of

injection volume (37). HGB1966, 1967, and 1968 were re-suspended in PBS supplemented with 7.5 μg/ml tetracycline to maintain plasmids. Insect survival was monitored at 8-24 h intervals post injection.

Assessment of progeny yield and percent productive infection. A White-trap was set up for each individual insect cadaver on day 7 post-injection (63), and monitored for IJ emergence at 24 h intervals thereafter. The proportion of infected insects that yielded nematodes at each time point was calculated as percent productive infection. The number of IJs produced in each insect cadaver was also determined by removing water from the White trap and estimating the number of IJs/μl. Samples of IJs were counted every other day for 14 d and total number of IJs per insect was estimated by IJs/μl multiplied by sample volume. Three biological replicates were performed (37). Insect cadavers that produced at least 50 IJs were scored as productive infection, and non-productive infection otherwise.

Pepsin digestion of insect cadavers. Pepsin digestion of infected insect cadavers was used to allow observation and counting of non-emerged nematodes. At various time points after co-injection of bacteria and nematodes, individual *G. mellonella* cadaver were rinsed in distilled water, dissected, and digested in 10 ml pepsin solution (0.83% w/v pepsin (Carolina Biological, Burlington, NC), 24% w/v NaCl, 2% v/v HCl in distilled water) (63) for 3 hours at 37°C (32). Nematodes from all developmental stages were counted using a dissecting scope.

Mathematical Model of Nematode Reproduction and Emergence

We developed a simplified mathematical model to assess relative contributions of development, reproduction, and emergence to our observed counts of nematodes from in vivo assays. The model was constructed under the assumptions (1) that all 50 aposymbiotic IJs injected into the insect survived and developed into adults, (2) that reproductive cycles were consecutive with no overlaps, (3) that insect cadavers were not infected by competitive

microbes such as fungi, (4) that carcass of dead nematodes did not decay, and (5) that among different reproductive cycles, population expansion (parameter a), the percentage of population that form IJs (parameter b), and the percentage of IJs that emerged out of the insect cadaver (parameter c) were constant, except for the first reproduction cycle in which no IJs are formed (b_1=0, otherwise b>0) (16).

For the n^{th} reproductive cycle, the total number of nematodes (including parental and progeny nematodes) from the current productive cycle is approximated as:

$$50 \cdot a^n \cdot (1 - b)$$

The number of emerged IJs from the n^{th} reproductive cycle is approximated by:

$$50 \cdot a^n \cdot (1 - b) \cdot b \cdot c$$

The number of 'trapped IJs' only from the n^{th} reproductive cycle is approximated by:

$$50 \cdot a^n \cdot (1 - b) \cdot b \cdot (1 - c)$$

The number of non-emerged nematodes after n^{th} reproductive cycle is approximated by:

$$50 \cdot a^n \cdot (1 - b) \cdot (1 - b \cdot c) + \sum_{2}^{n-1} 50 \cdot a^n \cdot (1 - b) \cdot b \cdot (1 - c)$$

After *d* rounds of reproductive cycles, the number of emerged IJs is approximated by:

$$Em = \sum_{n=2}^{d} 50 \cdot a^n \cdot (1 - b) \cdot b \cdot c$$

The number of non-emerged nematodes is approximated by:

$$Ne = 50 \cdot a^d \cdot (1 - b) \cdot (1 - b \cdot c) + \sum_{n=2}^{d-1} 50 \cdot a^n \cdot (1 - b) \cdot b \cdot (1 - c)$$

Total number of nematodes is approximated by:

$$T = 50 \cdot a^d \cdot (1 - b) + \sum_{n=2}^{d-1} 50 \cdot a^n \cdot (1 - b) \cdot b$$

The theoretical numbers of emerged IJs (Em), non-emerged IJs (Ne), and total number of nematodes (T) were simulated in Mathematica (Wolfram Research, Champaign, IL). The

initial condition was set using parameter values: a=3.3, b=0.5, c=0.2, d=5. To predict the outcomes of these hypotheses, we manipulated parameter values within ranges (2<a<20, 0<b<1, 0<c<1, 2<d<10) and generated the simulated data (Table 2.2).

In-vitro and in-vivo colonization assay

Colonization assays were performed using bacterial strains with in-genome constructs HGB 2261 (no-*lrp*), HGB 2262 (low-*lrp*), and HGB 2263 (high-*lrp*) both using lipid agar (in-vitro) and in *G. mellonella* (in-vivo). IJs emerged from either the bacterial lawns or insect cadavers after co-injected with bacteria and nematodes were collected 7 d post water trap. For each cadaver, ~100-150 IJs (a minimum of 50 IJs was necessary) were paralyzed using 2 nM levamisole and screened for bacterial colonization, indicated by red fluorescence from constitutive RFP expression, using a Nikon Eclipse TE300 inverted microscope (Nikon, Melville, NY, USA). Percent colonization was calculated as: (colonized IJs/the total number of IJs counted) x 100 (27). Percent colonization from three water traps were used as technical replicates and averaged for each bacterial strain. Five biological replicates were performed. A minimum of 50 IJs was deemed necessary to screen for colonization.

Sand-trap Assay

To conduct sand trap assays, 6 g of silica sand (Meeco, Seattle, WA) was distributed into individual 60 x 15mm diameter petri dishes. Infective juvenile nematodes colonized with the various in-genome test strains were inoculated at approximately 100 IJs per plate, and 6 *G. mellonella* larvae were added to each plate. Insects were monitored for survival, and placed into individual White traps about 7 d post-death. Emergent nematodes were monitored every 24 h, and the percent of insects that yielded nematodes were recorded as percent productive infection.

Statistical analysis

Data were processed and analyzed in PRISM6 using one-way or two-way ANOVA tests followed by Tukey's multiple comparisons test among bacterial strains with each time point as an independent comparison. Samples that showed no significant differences among them were grouped by the same letter. Statistical significance and P value ranges are indicated by asterisks (ns: $P>0.05$; *$P\leq0.05$; ** $P\leq0.01$; *** $P\leq0.001$; **** $P\leq0.0001$).

Acknowledgements

We thank Prof. Dr. David H. Brown (Colorado College) for his lectures, encouragement, and guidance in mathematical modeling of biological systems.

References

1. **van der Woude MW**, **Bäumler AJ**. 2004. Phase and antigenic variation in bacteria. Clin Microbiol Rev **17**:581–611.
2. **Herbert EE**, **Goodrich-Blair H**. 2007. Friend and foe: the two faces of *Xenorhabdus nematophila*. Nat Rev Microbiol **5**:634–646.
3. **Richards GR**, **Goodrich-Blair H**. 2009. Masters of conquest and pillage: *Xenorhabdus nematophila* global regulators control transitions from virulence to nutrient acquisition. Cell Microbiol **11**:1025–1033.
4. **Martens EC**, **Heungens K**, **Goodrich-Blair H**. 2003. Early Colonization Events in the Mutualistic Association between *Steinernema carpocapsae* Nematodes and *Xenorhabdus nematophila* Bacteria. J Bacteriol **185**:3147–3154.
5. **Orchard SS**, **Goodrich-Blair H**. 2004. Identification and functional characterization of a *Xenorhabdus nematophila* oligopeptide permease. Appl Environ Microbiol **70**:5621–7.
6. **Phalaraksh C**, **Lenz EM**, **Lindon JC**, **Nicholson JK**, **Farrant RD**, **Reynolds SE**, **Wilson ID**, **Osborn D**, **Weeks JM**. 1999. NMR spectroscopic studies on the haemolymph of the tobacco hornworm, *Manduca sexta*: assignment of ^{1}H and ^{13}C NMR spectra. Insect Biochem Mol Biol **29**:795–805.
7. **Jubelin G**, **Pagès S**, **Lanois A**, **Boyer M-H**, **Gaudriault S**, **Ferdy J-B**, **Givaudan A**. 2011. Studies of the dynamic expression of the *Xenorhabdus* FliAZ regulon reveal atypical iron-dependent regulation of the flagellin and haemolysin genes during insect infection. Environ Microbiol **13**:1271–1284.
8. **Vivas EI**, **Goodrich-Blair H**. 2001. *Xenorhabdus nematophilus* as a model for host-bacterium interactions: *rpoS* is necessary for mutualism with nematodes. J Bacteriol **183**:4687–93.
9. **Forst S**, **Dowds B**, **Boemare N**, **Stackebrandt E**. 1997. *Xenorhabdus* and *Photorhabdus* spp.: bugs that kill bugs. Annu Rev Microbiol **51**:47–72.

10. **Martens EC**, **Russell FM**, **Goodrich-Blair H**. 2005. Analysis of *Xenorhabdus nematophila* metabolic mutants yields insight into stages of *Steinernema carpocapsae* nematode intestinal colonization. Mol Microbiol **58**:28–45.

11. **Flores-Lara Y**, **Renneckar D**, **Forst S**, **Goodrich-Blair H**, **Stock P**. 2007. Influence of nematode age and culture conditions on morphological and physiological parameters in the bacterial vesicle of *Steinernema carpocapsae* (Nematoda: Steinernematidae). J Invertebr Pathol **95**:110–118.

12. **Crawford JM**, **Portmann C**, **Zhang X**, **Roeffaers MBJ**, **Clardy J**. 2012. Small molecule perimeter defense in entomopathogenic bacteria. Proc Natl Acad Sci U S A **109**:10821–6.

13. **Hwang J**, **Park Y**, **Kim Y**, **Hwang J**, **Lee D**. 2013. An entomopathogenic bacterium, *Xenorhabdus nematophila*, suppresses expression of antimicrobial peptides controlled by toll and imd pathways by blocking eicosanoid biosynthesis. Arch Insect Biochem Physiol **83**:151–169.

14. **Casanova-Torres ÁM**, **Goodrich-Blair H**. 2013. Immune Signaling and Antimicrobial Peptide Expression in *Lepidoptera*. Insects **4**:320–38.

15. **Sicard M**, **Brugirard-ricaud K**, **Page S**, **Lanois A**, **Boemare NE**, **Brehe M**, **Givaudan A**, **Gpia L**. 2004. Stages of Infection during the Tripartite Interaction between *Xenorhabdus nematophila* , Its Nematode Vector , and Insect Hosts. Appl Environ Microbiol **70**:6473–6480.

16. **Chaston JM**, **Murfin KE**, **Heath-Heckman EA**, **Goodrich-Blair H**. 2013. Previously unrecognized stages of species-specific colonization in the mutualism between *Xenorhabdus* bacteria and *Steinernema* nematodes. Cell Microbiol **15**:1545–1559.

17. **Martens EC**, **Goodrich-Blair H**. 2005. The *Steinernema carpocapsae* intestinal vesicle contains a subcellular structure with which *Xenorhabdus nematophila* associates during colonization initiation. Cell Microbiol **7**:1723–1735.

18. **Yip ES**, **Grublesky BT**, **Hussa EA**, **Visick KL**. 2005. A novel, conserved cluster of

genes promotes symbiotic colonization and σ ^{54} -dependent biofilm formation by *Vibrio fischeri*. Mol Microbiol **57**:1485–1498.

19. **Forst S**, **Clarke D**. 2002. Bacteria-nematode symbiosis., p. 57–77. *In* Gaugler, R (ed.), Entomopathogenic nematology. CABI, Wallingford.
20. **Volgyi A**, **Fodor A**, **Szentirmai A**, **Forst S**. 1998. Phase Variation in *Xenorhabdus nematophilus*. Appl Environ Microbiol **64**:1188–1193.
21. **Givaudan A**, **Baghdiguian S**, **Lanois A**, **Boemare N**. 1995. Swarming and Swimming Changes Concomitant with Phase Variation in *Xenorhabdus nematophilus*. Appl Environ Microbiol **61**:1408–1413.
22. **Park Y**, **Herbert EE**, **Cowles CE**, **Cowles KN**, **Menard ML**, **Orchard SS**, **Goodrich-Blair H**. 2007. Clonal variation in *Xenorhabdus nematophila* virulence and suppression of *Manduca sexta* immunity. Cell Microbiol **9**:645–656.
23. **Hussa EA**, **Casanova-Torres ÁM**, **Goodrich-Blair H**. 2015. The global transcription factor Lrp controls virulence modulation in *Xenorhabdus nematophila*. J Bacteriol **197**:3015–3025.
24. **Platko J V**, **Calvo JM**. 1993. Mutations affecting the ability of *Escherichia coli* Lrp to bind DNA, activate transcription, or respond to leucine. J Bacteriol **175**:1110–1117.
25. **Tani TH**, **Khodursky A**, **Blumenthal RM**, **Brown PO**, **Matthews RG**. 2002. Adaptation to famine: a family of stationary-phase genes revealed by microarray analysis. Proc Natl Acad Sci U S A **99**:13471–13476.
26. **Yokoyama K**, **Ishijima SA**, **Clowney L**, **Koike H**, **Aramaki H**, **Tanaka C**, **Makino K**, **Suzuki M**. 2006. Feast/famine regulatory proteins (FFRPs): *Escherichia coli* Lrp, AsnC and related archaeal transcription factors. FEMS Microbiol Rev **30**:89–108.
27. **Cowles KN**, **Cowles CE**, **Richards GR**, **Martens EC**, **Goodrich-Blair H**. 2007. The global regulator Lrp contributes to mutualism, pathogenesis and phenotypic variation in the bacterium *Xenorhabdus nematophila*. Cell Microbiol **9**:1311–1323.

28. **Cowles KN**, **Goodrich-Blair H**. 2005. Expression and activity of a *Xenorhabdus nematophila* haemolysin required for full virulence towards *Manduca sexta* insects. Cell Microbiol **7**:209–219.

29. **Martens EC**. 2005. Initiation and maintenance of *Steinernema carpocapsae* nematode colonization by *Xenorhabdus nematophila* bacteria *(Doctoal Thesis)* . University of Wisconsin-Madison.

30. **Park D**, **Forst S**. 2006. Co-regulation of motility, exoenzyme and antibiotic production by the EnvZ-OmpR-FlhDC-FliA pathway in *Xenorhabdus nematophila*. Mol Microbiol **61**:1397–412.

31. **Richards GR**, **Goodrich-Blair H**. 2010. Examination of *Xenorhabdus nematophila* lipases in pathogenic and mutualistic host interactions reveals a role for *xlpA* in nematode progeny production. Appl Environ Microbiol **76**:221–229.

32. **Mitani DK**, **Kaya HK**, **Goodrich-Blair H**. 2004. Comparative study of the entomopathogenic nematode, *Steinernema carpocapsae*, reared on mutant and wild-type *Xenorhabdus nematophila*. Biol Control **29**:382–391.

33. **Bogino PC**, **Oliva M de las M**, **Sorroche FG**, **Giordano W**. 2013. The role of bacterial biofilms and surface components in plant-bacterial associations. Int J Mol Sci **14**:15838–59.

34. **Morris AR**, **Visick KL**. 2010. Control of biofilm formation and colonization in *Vibrio fischeri*: a role for partner switching? Environ Microbiol **12**:2051–9.

35. **Cowles CE**, **Goodrich-Blair H**. 2008. The *Xenorhabdus nematophila nilABC* genes confer the ability of *Xenorhabdus* spp. to colonize *Steinernema carpocapsae* nematodes. J Bacteriol **190**:4121–4128.

36. **Goetsch M**, **Owen H**, **Goldman B**, **Forst S**. 2006. Analysis of the PixA inclusion body protein of *Xenorhabdus nematophila*. J Bacteriol **188**:2706–2710.

37. **Murfin KE**, **Lee MM**, **Klassen JL**, **McDonald BR**, **Larget B**, **Forst S**, **Stock SP**, **Currie**

CR, **Goodrich-Blair H**. 2015. *Xenorhabdus bovienii* strain diversity impacts coevolution and symbiotic maintenance with *Steinernema* spp. nematode hosts. MBio **6**:1–10.

38. **Cowles CE**, **Goodrich-Blair H**. 2006. *nilR* is necessary for co-ordinate repression of *Xenorhabdus nematophila* mutualism genes. Mol Microbiol **62**:760–771.
39. **Engel Y**, **Windhorst C**, **Lu X**, **Goodrich-Blair H**, **Bode HB**. 2017. The Global Regulators Lrp, LeuO, and HexA Control Secondary Metabolism in Entomopathogenic Bacteria. Front Microbiol **8**:209.
40. **Kaplan F**, **Alborn HT**, **von Reuss SH**, **Ajredini R**, **Ali JG**, **Akyazi F**, **Stelinski LL**, **Edison AS**, **Schroeder FC**, **Teal PE**. 2012. Interspecific nematode signals regulate dispersal behavior. PLoS One **7**:e38735.
41. **San-Blas E**, **Pirela D**, **García D**, **Portillo E**. 2014. Ammonia concentration at emergence and its effects on the recovery of different species of entomopathogenic nematodes. Exp Parasitol **144**:1–5.
42. **Veening J-W**, **Smits WK**, **Kuipers OP**. 2008. Bistability, Epigenetics, and Bet-Hedging in Bacteria. Annu Rev Microbiol **62**:193–210.
43. **Veening J-W**, **Stewart EJ**, **Berngruber TW**, **Taddei F**, **Kuipers OP**, **Hamoen LW**. 2008. Bet-hedging and epigenetic inheritance in bacterial cell development. Proc Natl Acad Sci U S A **105**:4393–4398.
44. **Van Der Woude M**, **Braaten B**, **Low D**. 1996. Epigenetic phase variation of the *pap* operon in *Escherichia coli*. Trends Microbiol **4**:5–9.
45. **Koike H**, **Ishijima SA**, **Clowney L**, **Suzuki M**. 2004. The archaeal feast/famine regulatory protein: potential roles of its assembly forms for regulating transcription. Proc Natl Acad Sci U S A **101**:2840–5.
46. **Unoarumhi Y**, **Blumenthal RM**, **Matson JS**. 2016. Evolution of a global regulator: Lrp in four orders of γ-Proteobacteria. BMC Evol Biol **16**:111.
47. **Morran LT**, **Penley MJ**, **Byrd VS**, **Meyer AJ**, **O'Sullivan TS**, **Bashey F**, **Goodrich-Blair**

H, **Lively CM**. 2016. Nematode-Bacteria Mutualism: Selection Within the Mutualism Supersedes Selection Outside of the Mutualism. Evolution (N Y) **7**:687–695.

48. **Vadyvaloo V**, **Jarrett C**, **Sturdevant DE**, **Sebbane F**, **Hinnebusch BJ**. 2010. Transit through the flea vector induces a pretransmission innate immunity resistance phenotype in *Yersinia pestis*. PLoS Pathog **6**:e1000783.
49. **Corcoran CP**, **Dorman CJ**. 2009. DNA relaxation-dependent phase biasing of the *fim* genetic switch in *Escherichia coli* depends on the interplay of H-NS, IHF and LRP. Mol Microbiol **74**:1071–1082.
50. **Nielsen AT**, **Dolganov NA**, **Rasmussen T**, **Otto G**, **Miller MC**, **Felt SA**, **Torreilles S**, **Schoolnik GK**. 2010. A bistable switch and anatomical site control *Vibrio cholerae* virulence gene expression in the intestine. PLoS Pathog **6**:e1001102.
51. **Jansen G**, **Crummenerl LL**, **Gilbert F**, **Mohr T**, **Pfefferkorn R**, **Thänert R**, **Rosenstiel P**, **Schulenburg H**. 2015. Evolutionary transition from pathogenicity to commensalism: Global regulator mutations mediate fitness gains through virulence attenuation. Mol Biol Evol **32**:2883–2896.
52. **Miller JH**. 1972. Experiments in molecular genetics. Cold Spring Harb Lab Press Cold Spring Harb NY **433**:352–355.
53. **Xu J**, **Hurlbert RE**. 1990. Toxicity of Irradiated Media for *Xenorhabdus* spp. Appl Environ Microbiol **56**:815–8.
54. **Mccann J**, **Stabb E V**, **Millikan DS**, **Ruby EG**. 2003. Population Dynamics of *Vibrio fischeri* during Infection of *Euprymna scolopes* Population Dynamics of *Vibrio fischeri* during Infection of *Euprymna scolopes*. Appl Environ Microbiol **69**:5928–5934.
55. **Dunn AK**, **Millikan DS**, **Adin DM**, **Bose JL**, **Stabb E V**. 2006. New *rfp*- and pES213-derived tools for analyzing symbiotic *Vibrio fischeri* reveal patterns of infection and *lux* expression in situ. Appl Environ Microbiol **72**:802–10.
56. **Bhasin A**, **Chaston JM**, **Goodrich-Blair H**. 2012. Mutational analyses reveal overall

topology and functional regions of NilB, a bacterial outer membrane protein required for host association in a model of animal-microbe mutualism. J Bacteriol **194**:1763–76.

57. **Chaston JM**, **Suen G**, **Tucker SL**, **Andersen AW**, **Bhasin A**, **Bode E**, **Bode HB**, **Brachmann AO**, **Cowles CE**, **Cowles KN**, **Darby C**, **de Léon L**, **Drace K**, **Du Z**, **Givaudan A**, **Herbert Tran EE**, **Jewell K a**, **Knack JJ**, **Krasomil-Osterfeld KC**, **Kukor R**, **Lanois A**, **Latreille P**, **Leimgruber NK**, **Lipke CM**, **Liu R**, **Lu X**, **Martens EC**, **Marri PR**, **Médigue C**, **Menard ML**, **Miller NM**, **Morales-Soto N**, **Norton S**, **Ogier J-C**, **Orchard SS**, **Park D**, **Park Y**, **Qurollo B a**, **Sugar DR**, **Richards GR**, **Rouy Z**, **Slominski B**, **Slominski K**, **Snyder H**, **Tjaden BC**, **van der Hoeven R**, **Welch RD**, **Wheeler C**, **Xiang B**, **Barbazuk B**, **Gaudriault S**, **Goodner B**, **Slater SC**, **Forst S**, **Goldman BS**, **Goodrich-Blair H**. 2011. The entomopathogenic bacterial endosymbionts *Xenorhabdus* and *Photorhabdus*: convergent lifestyles from divergent genomes. PLoS One **6**:e27909.

58. **Bao Y**, **Lies DP**, **Fu H**, **Roberts GP**. 1991. An improved Tn7-based system for the single-copy insertion of cloned genes into chromosomes of gram-negative bacteria. Gene **109**:167–168.

59. **Forst SA**, **Tabatabai N**. 1997. Role of the histidine kinase, EnvZ, in the production of outer membrane proteins in the symbiotic-pathogenic bacterium *Xenorhabdus nematophilus*. Appl Environ Microbiol **63**:962–8.

60. **Hussa E**, **Goodrich-Blair H**. 2012. Rearing and injection of *Manduca sexta* larvae to assess bacterial virulence. J Vis Exp **70**:1–5.

61. **Merritt JH**, **Kadouri DE**, **O'Toole GA**. 2005. Growing and analyzing static biofilms. Curr Protoc Microbiol **Chapter 1**:Unit 1B.1.

62. **Murfin KE**, **Chaston J**, **Goodrich-Blair H**. 2012. Visualizing bacteria in nematodes using fluorescent microscopy. J Vis Exp.

63. **Kaya HK**, **Patricia Stock S**. 1997. Chapter VI – Techniques in insect nematology, p.

281–324. *In* Manual of Techniques in Insect Pathology.

64. **Stabb E V**, **Ruby EG**. 2002. RP4-based plasmids for conjugation between *Escherichia coli* and members of the *Vibrionaceae*. Methods Enzymol **358**:413–26.

65. **Visick KL**, **Skoufos LM**. 2001. Two-component sensor required for normal symbiotic colonization of *Euprymna scolopes* by *Vibrio fischeri*. J Bacteriol **183**:835–42.

Tables and Figures

Table 2.1. Bacterial strains used in Chapter 2.

Strain or plasmid	Relevant genetic characteristic(s)	Fluorescent phenotype[a]	Source/ Reference
Strains			
HGB1059	*X. nematophila* HGB800 *lrp-2::kan*	NA	(27)
HGB1685	*E. coli* S17 pir carrying plasmid pEH69	GFP- RFP+	This study
HGB1974	*E. coli* S17 pir carrying plasmid pMYC1	GFP+ RFP+	This study
HGB2261	HGB1059 *att*Tn*7*::P_{fliC}-*gfp*	GFP- RFP+	This study
HGB2262	HGB2261 *kefA::*pMYC4 (low Lrp).	GFP- RFP+	This study
HGB2263	HGB2261 *kefA::*pMYC5 (high Lrp).	GFP+ RFP+	This study
HGB2267	*E. coli* S17 pir carrying plasmid pMYC4 (low Lrp)	NA	This study
HGB2268	*E. coli* S17 pir carrying plasmid pMYC5 (high Lrp)	NA	This study
HGB1966	*X. nematophila lrp-2::kan* plus pKV69 (vector)	NA	(23)
HGB1967	*X. nematophila lrp-2::kan* plus pEH54 (low Lrp plasmid)	NA	(23)
HGB1968	*X. nematophila lrp-2::kan* plus pEH56 (high Lrp plasmid)	NA	(23)
Plasmids			
pEVS107	ori6K mini-Tn7 delivery vector; Erm^R, Kan^R		(64)
pEH69	pEVS107 Tn7-promoterless *gfp/* P_{lac}-*rfp;* Erm^R, Kan^R		This study
pMYC1	pEH69 with *fliC* promoter fused upstream of *gfp;*		This study
pKV69	Multicopy mobilizable vector; Cm^R, Tet^R		(65)
pEH54	pKV69 with *lrp* in oppositie orientation relative to P_{lac}		(23)
pEH56	pKV69 with *lrp* under control of P_{lac}		(23)
pMYC4	ori6K-pEH54 with *kefA* fragment		This study
pMYC5	ori6K-pEH56 with *kefA* fragment		This study

[a]LB agar colony fluorescence scored as + or - based on fluorescence microscopy.

Table 2.2. Comparison of experimental and theoretical trends

Data type	Conditions	Emerged IJs	Non-emerged nematodes	Total nematodes
Experimental[1]	High-*lrp* vs. low-*lrp*	(+)	(=)	(+)
Theoretical[2]	Increase parameter[3] a	(+)	(+)	(+)
Theoretical	Increase parameter b	(+) then (-)	(-)	(-)
Theoretical	Increase parameter c	(+)	(-)	(=)
Theoretical	Increase parameter d	(+)	(+)	(+)

[1]Experimental data were extracted from Fig. 4 showing if high-*lrp* strains supports better (+) or equal (=) numbers of nematode production in each category in comparison to a low-*lrp* strain.
[2]Theoretical trends were simulated based on the mathematical model (see materials and methods). An initial condition was set as theoretical low-*lrp* outcomes (using parameter values: a=3.3, b=0.5, c=0.2, d=5). Parameters a, b, c, and d were individually and continuously increased in Mathematica. By increasing each of the parameters, the trend of simulated outcomes in comparison to outcomes under initial conditions (emerged IJs, non-emerged nematodes, or total nematodes) were recorded as increase (+), decrease (-), or equal (=).
[3]Parameter a: population expansion per reproductive cycle; b: percent population that forms IJ in the current reproductive cycle; c: percent of IJs that emerged in the current reproductive cycle; d: number of reproductive cycle before insect dissection.

Figure 2.1. The tripartite life cycle and mutualistic symbiosis among *Xenorhabdus* bacteria and *Steinernema* nematodes.

During the transmission stage, infective juvenile (IJ) nematodes carry Xenorhabdus bacteria (shown in yellow) in an intestinal pocket known as the receptacle. In the infection stage, an IJ enters the insect larva, releases bacterial symbiont; together they kill the insect host. During the reproduction stage, bacteria replicate, colonize nematodes, and support nematode reproduction. Upon nutrient depletion, juvenile nematodes form IJs and emerge out of the insect cadaver. See text for additional details.

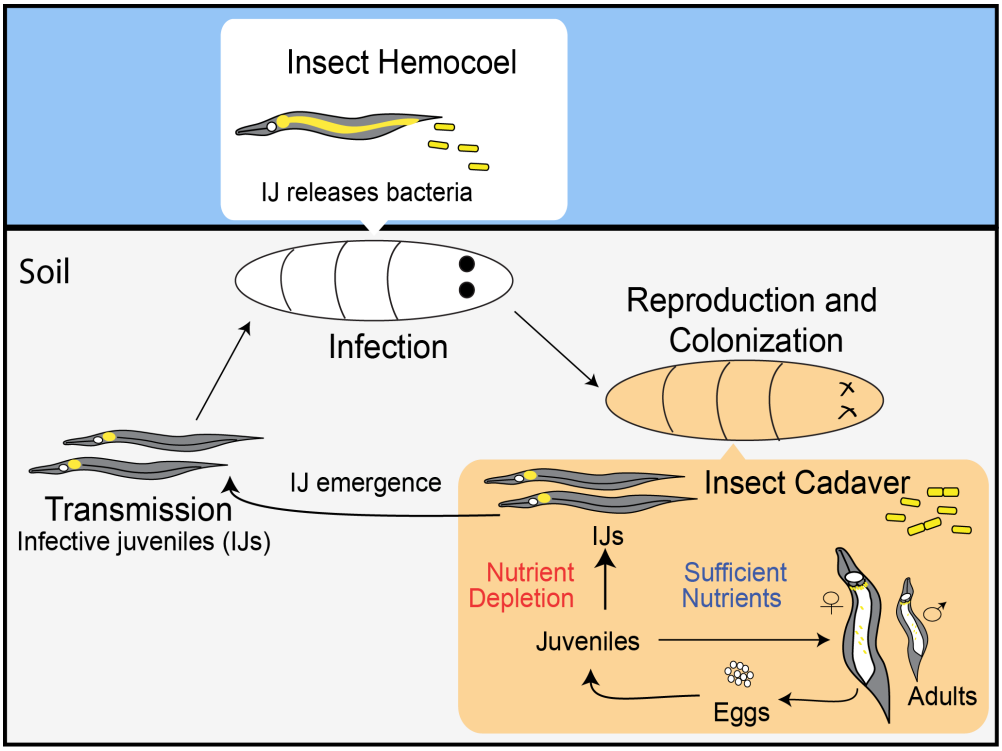
Insect Hemocoel
IJ releases bacteria
Soil
Infection
Reproduction and
Colonization
Transmission
Infective juveniles (IJs)
IJ emergence
Insect Cadaver
IJs
Nutrient
Depletion
Sufficient
Nutrients
Juveniles
Eggs
Adults

Figure 2.2. Lrp expression levels and virulence of bacteria with no-*lrp,* low-*rp,* and high-*lrp* in-genome fixed strains.

(A) High-*lrp* and low-*lrp* in-genome fixed strains were analyzed for Lrp protein expression levels via semiquantitative Lrp Western blotting using an antibody specific to *E. coli* Lrp. The total protein extracted from both strains were compared using serial of 2-folds dilutions. The difference in Lrp expression levels in between the two strains were estimated to be around 32 folds (See Materials and Methods). (B) Virulence of bacterial strains with *lrp* constructs in genome in *Manduca sexta* insects. Bacteria expressing no-*lrp,* low-*lrp,* and high-*lrp* in genome were grown overnight and sub-cultured for 8h. Samples were diluted to ~10^3 cfu in 10µL and injected into the hemocoel of *M. sexta* 4^{th} instar larvae. Three biological replicates of bacteria were used for each strain. Each replicate was injected into 10 insects.

A

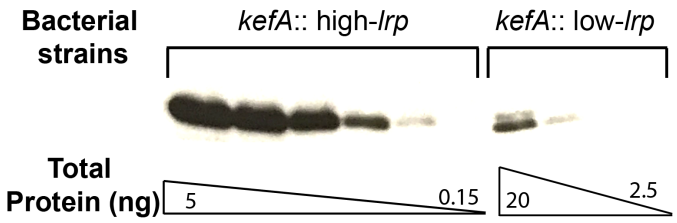
Bacterial strains
kefA:: high-lrp
kefA:: low-lrp
Total Protein (ng)
5
0.15
20
2.5

B

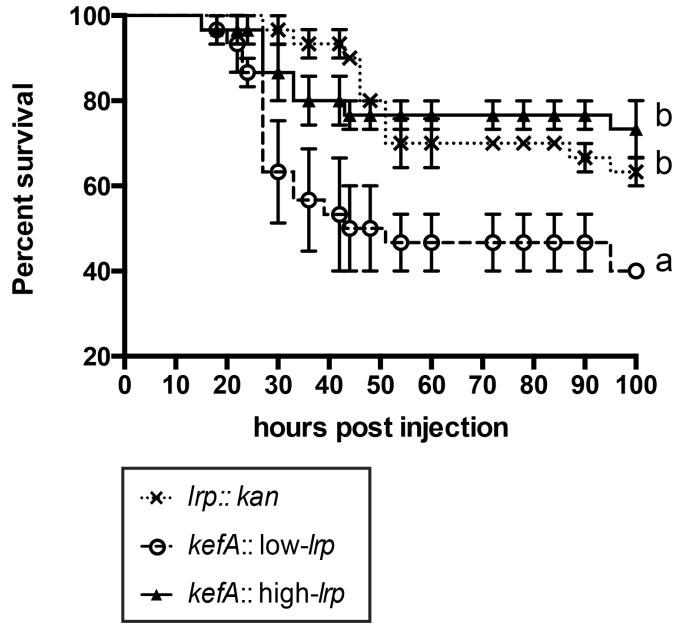
Percent survival
100
80
60
40
20
0 10 20 30 40 50 60 70 80 90 100
hours post injection
b
b
a
lrp:: kan
kefA:: low-lrp
kefA:: high-lrp

Figure 2.3. Biofilm formation of bacterial strains expressing fixed levels of Lrp.

Bacterial strains expressing fixed levels of Lrp from plasmids were grown for 6 days in static culture to cultivate biofilms. Biofilm materials were subsequently stained with crystal violet and visualized (A). Stained materials were then solubilized and quantitated using spectrophotometry (B). One-way ANOVA and Tukey's multiple comparisons tests were used to establish statistical groups (**).

A

genome	*lrp:: kan*	*lrp:: kan*	*lrp:: kan*
plasmid	vector	low-*lrp*	high-*lrp*

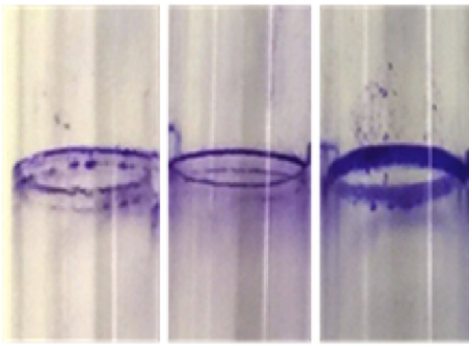

B

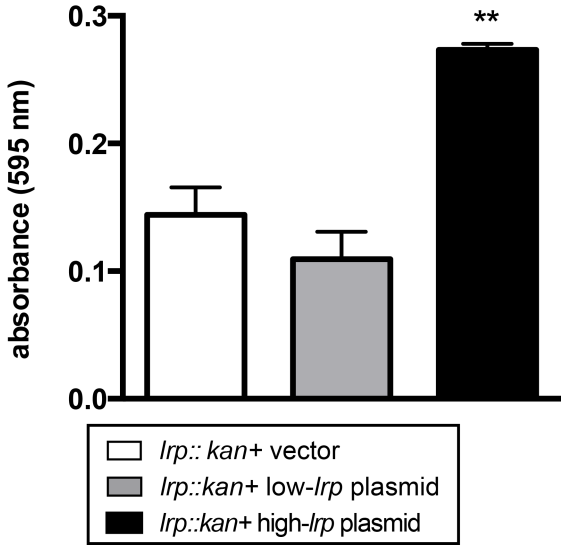

Figure 2.4. Mutualistic symbiosis phenotypes in vitro and in vivo.

Mutualistic symbiosis phenotypes in vitro (A, B, and C) and in vivo (D, E, and F) of IJ nematodes with bacterial strains expressing fixed levels of Lrp either from plasmids (A and D) or from in-genome constructs (B, C, E, and F). Nematode fecundity is shown as cumulative IJs (A, B and E) or percent productive infection (D). IJ colonization frequency was calculated as percentage of colonized IJs among the emerged IJs (E and F). Data are shown as averaged measurements (n=5 for A and E; n=3 for B, C, D, and F); error bars represent standard errors. Two-way ANOVA (A, B, D, E) or one-way ANOVA (C and F) and Tukey's multiple comparisons tests were used to establish statistical groups. Statistical significance and P value ranges are indicated by asterisks (ns: $P>0.05$; *$P\leq0.05$; ** $P\leq0.01$; *** $P\leq0.001$; **** $P\leq0.0001$). Different letters are assigned to different statistical groups.

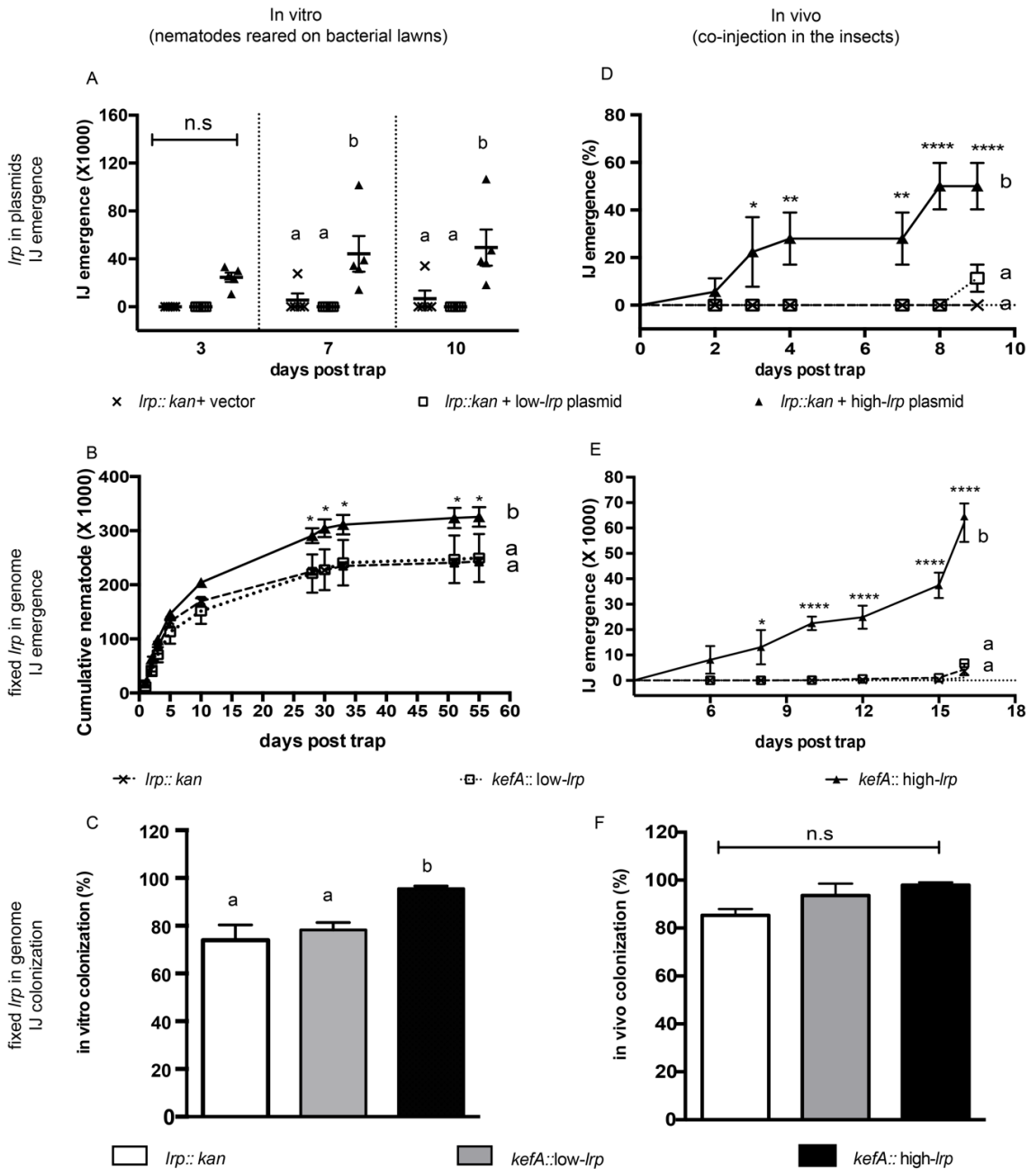
In vitro
(nematodes reared on bacterial lawns)
In vivo
(co-injection in the insects)
lrp in plasmids
IJ emergence
A
D
IJ emergence (X1000)
n.s
days post trap
IJ emergence (%)
lrp:: kan+ vector
lrp::kan + low-lrp plasmid
lrp::kan + high-lrp plasmid
fixed lrp in genome
IJ emergence
B
E
Cumulative nematode (X 1000)
IJ emergence (X 1000)
lrp:: kan
kefA:: low-lrp
kefA:: high-lrp
fixed lrp in genome
IJ colonization
C
F
in vitro colonization (%)
in vivo colonization (%)
lrp:: kan
kefA::low-lrp
kefA:: high-lrp

Figure 2.5. Total nematodes per insect.

Galleria insects co-injected with the combinations of nematodes and bacteria expressing fixed levels of Lrp either from plasmids (A) or from in-genome constructs (B, C). Individual insect cadavers were dissected for nematode counts either without (A) or with (B, C) determining if the cadaver was productive via water-trapping IJs. Insect cadavers that produced more than 50 emerged IJs were categorized as productive insects. Each data point represents the total nematode count from an individual insect as the sum of emerged and non-emerged nematodes.

A Bacteria carrying plasmids

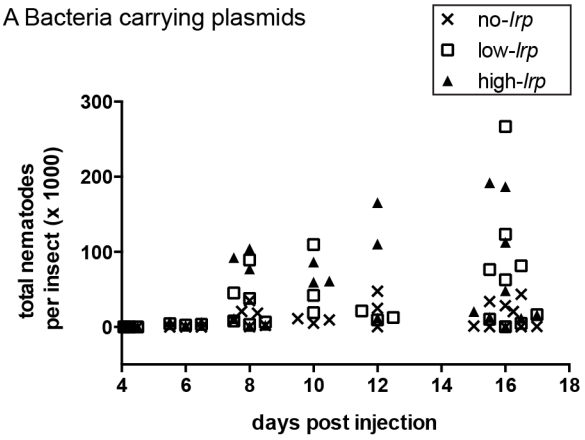

B Bacteria with in-genome constructs

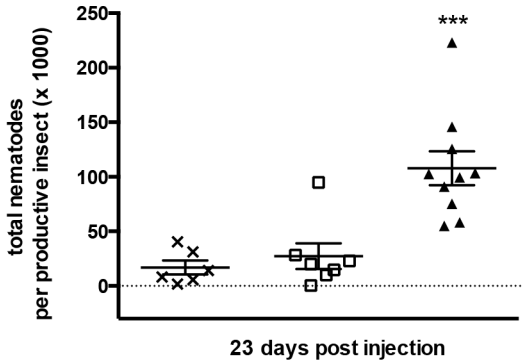

C Bacteria with in-genome constructs

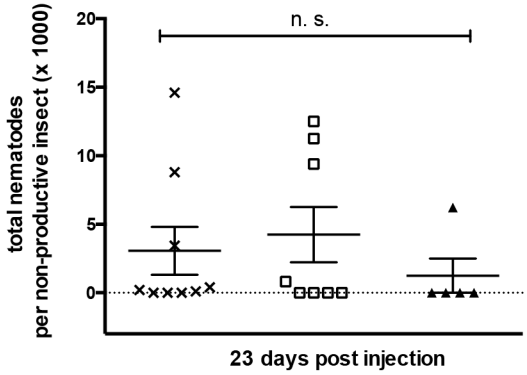

Figure 2.6. Nematode fecundity in *Galleria* insects shown as emerged IJs, non-emerged nematodes, and total nematodes.

Data were taken 23 days post co-injection of insects with aposymbiotic IJs and bacterial strains expressing fixed levels of Lrp. Nematodes per insect represent averages of each set of data (5 insects were used per bacterial strain in each biological replicates, n=3), and error bars represent standard errors.

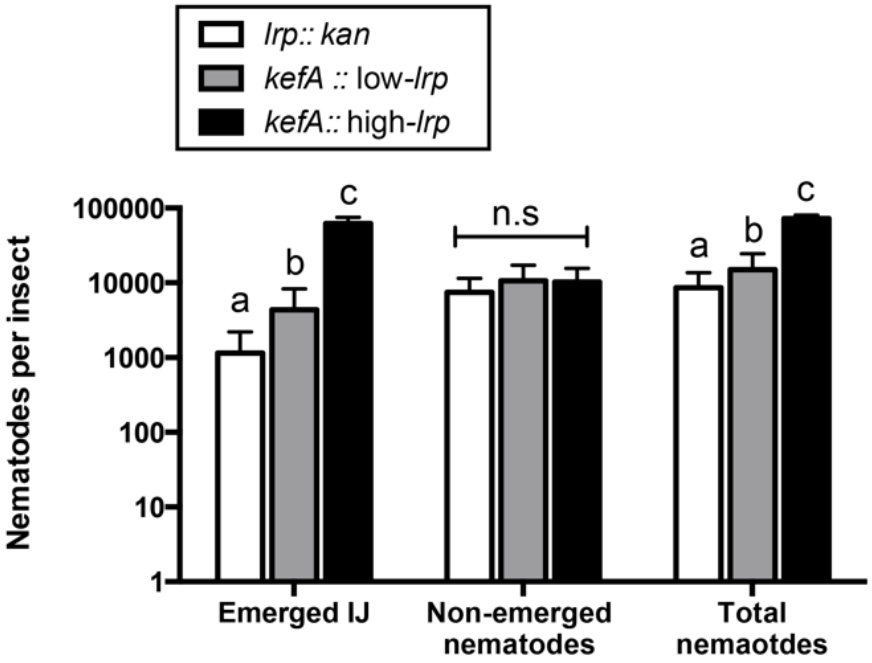
lrp:: kan
kefA :: low-lrp
kefA:: high-lrp
Nematodes per insect
100000
10000
1000
100
10
1
a
b
c
n.s
a
b
c
Emerged IJ
Non-emerged nematodes
Total nemaotdes

Figure 2.7. Comparison of experimental and theoretical numbers of emerged IJs, non-emerged nematodes, and total nematodes.

The theoretical numbers were estimated using the mathematical model (see Materials and Methods). Parameter values (a= 3.3, b= 0.5, c= 0.2, d=5) and (a=4.5, b=0.7, c=0.9, d=5) were used in the mathematical model to show one example of nematode numbers per insect if injected with the low-*lrp* strain or the high-*lrp* strain, respectively. a: population expansion per reproductive cycle; b: percent population that forms IJ in the current reproductive cycle; c: percent of IJs that emerged in the current reproductive cycle; d: number of reproductive cycle before insect dissection. The experimental data of low-*lrp* and high-*lrp* strains were averaged number of emerged IJ, non-emerged nematodes, and total nematodes extracted from data shown in Fig. 2.6

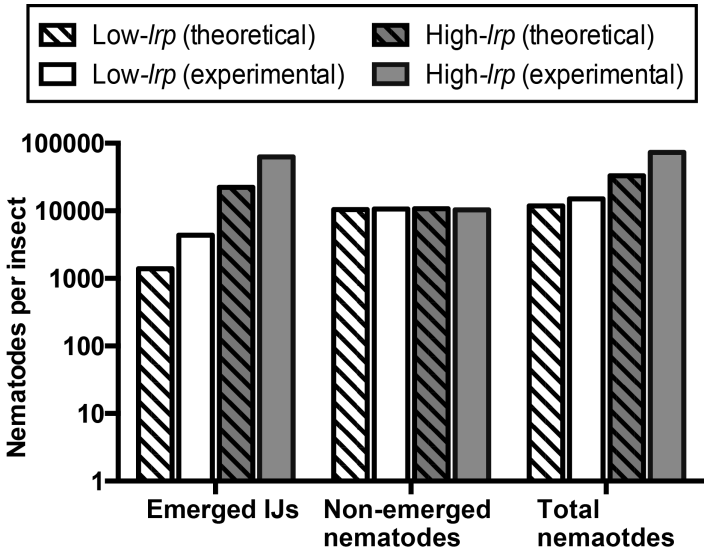

Figure 2.8. In vivo mutualism phenotypes.

Bacterial strains with in-genome constructs expressing fixed levels of Lrp were co-injected into five *Galleria* insects per treatment. Insects that produced more than 50 emerged IJs were considered productive insects. Percent productive insect is calculated by percentage of productive insects out of the total number of insects infected per experiment (A) Emerged and colonized IJs per productive insect were calculated as colonization frequency multiplied by number of emerged IJs per productive insect (B). Data are presented as means with standard errors (n=3 biological replicates, each biological replicate is the average of five insects). One-way ANOVA was used to determine statistical significance.

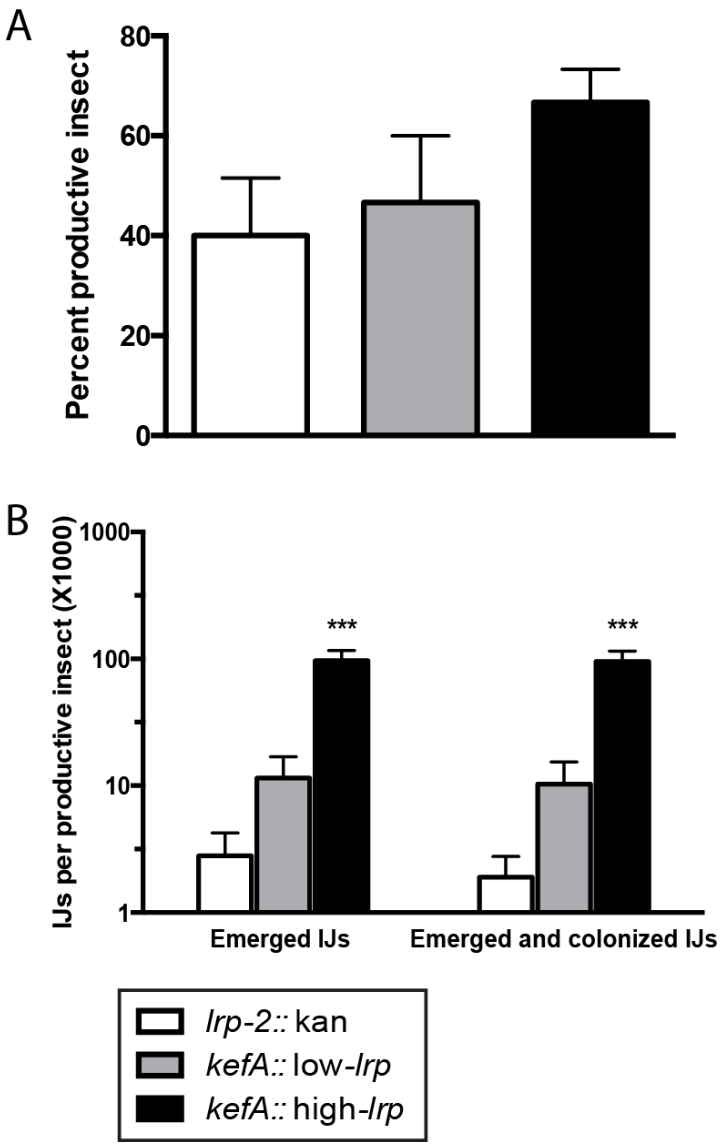
A
Percent productive insect
80
60
40
20
0
B
IJs per productive insect (X1000)
1000
100
10
1
***
***
Emerged IJs
Emerged and colonized IJs
lrp-2:: kan
kefA:: low-lrp
kefA:: high-lrp

Figure 2.9. Mutualistic interactions measurements in the natural infection of insects with colonized IJs.

(A) Survival rate of *Galleria* insects after naturally infected by IJs colonized with bacteria expressing fixed levels of Lrp in the sand trap. (B) Percent productive infection was calculated by percentage of insects that produces IJ nematodes in the water-traps. For each biological replicate, 15 insects were used for sand-trap assay and 8-12 insect cadavers were used for water-trapping IJ nematodes. Data points represent the averaged measurements (n=3), and error bars represent standard errors.

A

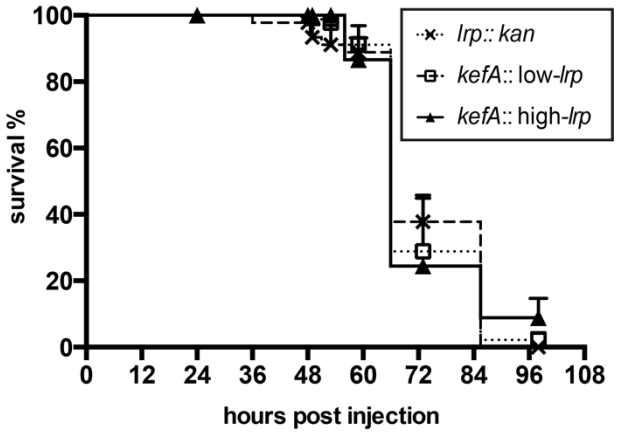
100
80
60
40
20
0
survival %
0
12
24
36
48
60
72
84
96
108
hours post injection
lrp:: kan
kefA:: low-lrp
kefA:: high-lrp

B

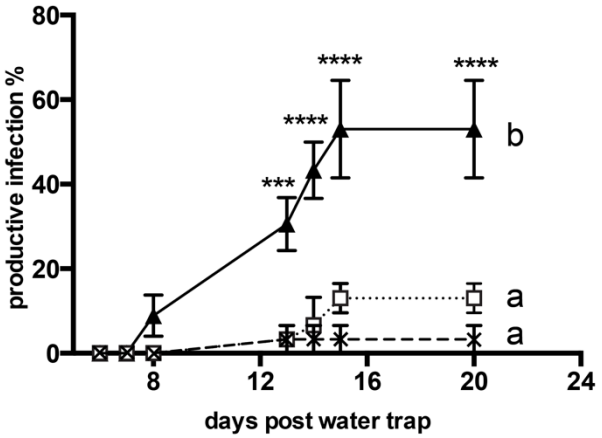
80
60
40
20
0
productive infection %
***
****
****
****
b
a
a
8
12
16
20
24
days post water trap

Chapter 3

Nutritional conditions influence *Xenorhabdus nematophila* Lrp-dependent phenotypic variation

Mengyi Cao: Hypothesis, experiments, data analysis, figures, writing

Ellen Gough: conducted experiments for Fig. 3.2: Lrp semi-quantitative immunoblotting

Heidi Goodrich-Blair: Hypothesis, experiments, data analysis, figures, writing

Abstract

Within a clonal population of bacteria, environmental changes and gene expression regulatory pathways can contribute to phenotypic population heterogeneity. The symbiotic bacterium *Xenorhabdus nematophila* exhibits phenotypic heterogeneity with respect to host interactions, in a process termed virulence modulation (VMO) that is controlled by the transcription factor Lrp (leucine-responsive regulatory protein). In VMO, bacteria vary between two symbiotic phenotypes: a low-Lrp expressing population that is virulent towards insects and a high-Lrp population that is mutualistic towards nematodes. To investigate the molecular mechanisms by which VMO occurs in *X. nematophila*, I employed Lrp-dependent-*gfp/*constitutive P*lac-rfp* fluorescent reporters that allow accurate assessments of Lrp-dependent gene expression in individual bacterial colonies. One reporter, *PfliC-gfp/Plac-rfp,* shows that the ratio of GFP/RFP fluorescence positively correlates with Lrp levels and inversely correlates with virulence (Chapter 2). In wild type *X. nematophila*, *PfliC-gfp/Plac-rfp* revealed two major colony phenotypes: a low-Lrp (low GFP/RFP intensity) colony and a high-Lrp (high GFP/RFP intensity) colony phenotype. A wild type clonal population composed of bi-stable expression of both low-Lrp colonies and high-Lrp colonies, referred to as a 'heterogeneous population', is more virulent towards *Manduca sexta* insect larvae than is a 'homogeneous population' composed of mono-stable expression of high-Lrp colonies. FACS analysis of single colonies suggests that the switch among low-Lrp and high-Lrp colonies are reflected by consistent shifts among four subpopulations within the colony expressing off, medium, on, or high levels of *PfliC*. To assess the influence of environmental conditions on the frequency of either high- or low-Lrp expressers in a population, I used percent low-Lrp colonies as an indicator of population heterogeneity and found that high-to-low Lrp switch and population heterogeneity are promoted in nutrient-limiting conditions particularly when casamino acids are present, but could be inhibited by glucose. In addition, the bacterial growth yield in glucose is positively correlated to population heterogeneity in casamino acids among isolates derived from a wild type virulent strain, but these two factors

showed no correlation among those isolates derived from the virulence-attenuated strain. My data indicate that the correlation in between Lrp-dependent heterogeneity and adaptive performance in glucose is reflective of bacterial virulence towards insects. Together, these data suggest particular host-derived nutrients, especially amino acids (i.e. in IJ receptacle) and glucose (i.e. in insect hemolymph) could impact Lrp switch and population heterogeneity, which could be crucial to bacterial adaptive behaviors, such as growth yield and virulence, during environmental changes in the symbiotic life cycle.

Introduction

Within an isogenic population of bacteria, cell-to-cell differences in gene regulation, such as transcriptional noises, occur and could lead to population heterogeneity, which facilitates responses and survival in fluctuating environments. One mechanism that creates population heterogeneity is termed phenotypic (or phase) variation, which can be initiated by stochastic molecular processes such as fluctuating gene expression, and amplified by genetic or epigenetic switching mechanisms, leading to bi- or multi- stable behaviors within bacterial populations (1)[1]. Such population heterogeneity causes spatial or temporal diversity within a single species of bacterium that could provide opportunities for 'social benefits' such as cooperation and bet hedging. In cooperation, for instance, a particular and costly phenotype (such as siderophore production in *Pseudomonas aeruginosa*) could benefit neighboring cells, resulting in better fitness such as virulence towards a host (2). In bet hedging, individual subpopulations express distinctive traits that may be adaptive for future environments such that the population as a whole is pre-adapted for success in multiple potential future environments (3). In many types of pathogenic bacteria, such as *Escherichia coli, Vibrio cholerae, Neisseria*

[1]. The terms 'phase' and 'phenotypic' variation are both used in the literature, but the concepts of the two are not always clearly distinguished. Here I use 'phenotypic variation' to represent the idea of both 'phase' and 'phenotypic' variation, regardless of switching mechanisms (genetic or epigenetic), switching frequency, or the consequences of this phenomenon. Another term, 'antigenic variation' is used here to describe a phenotypic/phase variation that occurs via modulation of surface-exposed proteins.

gonorrhea, P. aeruginosa, switching among different phenotypes drives heterogeneity that can increase fitness during the transition from free-living to host-associated states (4). For instance, in a process known as antigenic variation some pathogenic bacteria change the type of molecules exposed on their surface in order to bypass the host immunity (4).

Multi-stable states phenotypic variation can result from networks of transcriptional regulation (5). However, beneficial population heterogeneity can also result from shifts in transcriptional profiles among some cells within a population without leading to bi- or multi-stability(6, 7). For example, the *lac* operon can be expressed in either mono- or bi-stable states via a combination of transcriptional activation, repression, and nutrient availability. Under specific environmental conditions when the transcriptional repressor LacI is overexpressed and lactose is at intermediate level, *lac*-ON and *lac*-OFF subpopulations co-exist (bi-modal/two-peak distribution) in a bi-stable expression (8). In contrast, the presence of specific sugar or inducer, such as lactose or IPTG, only leads to a normal distribution of either promoter-ON or OFF cells, a phenomenon called mono-modality (one-peak distribution). Although mono-modality of a gene(s) expression is not considered true switching among stable states (phenotypes) in a biological system, environmental signals such as increased level of lactose or IPTG in this case, could cause a graded response: a ‘shift’ of the subpopulation percentage (i.e. a right-shift from 50% promoter-ON cells to 80% promoter-ON cells) or an amplified gene expression (i.e. from an intermediate to a maximal gene expression in the induction curve) (8).

Population heterogeneity caused by transcriptional profile shifting could also serve as a crucial strategy in bacterial adaptive behaviors under environmental changes and during microbe-host interactions. For instance, in the agricultural pest glassy-winged sharpshooter, the obligate bacterial symbiont *Baumania* associates with the host embryo as a single inoculum (one clonal population derived from a parental cell). Later in insect host development, *Baumania* localizes to two distinct tissues in the same host as two different bacteriomes (9). Resent research revealed that *Baumania* isolated from different bacteriomes of the same insect showed

significantly different transcriptional profiles that indicate distinctive roles in either nutrition or transmission during host-microbe interactions (10). In this case, the transcriptional profile shift occurred within a clonal population of bacteria when subpopulations bifurcated to occupy two distinct host niches, causing the phenotypic shift and functional differences in the mutualistic symbiosis. This phenotypic shift is suggested to derive from long-term co-adaptation or co-evolution within a specific symbiosis pair between particular species of bacteria and hosts (termed species-specific interaction). Unlike bet hedging in random environments, transcriptional-shift in species-specific interaction drives population heterogeneity that facilitates bacterial adaptive behaviors in predictable environments.

This chapter focuses on the virulence modulation (VMO) in bacterium *Xenorhabdus nematophila,* which is considered to be a phenotypic variation phenomenon. The symbiotic bacterium *Xenorhabdus nematophila* has a species-specific relationship with its nematode host *Steinernema carpocapsae*. The *X. nematophila* life cycle includes three distinct environments: the insect cadaver (reproductive stage), the species-specific nematode host intestine or other tissues (transmission stage), and the blood cavity of the relatively broad range of insect hosts infected by the nematode (infection stage). The transitions among these life stages are associated with host environmental changes, including in nutritional conditions. One nutritional shift occurs when bacteria move from the nutrient-rich insect cadaver (which contains ample lipids, amino acids, and sugars (11)) to the intestinal receptacle of the transmission stage IJ nematode, which is thought to be nutrient-limiting (with some, but not all amino acids available in sufficient quantities to support the growth of *X. nematophila* auxotrophs) (12). Another nutritional shift occurs when bacteria are transitioning from the IJ receptacle into the blood cavity of a new insect host (13, 14). Insect hemolymph (blood) is rich in sugars such as glucose and trehalose (15). To smoothly transit among hosts and succeed in the symbiotic life cycle, *X. nematophila* populations may respond and survive the nutritional changes in the host environments.

In the previous chapter, I presented my findings that in wild type populations of *X. nematophila* varying expression levels of a global transcription factor Lrp mediates the modulation between bacterial mutualistic (high-Lrp, virulence-, mutualism+) and pathogenic (low-Lrp, virulence+, mutualism-) phenotypes, in a process termed VMO. Lrp is a member of a larger family of transcription factors conserved across bacteria and archaea and known as feast-or-famine regulators because they generally sense and respond to nutritional changes (16). I hypothesized that *X. nematophila* heterogeneity in Lrp expression levels and the consequent Lrp-dependent expression of either mutualistic or pathogenic traits is driven by nutritional changes when bacteria transit between insect and nematode hosts.

The experiments in published literature and my thesis have established that *X. nematophila* VMO is a phenotypic variation phenomenon that is controlled by Lrp levels. However, it is not yet clear if Lrp levels are mono-, bi- or multi-stable. Historically, the phenotypic variation phenomenon was observed via switching of colony morphology, such as opacity, surface smoothness, pigment production, bioluminescence expression, dye binding, or colony size (4, 17, 18). The tools of bacterial genetics, such as promoter fusions to *lacZ* and *gfp* reporters facilitate the investigation of transcriptional regulation underlying phenotypic variation. In addition, the more recently developed technologies of fluorescence based analyses, such as FACS (Fluorescence Activated Cell Sorting), allows single-cell and quantification of population heterogeneity which can reveal the underlying mechanisms of phenotypic variation (19). In this chapter, I present my investigation of *X. nematophila* Lrp-dependent phenotypic variation using Lrp-dependent fluorescent reporters. Based on both colony and single-cell observations of cells expressing the *PfliC-gfp/Plac-rfp* reporter, my current data show that under a specific nutritional condition (LB agar), an isogenic population of *X. nematophila* could express either one or two stable profile(s) of Lrp-dependent gene expression (*PfliC*), correlating to mono- or bi-stable expression of Lrp. Wild type populations with bi-stable expression of Lrp (heterogeneous) are

more virulent than those with mono-stable expression of high levels of Lrp (homogeneously-high) Nutritional change could impact the Lrp mono-, bi-, or multi- stable expression in the bacterial populations. Such variation in population heterogeneity impacts the bacterial adaptive behaviors, such as growth yield in glucose and virulence towards insects.

Results

X. nematophila Lrp-dependent *fliC* reporter gene expression exhibits colony-to-colony variation

Bacterial phenotypic variation or global transcriptional profiles change typically results in population heterogeneity with respect to the phenotype that is varying. Monitoring changes in heterogeneity can reveal the timing of and influence of environmental conditions on the switch (or shifts) among phenotypes (3). To investigate the VMO between mutualistic (high-Lrp) and pathogenic (low-Lrp) phenotypes in the life cycle of *X. nematophila,* I constructed an Lrp-dependent fluorescence reporter to visualize and quantify the number of each cell type, and variation in this number, in living bacterial populations (Fig. 3.1). As a reporter of Lrp expression I chose the promoter activity of *fliC* (a gene encoding flagellin subunit) which is positively regulated by Lrp (Hussa et al., 2015), resulting in as much as 803-fold higher *fliC* expression, measured by reverse-transcriptase quantitative PCR (RT-qPCR) in the presence vs. absence of Lrp. A construct was created with two reporters, *PfliC-gfp* and *Plac-rfp* (to serve as an internal control for cellular expression levels) (Fig. 3.1A). When this construct is integrated stably into the genomes of *X. nematophila* strains, measurement of GFP/RFP ratios accurately reflects Lrp-dependent gene expression (see materials and methods and Chapter 2, Table 2.1).

To visualize population heterogeneity of Lrp-dependent gene expression, the reporter construct was integrated into the genome of wild type *X. nematophila*. Individual exconjugants were isolated, cultured in fresh medium to create clonal populations, and stored as frozen stocks. When these frozen stocks were streaked onto LB agar, diverse population phenotypes were observed among bacterial isolates, including: a heterogeneous (HET) population composed of both smaller low-Lrp colonies (low GFP/RFP intensity) and larger high-Lrp colonies (high GFP/RFP intensity) (Fig. 3.1 B-D); and a homogeneous (HOM) population composed exclusively of high-Lrp colonies (Fig. 3.1 E-G) regardless of colony size. A third population phenotype was exclusively small colony (SC), low-Lrp (low GFP/RFP). This

population was the focus of undergraduate Ellen Gough's senior thesis and is not presented here in detail. One of the major differences between low-Lrp colonies from HET populations vs. SC populations is that the former, but not the latter, frequently switch to high-Lrp progeny colonies. When picked using a sterile toothpick and streaked onto a new LB agar plate, low-Lrp colonies from HET populations develop into heterogeneous populations with co-existing low-Lrp and high-Lrp colonies. In contrast, low-Lrp from SC populations gives rise only to low-Lrp small colonies. Immunoblotting to semi-quantitatively measure Lrp levels confirmed that isolates of the HET, HOM, and SC populations described above express expected levels of Lrp (Figure 3.2, adapted from EG thesis). Single colony Lrp immunoblotting was attempted but was unsuccessful due to insufficient levels of total protein extracted from each colony (data not shown).

Other colony phenotypes, including those with sectors and concentric rings of alternating high and low GFP/RFP intensity, were observed after growing in minimal medium supplemented with casamino acids (MM+CAA) for more than a week (Fig. S3.1). These diverse Lrp-dependent mosaics within individual colonies suggest the possibility of bi- or multi-state stability of Lrp expression levels in an isogenic population under certain laboratory culturing conditions. Here I focus on two population phenotypes, HET and HOM, since these two populations reproducibly generated under controlled laboratory conditions and consistent with virulent and virulence-attenuated phenotypes, respectively.

Population heterogeneity of Lrp-regulated gene expression is not exclusive to genes within the flagellar pathway

Lrp is a global regulator of gene expression in *X. nematophila* and regulates genes both within and outside of the flagellar regulatory pathway (20). Since previous reports had established that expression of the *X. nematophila* (strain F1) flagellar pathway (including *fliC*) is subject to population heterogeneity due to fluctuations in Lrp-dependent *fliZ* expression (21), we

assessed the heterogeneity of expression of an Lrp-regulated gene outside of the flagellar pathway. For this purpose I used an Lrp-dependent fluorescence reporter (*PXNC1_2826-gfp/Plac-rfp*). XNC1_2826 (XNC3v2_1350002 in F1) is predicted to encode a phospho-transferase system protein. Microarray analysis indicates that in *X. nematophila* this gene is negatively regulated by Lrp (~4.3 fold) (20) while RNAseq data indicate it is not part of the flagellar regulatory pathway (21). When this reporter construct was integrated in single copy in the wild type bacterial genome, I again visualized colony-to-colony variation. A heterogeneous population was composed of colonies with low ratios of GFP/RFP, indicating high-Lrp levels (since Lrp is a negative regulator of XNC1_2826) and those with high ratios of GFP/RFP, indicating low-Lrp levels (Fig. 3.1 H-J), with the latter showing smaller colony sizes than the former. These differences in fluorescence intensity using *PXNC1_2826-gfp/Plac-rfp* reporter were detectable on minimal medium agar supplemented with casamino acids. I was unable to discern differences when colonies were grown on LB agar, since the colonies were all uniformly low GFP. This may be due to additional regulatory controls that limit XNC1_2826 expression on LB agar, or to the interference of autofluorescence from LB agar in discerning the subtle fold differences in high vs. low expression of the XNC1_2826 reporter. Regardless, these data indicate that heterogeneity of Lrp-dependent regulation is not exclusive to genes within the flagellar pathway.

Colonies expressing high GFP/RFP intensity by *PXNC1_2826-gfp/Plac-rfp* reporter (low-Lrp colonies) are relatively small after 18-24 hours of incubation on MM+CAA agar (Fig. 3.1 H-J), consistent with observations using the *PfliC-gfp/Plac-rfp* reporter on LB agar. This raises the possibility that Lrp levels gradually rise during colony growth, and that the observed heterogeneity is due to colony growth rate, not directly due to Lrp levels. To test this possibility, I grew and screened wild type bacterial colonies carrying *PfliC-gfp/Plac-rfp* or *PXNC1_2826-gfp/Plac-rfp* on MM+CAA agar for consecutive 4 days (Fig. S3.2). My data showed that over the time course, the low-Lrp sectors per colony significantly increase in *PfliC-gfp/Plac-rfp* (high

GFP/RFP) and *PXNC1_2826-gfp/Plac-rfp* (low GFP/RFP) reporters, respectively (Fig. S3.2). These data confirmed that both Lrp-dependent reporters show the same trend of an increase in low-Lrp populations when nutrients depleted, not limited to a transient early growth stage or the colony size. The inverse trends of fluorescence intensity (GFP/RFP) versus colony size of the *PXNC1_2826-gfp* and *PfliC-gfp* reporters (Fig.3.1B-D) is consistent with the inverse regulatory effects of Lrp on these two promoters, and further supports that the observed heterogeneity in gene expression is due to Lrp-dependent regulation of genes both within and outside of the flagellar pathway. Lrp has more dramatic effects on *fliC* expression (803-fold by RT qPCR) than it does on XNC1_2826 expression (-4.3-fold by microarray) (20). Therefore, I chose to use *PfliC-gfp/Plac-rfp* to further study the impact of growth conditions on Lrp-dependent population heterogeneity.

HET populations are more virulent than HOM populations.

Previous research has established that cells expressing low levels of Lrp are more virulent than those expressing high levels of Lrp (20, 22). Based on this, I predicted that naturally occurring HET populations that contain both high-Lrp and low-Lrp colonies are more virulent than naturally occuring HOM high-Lrp populations. To test this prediction, I isolated multiple populations of *PfliC-gfp/Plac-rfp* reporter exconjugants from a virulent HGB1969 (herein referred to as vir-69) *X. nematophila* wild type parental strain (20). Of the 102 exconjugants tested, ~55% were heterogeneous (herein referred to as vir-69-HET) and ~45% were homogeneous (herein referred to as vir-69-HOM) with respect to the reporter. In addition, I isolated reporter exconjugants from a virulence-attenuated variant HGB1970 (att-70) (20). In

this background, of the 10 exconjugants tested I observed only homogeneously high-Lrp populations (herein referred to as att-70-HOM)[2].

I assessed virulence of representatives of the three populations (vir-69-HET, vir-69-HOM, and att-70-HOM), by injecting overnight cultures into *Manduca sexta* 4th instar larvae and monitoring insect survival (Fig. 3.3). Consistent with my prediction, HET populations were significantly more virulent than either of the two HOM populations (Fig. 3.3 A, B, and C), supporting my hypothesis that HET populations with both high-Lrp and low-Lrp cells are better adapted for infection compared to their HOM high-Lrp counterparts. In addition, vir-69-HOM from the virulent parental background is significantly more virulent than is att-70-HOM derived from the virulence-attenuated strain (Fig. 3.3 B and C). These data indicate that lineage history impacts the progeny virulence phenotype. This finding also suggests that HOM populations derived from virulent and virulence-attenuated parental strains may have different underlying mechanisms contributing to virulence attenuation.

Single cell fluorescence analysis of *fliC* expression profiles within colonies reveals bi-stable Lrp expression in wild type *X. nematophila*

The data presented above indicates that population heterogeneity of Lrp-dependent *PfliC-gfp* expression in colonies is positively associated with virulence (Fig. 3.3). However, observing overall colony phenotypes does not reveal the distribution of Lrp-dependent gene expression among individual cells within the colony. For example, all the cells in a low-Lrp colony may express relatively low, homogenous levels of Lrp-dependent gene, or the colony may be comprised of both "ON" and "OFF" cells of Lrp-dependent genes, and the latter are the majority.

[2] Note that the homogeneous, non-reversible, low-Lrp SC populations were also isolated exclusively from homogeneously-high Lrp populations at very low frequency (a total 3 isolates after repeated trials of isolation from HGB 800, HGB 1087, HGB 1969, and HGB 1970). However, since the low-Lrp colonies from a heterogeneous population constantly switch to high-Lrp colonies on LB, I was not able to obtain a homogeneous population of switchable low-Lrp colonies.

To distinguish between these possibilities, I used fluorescence activated cell sorting (FACS) to analyze individual cells and subpopulations within colonies. To set gating standards for FACS analysis, I used bacterial colonies expressing no-*lrp* (Fig. 3.4A), fixed low-*lrp* (Fig.3.4B) and fixed high-*lrp* (Fig. 3.4C). Based on these fixed-*lrp* strains, FACS analysis revealed a total four subpopulations distinguished by differences in *fliC* expression: a *PfliC*-OFF gate (GFP-low/RFP-low), a *PfliC*-ON gate (GFP-high/RFP-low), a *PfliC*-Medium gate (GFP-high/RFP-high), and a GFP-low/RFP-high population. This last population was non-viable based on its inability to grow post-sorting (data not shown) and was not considered further. As expected, the profile of *PfliC* expression is dependent on Lrp expression levels: a colony expressing no Lrp only shows mono-modal of *PfliC*-OFF population (Fig.3.4A); a fixed low-Lrp colony is composed of bi-modal expression of *PfliC*-ON and OFF subpopulations (Fig.3.4B), while a fixed high-Lrp colony is composed of tri-modal expression of *PfliC*-ON, OFF, and Medium subpopulations (Fig.3.4C). Using this standard gating method, I analyzed the compositions of low-Lrp colonies from a HET population (Fig. 3.4D), high-Lrp colonies from a HET population (Fig. 3.4E), and high-Lrp colonies from a HOM population (Fig. 3.4F). Corresponding to the varying levels of Lrp expression in these wild type colonies (Fig. 3.4DEF), the *PfliC* expression profiles revealed the shifts among three subpopulations: OFF, ON, and Medium.

A difference in between Lrp expression shift (graded response model) vs. Lrp switch (bi- or multi- stable model) is whether the bacterial colonies show one or multiple stable states of Lrp-dependent gene expression profiles. For instance, in the 'Lrp-shift' (graded response) model, under a specific growth condition such as on the LB agar, Lrp expression is expected to show a mono-modal distribution among colonies derived from an isogenic population of bacteria. In this case, when multiple colonies are analyzed from the same agar plate, the Lrp-dependent genes expression profile (such as *fliC*) among these colonies should be stabilized in one *fliC* expression profile (i.e. 40%-ON, 40%-OFF) with fluctuation mostly within standard

deviation (i.e. minority of colonies would show 35%-ON/45%-OFF, one out of hundreds might show 20%ON/60%-OFF). In the 'Lrp-switch' (i.e. bi-stable) model, the *fliC* expression profiles are expected to stabilize at two compositions (i.e. the majority of colonies would be either 40%-ON/40%-OFF, or 10%-ON/70%-OFF). I hypothesize that each colony phenotype I have observed in wild type populations is one stable state of *fliC* expression profile, thus a HET population shows bi-stable Lrp expression, while the HOM population shows mono-stable Lrp expression. To investigate the profiles of *PfliC* expressing subpopulations within each wild type colony phenotype, I quantified individual colonies by FACS and assessed the percentages of individual viable cells within each expression category: *PfliC*-ON, *PfliC*-OFF, and *PfliC*-Medium (Fig.3.5A). My data show that low-Lrp colonies have significantly lower frequencies of *PfliC*-ON ($P \leq 0.0001$) and *PfliC*-Medium ($P \leq 0.05$) cells relative to high Lrp colonies, confirming the observable low-Lrp and high-Lrp colonies represent two significantly different stable states of Lrp expression. These data support the bi-stable model of Lrp in the wild type HET population.

To further interpret my data of FACS analysis, another possible *PfliC* expression profile in the high-Lrp colony phenotype is if individual *PfliC*-ON cells express higher cellular levels of *fliC*, relative to *PfliC*-ON cells from low-Lrp colonies (Fig. 3.5D). This could lead to an additional *PfliC*-High subpopulation that is not revealed by scattered plot in Fig. 3.4. For instance, if a wt. low-Lrp colony is composed of *PfliC*-OFF, -Medium, and -ON subpopulations, while a high-Lrp colony is composed of *PfliC*-OFF, -Medium, and -High (a subpopulation in the *PfliC*-ON gate but express significantly higher *PfliC* than *PfliC*-ON cells in low-Lrp colony), the entire wild type HET population (low-Lrp and high-Lrp colonies) would show a tetra-modal, rather tri-modal expression of *PfliC*. Understanding such multi-modality in Lrp-dependent gene expression is crucial to studying the phenotypic switching/shifting phenomenon, because each peak (modal or subpopulation) could represent a stable phenotype in a biological system. To test this, I quantified average GFP/RFP intensity ratios in individual cells from each of the different colony types (Fig.3.5C). My data show that *PfliC*-ON subpopulations derived from low-Lrp colonies

have significantly lower average GFP/RFP intensity ratios than those derived from high-Lrp colonies (Fig.3.5C). This finding is consistent with the idea that high-Lrp colonies contain *PfliC*-ON cells, but these express significantly higher levels *of fliC* than *PfliC*-ON cells from low-Lrp colonies (Fig.3.5D), revealing an additional *PfliC*-High subpopulation.

The proportion (Fig. 3.5A and B) and average *fliC* expression levels of individual cells in the *PfliC*-ON category (Fig. 3.5 C and D) was similar in high-Lrp colonies regardless of whether the colony was isolated from a heterogeneous population or a homogenous population, indicating that population phenotype history influences neither the within-colony composition *of PfliC* expressing cells nor *the PfliC* expression levels within those cells. Together, my FACS data support the hypothetical model that a wt. *X. nematophila* population exhibits bi-stable Lrp switch that controls population shift among four viable and stable subpopulations based on *PfliC* expression profiles. The low-Lrp colony phenotype gives rise to one stable composition of *PfliC*-OFF, -Medium, and -ON subpopulations, and a high-Lrp colony phenotype gives rise to another stable composition of *PfliC*-OFF, -Medium, and -High subpopulations.

Growth conditions influence population heterogeneity of Lrp-dependent gene expression

My data show that the visible low- and high-Lrp colony phenotypes on LB agar are consistent with *pfliC* expression profiles representing the two stable states of Lrp expression. In addition, the ability to obtain low-Lrp colonies from heterogeneous populations is directly correlated with virulence (Fig. 3.3), I next sought to investigate environmental conditions that affect Lrp switch using the visible low- and high-Lrp colonies on agar plate as a proxy of population heterogeneity. As noted above, when streaked onto fresh LB agar plates, low-Lrp colonies give rise to both high- and low-Lrp colonies, indicating that nutrient replete conditions allow high-Lrp colonies to arise. Consistent with this idea, high-Lrp colonies yield only high-Lrp colonies when restreaked onto LB.

Based on these observations, I hypothesized that regardless of the initial state (starting phenotype), limiting nutrients could lead to the rise of low-Lrp colonies, while a nutrient-rich condition could lead to the rise of high-Lrp colonies. To test this hypothesis, I streaked from a frozen stock of a homogeneously-high-Lrp population onto LB agar (Fig.3.6A-C), 50% LB agar (Fig.3.6D-F), and 25% LB agar (Fig. 3.6G-I). I found that Low-Lrp colonies appear on diluted, but not full strength, LB agar (Fig.3.6D-I), such that on quarter-strength LB the population was predominantly homogenously low-Lrp, while on half-strength Lrp a heterogeneous population was observed (Fig.3.6D-F). These data suggest that during laboratory growth nutrient-rich conditions promote a population switch toward high-Lrp expressers, while nutrient limiting conditions promote a population switch toward low-Lrp expressers.

Heterogeneous expression of Lrp high- and low- states is promoted by growth in minimal medium supplemented with casamino acids and is inhibited by glucose

To further explore the impact of nutrients on the relative levels of high- or low-Lrp expression in populations, I examined the changes in frequencies of low-Lrp colonies in a population of cells transferred from rich to nutrient-limiting growth media, then back again (Fig. 3.7). I chose this regime because it provides a rough representation of the host conditions that may be experienced by *X. nematophila* during its life cycle from the insect cadaver to the transmission stage nematode to the insect cadaver. To create a nutrient-limiting condition, I used either minimal medium supplemented with casamino acids[3] (MM+CAA, Fig. 3.7A) or minimal medium supplemented with glucose (MM+GLU, Fig. 3.7B). I used six biological replicates (one test tube represents an individual population and a biological replicate) from three independent experiments. Over the time course of 5 days (1 overnight in LB followed by 3

[3] Minimal medium supplemented with casamino acids (MM+CAA) used in this chapter was made based on the protocol suggested by Elizabeth Hussa (personal communication), with additional trace amount of glutamate and aspartate. Note that I have preliminary data (not shown here) that the presence of extra trace amount of glutamate and aspartate is crucial to the Lrp-dependent phenotypic variation.

days in defined media and 1 overnight in LB), individual bacterial populations were sampled daily from each tube and serially diluted. For each dilution, three 10 µl droplets (three technical replicates) were plated onto LB agar to screen for population heterogeneity by epifluorescence microscopy. Qualitatively, diverse colony phenotypes could be observed among the heterogeneous population including low- and high- Lrp colonies mentioned above (Fig. 3.1-3.5). In addition, a translucent colony phenotype and small-sized colony phenotype (switchable, different from SC) also appear (data not shown). These diverse colony phenotypes suggest additional stable or transient compositions of *PfliC* expression profiles within the colonies, which could correlate to multi-stable expression of Lrp. To simplify the quantification of Lrp heterogeneity, I used the percentage of low-Lrp colony phenotype as a proxy of heterogeneity. I quantified population heterogeneity using CFU per culture, and counted the proportion of colonies that displayed the low-Lrp phenotype. Consistent with qualitative observations, my data show that samples taken from bacteria cultured in MM+CAA had higher percentage of low-Lrp colonies than the original stock grown in LB (Fig. 3.7A). In addition, populations expressing homogenously high levels of Lrp (vir-69-HOM and att-70-HOM) have lower increase in percent low-Lrp colonies compared to the heterogeneous population (vir-69-HET) (Fig.3.7A). These data show that casamino acids could drive a population switch from high-to-low Lrp expression thus increasing population heterogeneity. However, the switching frequency depends on the lineage and starting population status of bacterial isolates.

Incubation in minimal medium supplemented with glucose did not induce an increase in the proportion of low-Lrp colonies in any of the wild type bacterial populations (Fig. 3.7B), nor did incubation in minimal medium supplemented with a combination of glucose and amino acids (Fig. 3.7C). These data suggest that the presence of glucose inhibits population heterogeneity and the formation of low-Lrp colonies.

To further explore the connection between phenotypes observed in minimal medium supplemented with either glucose or CAA, I split individual LB overnight cultures (n=6 from the

same frozen stock) into minimal medium supplemented with either casamino acids or glucose (10^6-10^7 CFU/mL in the starting population), then measured growth yields and Lrp-dependent gene expression heterogeneity (Fig.3.8). I observed that while different wild type bacterial populations showed very similar growth yields after 3 days of growth in MM+CAA (~10^7 CFU/mL after 3 days), these same bacterial populations showed variability of growth yields when cultivated in MM+GLU (Fig. 3.8). Some cultures, which I term high-yield, reached above 10^8 CFU/mL after 3 d incubation in MM+GLU (Fig.3.8A-C), while others, which I term low-yield, attained sizes of only 10^5-10^8 CFU/mL in the same time period (Fig.3.8D-F). An additional subgroup did not grow, and in fact declined in size to under 10^4 CFU/mL over the incubation period (Fig.3.8G). The high-, low-, no- growth yield phenotypes in MM+GLU were repeatedly observed in three independent experiments regardless of the starting population size (10^6 or 10^7 CFU/mL). in the similar manner. The MM+GLU growth yield phenotype was independent of starting population size (10^6 or 10^7 CFU/mL) but was positively correlated with the MM+CAA population heterogeneity phenotype (Fig.3.8A), with both phenotypes being most frequently observed in populations derived from the vir-69-HET strain (4 high yield of 6 cultures tested, Fig. 3.8A and D), next most frequently in the att-70-HOM strain (3 high yield of 6 cultures tested; Fig. 3.8C and F), and least frequently observed in vir-69-HOM (1 high yield of 6 cultures tested, Fig. 3.8B, E, and G) (Fig. 3.7). The positive correlation between the maximum population size when grown in MM+GLU and the low-Lrp expressor phenotype may suggest that cells expressing low levels of Lrp have a growth advantage in MM+GLU, relative to high-Lrp expressers.

I have observed that out of the three isolates I tested (vir-69-HET, vir-69-HOM, att-70-HOM) the most heterogeneous bacterial isolate (vir-69-HET from Fig. 3.7) also showed the highest population yield in glucose (4 high yield of 6 cultures tested, Fig. 3.8), while the isolate with the least yield in glucose (vir-69-HOM) also showed the least heterogeneity (Fig 3.7 and 3.8). Thus I hypothesized that Lrp heterogeneity in CAA has a positive correlation with bacterial growth yield in glucose. To test this, I directly compared bacterial growth in glucose (Fig.3.8, left

y-axis) and their high-to-low Lrp switching ability in amino acids (Fig.3.8, right y-axis) In the two wild type strains derived from virulent parent, vir-69-HET (Fig. 3.8A and D) and vir- 69-HOM (Fig.3.8B, E, and G), my data showed a clear correlation in between growth yield in glucose and Lrp switching ability in amino acids: by 3 days of incubation, the populations with the high growth yield phenotype in MM+GLU showed high percentage (20-100%) of low-Lrp colonies in MM+CAA (Fig.3.8A and B), the low-yield populations in MM+GLU showed medium percentage (2-10%) of low-Lrp colonies in MM+CAA (Fig.3.8 D and E), and the no-growth yield populations in MM+GLU showed low percentage (<1.5%) of low-Lrp colonies in MM+CAA. These data support my hypothesis that in the bacterial isolates derived from a virulent parental strain, Lrp heterogeneity in casamino acids is positively correlated with population growth yield in glucose. In comparison to a homogeneous isolate (vir-69-HOM), a more heterogeneous isolate (vir-69-HET) exhibits better adaptive behaviors, such as growth yield in glucose (Fig. 3.8) and virulence towards insects (Fig. 3.3)

In contrary, the isolate derived from the virulence-attenuated strain, att-70-HOM, did not show a correlation between the MM+GLU growth yield and the MM+CAA population heterogeneity. By 3 days of incubation, the high-yield populations in glucose that were expected to correlate with high heterogeneity showed either high (20%-80%) or medium (2%-20%) percentages of low-Lrp colonies (Fig. 2.8C); the low-yield populations that were expected to correlate with medium heterogeneity showed either high (20%-80%) or low (<1.5%) percentages of low-Lrp colonies (Fig. 2.8F).

These data show that wild type *X. nematophila* growth yield in glucose is positively correlated with population heterogeneity in populations derived from a **virulent parental strain**, but not in those derived from a **virulence-attenuated parental strain**. These data support my hypothesis that the two homogeneously high-Lrp populations, vir-69-HOM and att-70-HOM, are attenuated in virulence caused by different mechanisms: the former has a low switching

frequency from high to low levels of Lrp while the latter showed a disrupted correlation in population heterogeneity vs. growth yield in glucose.

Conclusion

In this chapter, I presented my current data investigating Lrp-dependent VMO, a phenotypic variation phenomenon in *X. nematophila.* Using a single-coy in-genome construct of Lrp-dependnet reporter, *PfliC-gfp/Plac-rfp,* I identified two colony phenotypes among wild type bacteria (low-Lrp and high-Lrp colonies) each is a stable state of Lrp expression reflected by population shifts among for subpopulations of *PfliC* expression profiles. The population heterogeneity (bi-stable expression of high and low-Lrp colonies) could be promoted by casamino acids, and inhibited by glucose. Heterogeneous population with bi-stable expression of Lrp (high-Lrp + low-Lrp colonies) are more virulent and show higher growth yield in glucose than mono-stable expression of homogeneously high-Lrp colonies. In the two virulence-attenuated wild type isolates, vir-69-HOM has low switching frequency in high-to-low Lrp conversion and low growth yield in glucose, while att-70-HOM shows a normal population heterogeneity but a disrupted correlation in between population heterogeneity and adaptive performance in glucose.

Discussion

Construction of a fluorescence reporter for visualization of VMO phenotypic variation during *X. nematophila* growth in laboratory media

In this chapter, I developed Lrp-dependent fluorescence reporters that enabled visualization of colony-to-colony variation in Lrp expression levels within wild type populations. This is the first such dual-fluorescence reporter available for use in *Xenorhabdus* bacteria and facilitated accurate quantification and further analysis of VMO switch at single-cell level. One reporter, *PfliC-gfp/Plac-rfp* revealed four subpopulations of *fliC* expression profiles in two stable

states of Lrp expression. Previously, another research reported that transcription regulator FliZ controls *fliC* bi-modal expression in a graded response manner: by titrating FliZ using tetracycline-inducible system, the authors observed population shift from *fliC*-OFF to *fliC*-ON states shown by plasmid-based *PfliC-gfp* reporter. These previous data suggested a graded-response of *PfliC* bi-modal expression controlled by change in FliZ (21). Using single-copied reporter in genome in combination with an *rfp* reporter as an internal control, I identified two additional subpopulations, *PfliC*-Medium and *PfliC*-High that are engaged in wild type bacterial VMO. In contrary to graded response via manipulating FliZ expression shown in the previous research, my data show that in wild type population of *X. nematophila,* Lrp express to two discrete levels (low and high stable states) suggesting FliZ in wild type population also express could also express in a bi-stable manner dependent on Lrp. In addition, the *PXNC1_2826-gfp/Plac-rfp* reporter showed similar bi-stable expression of Lrp that are outside of the flagellar regulatory pathway, further confirmed the bi-stable expression of Lrp is independent of FliZ. However, more detailed analysis, such as plotting cell count vs. GFP/RFP intensity should be done to confirm bi- or multi- stability of the Lrp expression.

Nutrient availability promotes or inhibits population heterogeneity

Using the percent low-Lrp colonies in the population as a proxy, I quantified Lrp-dependent population heterogeneity and in response to nutrient limitation, the presence of casamino acids and (or) glucose. My data showed that population heterogeneity could be promoted by either lower-strength of LB medium or the presence of casamino acids, but would be inhibited by using full-strength LB medium or with the presence of glucose. The underlying mechanisms of either heterogeneity induction (by amino acids) or inhibition (by glucose) are not yet clear. In *E. coli,* Lrp (leucine-responsive regulatory protein) is known to respond to leucine. However, if *X. nematophila* Lrp responds to leucine or other species of amino acids is unknown. It is possible that the presence of particular species of amino acids could associate with Lrp and

affect the bi-stable switch of Lrp expression. In the future research, it would be crucial to identify specific amino acids or combinations of amino acids that *X. nematophila* Lrp is responsive to. In bacteria, glucose is known for repressing the catabolism of other nutrients such as amino acids (a process called catabolite repression). In *Staphylococcus aureus,* the catabolism of amino acids (i.e. glutamate) is relieved when glucose is limiting, and is crucial to pathogen survival in host niches where glucose is not abundant (23). It would be intriguing for the future researchers to explore if glucose also repress amino acids metabolism which could affect Lrp switch.

Mechanisms of virulence-attenuation in homogeneous populations

Based on low-Lrp and high-Lrp colonies phenotypes, I isolated heterogeneous population with bi-stable expression of Lrp (HET, high-Lrp and low-Lrp colonies) and homogeneous populations expressing mono-stable of high levels of Lrp (HOM, high-Lrp colonies only). My virulence assays showed that heterogeneous populations are more virulent than homogeneously-high Lrp populations. The populations derived from a virulent parental strain also showed positive correlation in between population heterogeneity and growth yield in glucose. HOM isolates either has low levels of heterogeneity (vir-69-HOM) or absence of correlation in between heterogeneity and growth yield in glucose (att-70-HOM) is attenuated in virulence towards insects. Whether bacterial virulence is directly caused by or affected the ability of bacterial adaptive behaviors in glucose is not clear and awaits testing. Understanding the links among amino acids-promoted population heterogeneity, growth in glucose, and bacterial virulence would be crucial to understand lineage-dependent virulence attenuation mechanisms in HOM populations.

Lrp-dependent switching between pathogenic and mutualistic phenotypes in the *X. nematophila* bacterial life cycle

My data show that alternating nutritional conditions, such as from relatively nutrient rich (full-strength LB) to nutrient limiting (quarter-to-half strength of LB) increases population heterogeneity which is crucial for adaptive behaviors such as virulence and growth yield in glucose. Heterogeneity could be promoted by amino acids and inhibited by glucose in vitro. Based on my data, I hypothesize that the transition of life stages with similar environmental changes, such as from insect cadaver (nutrient-rich, ample lipids, sugar, and amino acids) to IJ nematode receptacle (nutrient-limiting and contains some amino acid) promotes the Lrp high-to-low switch among *X. nematophila* symbionts. This high-to-low Lrp switch increases population heterogeneity and virulence prior to the infection stage of the life cycle (Fig.3.9). In the next chapter, I focus on investigating and pinpointing the specific developmental stage in which the VMO switch to low-Lrp expression occurs.

The insect blood is rich in sugars, such as glucose and trehalose (15), and these sugars could possibly serve as signals for host switch during infection stage. My data show that increased percentage of low-Lrp colonies in the populations (heterogeneity) also increases bacterial growth yield in glucose, suggesting glucose either promotes low-Lrp cells or inhibits the growth of high-Lrp cells. My data favor the latter explanation, because my data showed that glucose inhibits Lrp high-to-low switch (Fig 3.7 and 3.8). Together, my data suggest that glucose selects low-Lrp cells by inhibiting high-Lrp expressors, and those low-Lrp cells selected in the glucose environment switch to a homogeneous population expressing intermediate level of Lrp (translucent colonies). High-Lrp cells were shown to be immunogenic towards insects (22). I proposed in my current model (Fig. 3.9) that once a heterogeneous population is released from recovering IJ nematodes and exposed to glucose-rich insect hemolymph, the high-Lrp cells are inhibited by glucose, further preventing high-Lrp cells from inducing insect immune responses and ensuring the successful infection by low-Lrp subpopulations. At the meantime, glucose could signals the switch of low-to-intermediate level of Lrp prior to reproduction stage in which

higher levels of Lrp benefits bacteria and nematode reproduction and colonization. These ideas awaits testing.

Materials and Methods

Bacterial growth

Bacterial strains were grown in LB medium (24) either not exposed to light or supplemented 1% of 0.1% sodium pyruvate (25) at 30°C. Medium were supplemented with chloramphenicol (30μg mL^{-1}) for *E. coli* or (15 μg mL^{-1}) for *X. nematophila* to maintain plasmids(20), erythromycin (200μg mL^{-1}), kanamycin (50μg mL^{-1}). Bacterial liquid culture were grown using the cell roller in dark. Defined media were prepared as described in previous research (26, 27). For minimal media-glucose, 0.91% glucose and 0.25mM $MgCl_2$ were used as supplements. For minimal media-casamino acids, 0.1% casamino acids, 0.01% glutamate, and 0.25% aspartate were used as supplement. For minimal media+CAA-Glucose, all supplements described above were added. To sub-culture *X. nematophila* in defined media, bacterial overnight culture in LB was washed in PBS buffer for 3X and 1:100 diluted into defined media. Bacterial CFU/mL was calculated by serial dilution and colony counting on LB agar.

Plasmids and strains construction

PXNC1_2826-gfp/Plac-rfp was constructed by PCR amplification of the XN_2826 promoter using primers SphI-p2826-f and AvrII-p-2825-r, digested with SphI/AvrII and ligated into SphI/AvrII-digested pEH69 (Bradon McDonald and Beth Hussa constructed). The plasmid construct was electroporated into *E. coli* S17-lpir, creating the donor strain (HGB 1723). The *P2826-gfp/Plac-rfp* construct was transferred to attTn7 in wild type *X. nematophila* (HGB 800) via tri-parental conjugation using *E. coli* donor strain (HGB 1723) and helper strain (HGB 283), creating the wild type strain (HGB 2099). The same construct *P2826-gfp/Plac-rfp* was also inserted in an *lrp* mutant at attTn7 (HGB 2102). Fluorescence screen of wild type/Tn7-*P2826*-

gfp/Plac-rfp (HGB 2099) and *lrp* mutant/Tn7-*P2826-gfp/Plac-rfp* (HGB 2102) grown on MM-casAA agar showed that GFP/RFP intensity ratio in inversely regulated by Lrp, confirming Lrp negatively regulates *P2826* promoter activity.

Fluorescence screening and FACS analysis

Bacterial cells are diluted serially and plated onto LB or MM-CasAA (minimal media supplemented with casamino acids) agar with or without antibiotics, incubated at 30C in dark for 16-20 hours, and screened and imaged by fluorescence microscopy using a Nikon Eclipse TE300 inverted microscope (Nikon, Melville, NY, USA) at 4X magnification using FITC(GFP) and TRITC (RFP) double-channel. Images of bacterial colonies were colored and GFP and RFP images were overlaid using Figi (NIH Image (cite article on their website)) without further processing.

FACS was preformed at UWCCC Flow Cytometry laboratory. Individual colonies were screened using epifluorescence microscopy, picked by sterile toothpick and re-suspended in 100µL 1XPBS buffer. Cell samples were kept on ice, and sorted using BD FACS AriaII Multi-Color Benchtop Flow Cytometer at 4°C. To recover each subpopulation, the sorted cells were collected in sterile microfuge tubes and directly plated onto LB agar and incubated at 30°C overnight. FACS data analysis was performed using FlowJo single cell data analysis software (LLC).

Virulence assay

Manduca sexta insects were reared from eggs (Carolina Biological), and fed by wheat-germ diet (Carolina Biological). Bacterial were grown in LB liquid media overnight at 30°C on cell roller, subcultured into fresh LB media (1:100), and grown for 6-8 hours. Bacterial cultures were serially diluted in 1XPBS and 10^3 or 10^4 cfu/10uL of dilution was injected into each *M. sexta* 4th instar larvae. Insect death was monitored over the time course of 100 hours post

injection. For each biological replicate (one bacterial culture), 8 or 10 insects were used for injection (28).

Acknowledgements

I would like to thank the staff at FlowCCC at University of Wisconsin-Madison for their valuable suggestions for FACS experiments and analysis. I want to thank Bradon McDonald and Elizabeth Hussa for their *P2826-gfp/Plac-rfp* construct which contributed to the work in this Chapter.

References

1. **Van Der Woude MW**. 2011. Phase variation : how to create and coordinate population diversity. Curr Opin Microbiol **14**:205–211.
2. **Buckling A**, **Harrison F**, **Vos M**, **Brockhurst M a**, **Gardner A**, **West S a**, **Griffin A**. 2007. Siderophore-mediated cooperation and virulence in *Pseudomonas aeruginosa*. FEMS Microbiol Ecol **62**:135–41.
3. **Veening J-W**, **Smits WK**, **Kuipers OP**. 2008. Bistability, Epigenetics, and Bet-Hedging in Bacteria. Annu Rev Microbiol **62**:193–210.
4. **van der Woude MW**, **Bäumler AJ**. 2004. Phase and antigenic variation in bacteria. Clin Microbiol Rev **17**:581–611.
5. **Tyson JJ**, **Chen KC**, **Novak B**. 2003. Sniffers, buzzers, toggles and blinkers: dynamics of regulatory and signaling pathways in the cell. Curr Opin Cell Biol **15**:221–231.
6. **Smits WK**, **Kuipers OP**, **Veening J-W**. 2006. Phenotypic variation in bacteria: the role of feedback regulation. Nat Rev Microbiol **4**:259–271.
7. **Jansen G**, **Crummenerl LL**, **Gilbert F**, **Mohr T**, **Pfefferkorn R**, **Thänert R**, **Rosenstiel P**, **Schulenburg H**. 2015. Evolutionary transition from pathogenicity to commensalism: Global regulator mutations mediate fitness gains through virulence attenuation. Mol Biol Evol **32**:2883–2896.
8. **Zander D**, **Samaga D**, **Straube R**, **Bettenbrock K**. 2017. Bistability and Nonmonotonic Induction of the lac Operon in the Natural Lactose Uptake System. Biophysj **112**:1984–1996.
9. **Brooks MA**. 1966. Endosymbiosis of animals with plant microorganisms. J Invertebr Pathol **8**:428–429.
10. **Bennett GM**, **Chong RA**. 2017. Genome- -wide transcriptional dynamics in the companion bacterial symbionts of the glassy-winged sharpshooter (Cicadellidae: *Homalodisca vitripennis*) reveal differential gene expression in bacteria occupying

multiple host organs. G3 Genes, Genomes, Genet.

11. **Richards GR**, **Goodrich-Blair H**. 2009. Masters of conquest and pillage: *Xenorhabdus nematophila* global regulators control transitions from virulence to nutrient acquisition. Cell Microbiol **11**:1025–1033.
12. **Martens EC**, **Russell FM**, **Goodrich-Blair H**. 2005. Analysis of *Xenorhabdus nematophila* metabolic mutants yields insight into stages of *Steinernema carpocapsae* nematode intestinal colonization. Mol Microbiol **58**:28–45.
13. **Snyder H**, **Stock SP**, **Kim S-KK**, **Flores-Lara Y**, **Forst S**. 2007. New insights into the colonization and release processes of *Xenorhabdus nematophila* and the morphology and ultrastructure of the bacterial receptacle of its nematode host, *Steinernema carpocapsae*. Appl Environ Microbiol **73**:5338–5346.
14. **Martens EC**, **Goodrich-Blair H**. 2005. The *Steinernema carpocapsae* intestinal vesicle contains a subcellular structure with which *Xenorhabdus nematophila* associates during colonization initiation. Cell Microbiol **7**:1723–1735.
15. **Phalaraksh C**, **Lenz EM**, **Lindon JC**, **Nicholson JK**, **Farrant RD**, **Reynolds SE**, **Wilson ID**, **Osborn D**, **Weeks JM**. 1999. NMR spectroscopic studies on the haemolymph of the tobacco hornworm, *Manduca sexta*: assignment of ^{1}H and ^{13}C NMR spectra. Insect Biochem Mol Biol **29**:795–805.
16. **Yokoyama K**, **Ishijima SA**, **Clowney L**, **Koike H**, **Aramaki H**, **Tanaka C**, **Makino K**, **Suzuki M**. 2006. Feast/famine regulatory proteins (FFRPs): *Escherichia coli* Lrp, AsnC and related archaeal transcription factors. FEMS Microbiol Rev **30**:89–108.
17. **Nelson LK**, **Stanton MM**, **Elphinstone RE a**, **Helwerda J**, **Turner RJ**, **Ceri H**. 2010. Phenotypic diversification in vivo: Pseudomonas aeruginosa gacS- strains generate small colony variants in vivo that are distinct from in vitro variants. Microbiology **156**:3699–3709.
18. **Somvanshi VS**, **Sloup RE**, **Crawford JM**, **Martin AR**, **Heidt AJ**, **Kim K -s. KK -s.**,

Clardy J, **Ciche TA**. 2012. A single promoter inversion switches Photorhabdus between pathogenic and mutualistic states. Science **337**:88–93.

19. **Lidstrom ME**, **Konopka MC**. 2010. The role of physiological heterogeneity in microbial population behavior. Nat Chem Biol **6**:705–712.
20. **Hussa EA**, **Casanova-Torres ÁM**, **Goodrich-Blair H**. 2015. The global transcription factor Lrp controls virulence modulation in *Xenorhabdus nematophila*. J Bacteriol **197**:3015–3025.
21. **Jubelin G**, **Lanois A**, **Severac D**, **Rialle SS**, **Longin C**, **Gaudriault S**, **Givaudan A**. 2013. FliZ Is a Global Regulatory Protein Affecting the Expression of Flagellar and Virulence Genes in Individual Xenorhabdus nematophila Bacterial Cells. PLoS Genet **9**:e1003915.
22. **Casanova-Torres ÁM**, **Shokal U**, **Morag N**, **Eleftherianos I**, **Goodrich-Blair H**. 2017. The global transcription factor Lrp is both essential for and inhibitory to *Xenorhabdus nematophila* insecticidal activity. Appl Environ Microbiol AEM.00185-17.
23. **Halsey CR**, **Lei S**, **Wax JK**, **Lehman MK**, **Nuxoll AS**, **Steinke L**, **Sadykov M**, **Powers R**, **Fey PD**. 2017. Amino Acid Catabolism in *Staphylococcus aureus* and the Function of Carbon Catabolite Repression. MBio **8**:e01434-16.
24. **Miller JH**. 1972. Experiments in molecular genetics. Cold Spring Harb Lab Press Cold Spring Harb NY **433**:352–355.
25. **Xu J**, **Hurlbert RE**. 1990. Toxicity of Irradiated Media for *Xenorhabdus* spp. Appl Environ Microbiol **56**:815–8.
26. **Orchard SS**, **Goodrich-Blair H**. 2004. Identification and functional characterization of a *Xenorhabdus nematophila* oligopeptide permease. Appl Environ Microbiol **70**:5621–7.
27. **Bhasin A**, **Chaston JM**, **Goodrich-Blair H**. 2012. Mutational analyses reveal overall topology and functional regions of NilB, a bacterial outer membrane protein required for host association in a model of animal-microbe mutualism. J Bacteriol **194**:1763–76.

28. **Hussa E**, **Goodrich-Blair H**. 2012. Rearing and injection of *Manduca sexta* larvae to assess bacterial virulence. J Vis Exp **70**:1–5.

Figures

Figure 3.1. Lrp-dependent fluorescence reporters reveal colony heterogeneity among *X. nematophila* wild type populations.

(A) Diagram showing the construction of *PfliC-gfp/Plac-rfp* (Lrp-positively regulated). **(B-G)** A *Xenorhabdus nematophila* wild type populations carrying *PfliC-gfp/Plac-rfp* stably integrated in the genome were plated on LB agar plates and individual colonies were visualized using fluorescence microscopy to examine GFP and RFP levels. Images indicate colony-to-colony variation of GFP intensity, which is positively correlated to colony size. Wild type populations are either heterogeneous, with colonies expressing either high or low levels of Lrp-dependent GFP **(B-D)** or homogeneous, expressing high levels of Lrp-dependent GFP **(E-G)**. **(F-I)** An *X. nematophila* wild type population carrying the Lrp-negatively regulated promoter reporter *PXNC1_2826-gfp/Plac-rfp.* Cells were plated on minimal medium agar supplemented with casamino acids (MM-casAA) and visualization with fluorescence microscopy revealed colony variation of GFP intensity inversely correlated with colony size. Images were taken using 500ms **(B-G)** or 50ms **(H-J)** fluorescence exposure. Triangles and arrows indicate small (low-Lrp) colonies and large (high-Lrp) colonies, respectively. Scale bar=500 μm.

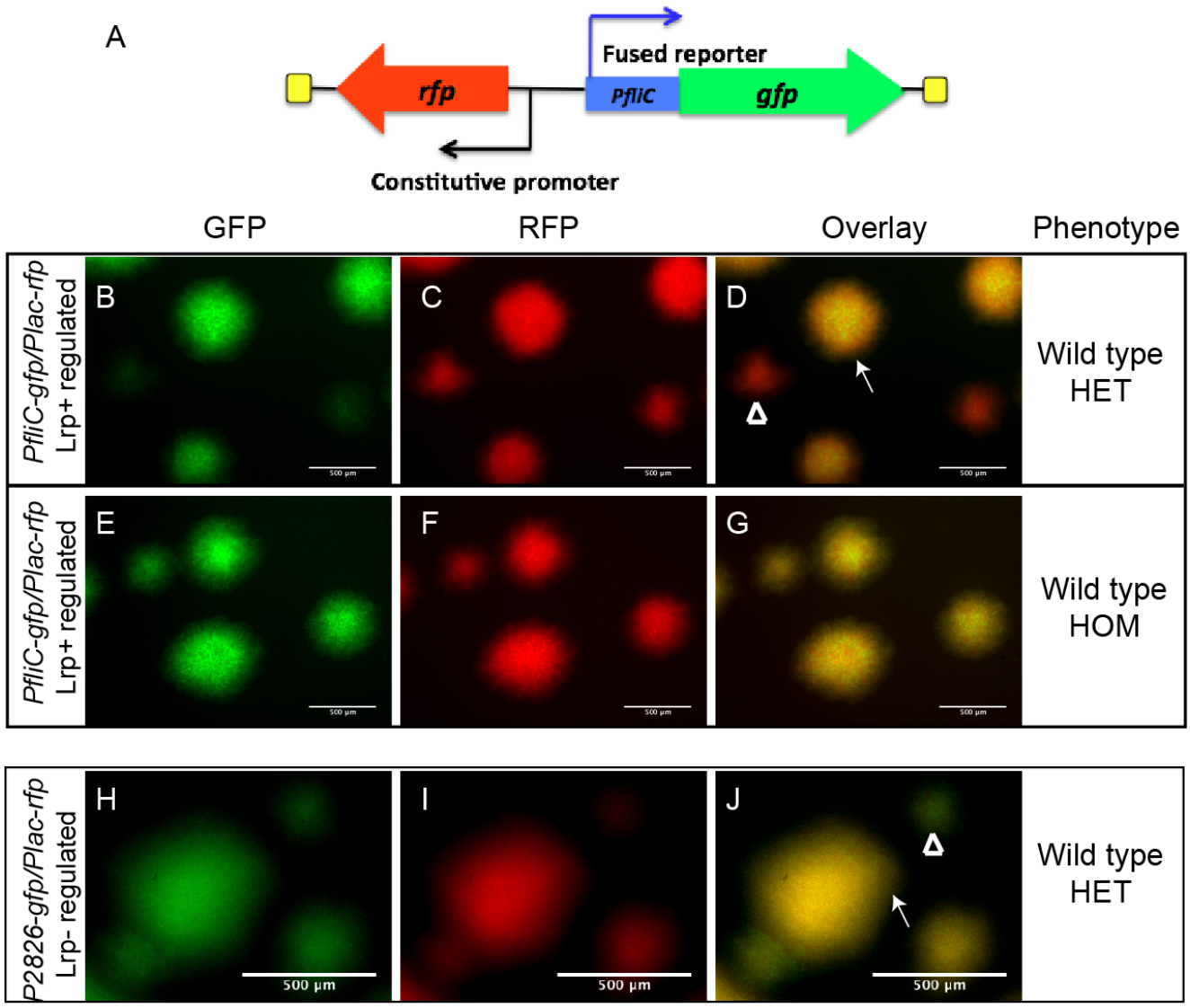
A
Fused reporter
rfp
PfliC
gfp
Constitutive promoter
GFP
RFP
Overlay
Phenotype
PfliC-gfp/Plac-rfp
Lrp+ regulated
B
C
D
Wild type
HET
PfliC-gfp/Plac-rfp
Lrp+ regulated
E
F
G
Wild type
HOM
P2826-gfp/Plac-rfp
Lrp- regulated
H
I
J
Wild type
HET
500 µm

Figure 3.2. Semi-quantitative immunoblotting of Lrp expression levels in the engineered control strains and wild type *X. nematophila* isolates with *PfliC-gfp/Plac-rfp* reporter.

Control strains include no-Lrp (*kefA::* no-*lrp),* low-Lrp (*kefA::* low-*lrp*), high-Lrp (*kefA::* high-*lrp*) (see Chapter 2 for details). Wild type strains include homogeneously low-Lrp SC isolate, homogeneously high-Lrp isolate derived from HGB 1970 (wt.70.HO), and heterogeneous population derived from HGB 1969 (wt.69.HE). A total of 10ng and 5ng of the protein samples were loaded into each well. All bands were shown on the same gel. Bacterial strains were inoculated directly from frozen stock into dark LB media and grew to stationary phase via overnight incubation.

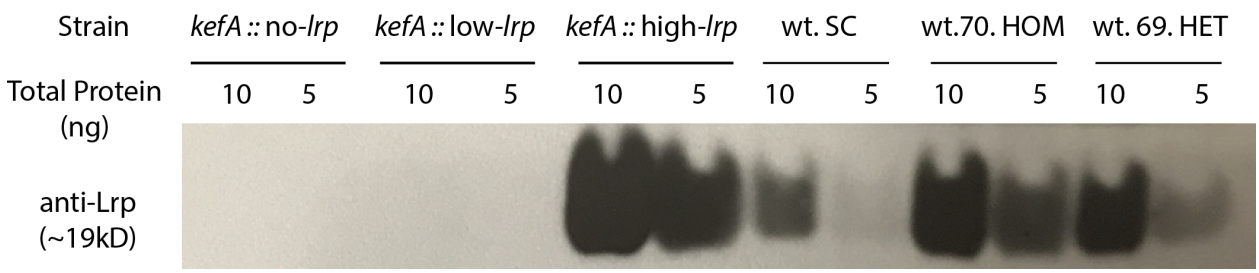

Figure 3.3. Heterogeneous populations are more virulent than homogeneously high-Lrp populations in *Manduca sexta* larvae.

Bacterial strains were grown in LB overnight from frozen stock, sub-cultured (1:100) into fresh LB for 6-8 hours, diluted with PBS and injected into *Manduca sexta* insects 4^{th} instar larvae. A, B, and C represent different independent experiments with different batches of insects. **(A)**: Three heterogeneous stocks (vir-69-HET: red curves) and three homogeneous stocks (vir-69-HOM: blue curves and black dotted curves) carrying Tn7-*PfliC-gfp/Plac-rfp* were isolated from a virulent parental wild type strain HGB 1969 (20). Approximately 2000 bacterial cfu were injected into each of 8 insects per bacterial strain. **(B)**: Three homogeneous stocks derived from a virulence-attenuated wild type *X. nematophila* stock HGB 1970 (20) were isolated (att-70-HOM: black) and assessed for virulence in comparison to the three heterogeneous stocks in panel A (vir-69-HET: red). Approximately 10^4 cells from each bacterial strain were injected into each of 10 insects. **(C):** Heterogeneous and homogeneous populations derived from either a virulent (HGB 1969) or a virulence-attenuated (HGB 1970) parental wild type stock (the same bacterial strains as in A and B) were assessed for virulence in *Manduca sexta.* Approximately 10^4 cfu per bacterial strain was injected into each insect. Either 8 or 10 insects were used for each biological replicate which is represented by one bacterial isolate. Six biological replicates per bacterial strain from two independent experiments (with different batches of insects) were shown. Statistics was analyzed using Two-way ANOVA test followed by Tuckey's multiple comparisons. Standard errors were indicated by error bars. Different letters indicate significantly different statistical groups.

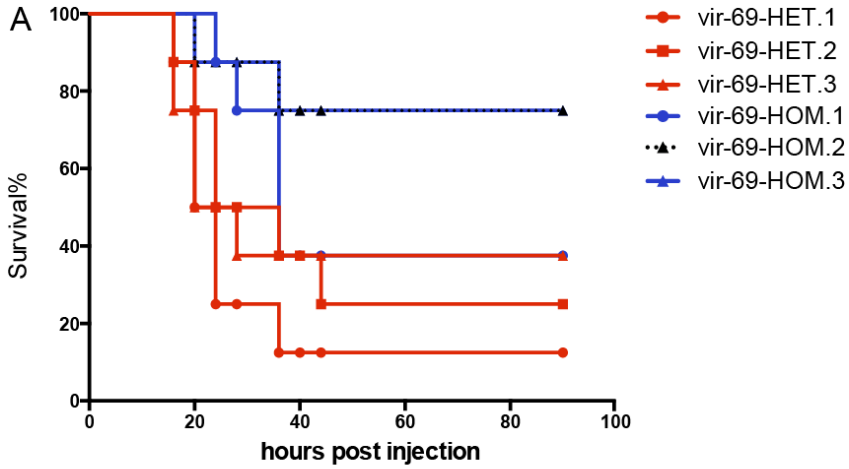
A
Survival%
hours post injection
vir-69-HET.1
vir-69-HET.2
vir-69-HET.3
vir-69-HOM.1
vir-69-HOM.2
vir-69-HOM.3

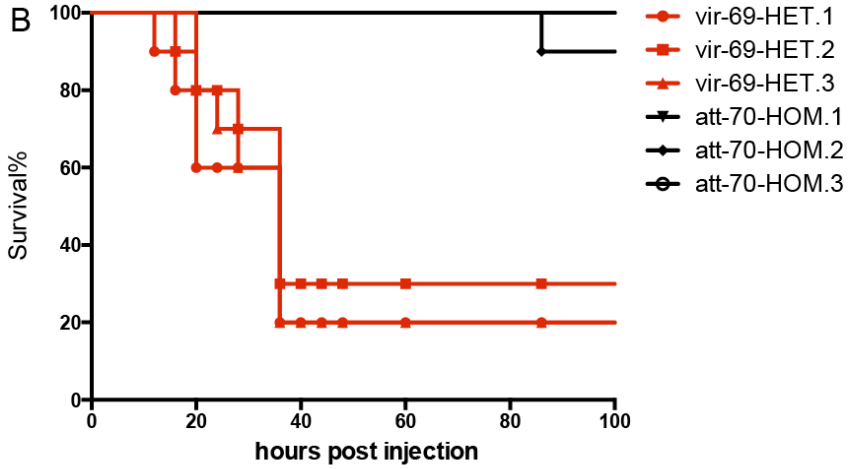
B
Survival%
hours post injection
vir-69-HET.1
vir-69-HET.2
vir-69-HET.3
att-70-HOM.1
att-70-HOM.2
att-70-HOM.3

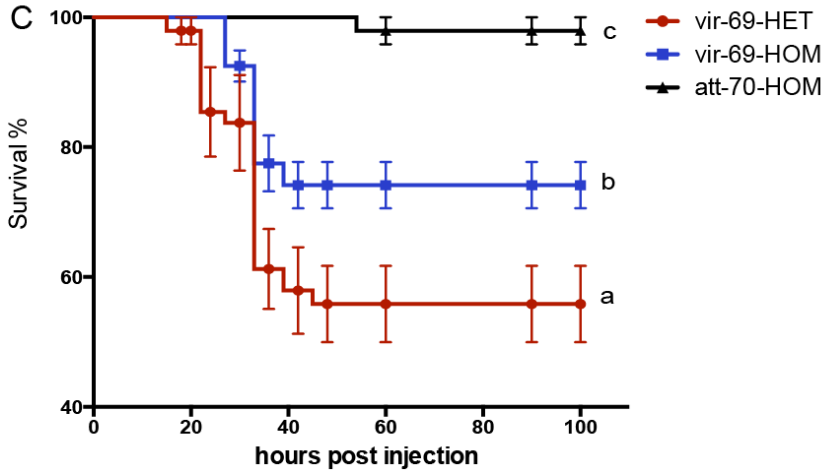
C
Survival %
hours post injection
vir-69-HET
vir-69-HOM
att-70-HOM
c
b
a

Figure 3.4. *PfliC-gfp/Plac-rfp* reporter and single-cell FACS analysis revealed three viable subpopulations in *Xenorhabdus nematophila* Lrp expression.

(**A-F**): Colony composition profiles showing single cells GFP intensity (y-axis) over RFP intensity (x-axis) in one representative colony per colony phenotype or bacterial strain. Percentage (or frequency) of subpopulation at each gate is shown in the figures. Bacterial strains carrying *PfliC-gfp/Plac-rfp* at attTn7 site were struck onto LB agar with (**B and C**) or without chloramphenicol (**A, D, E, and F**). After 16 hours of incubation at 30C, individual colonies were screened using fluorescence microscopy under GFP and RFP double channels, re-suspended in cold PBS buffer, and analyzed via FACS. Colonies expressing no *lrp* **(A),** fixed low-*lrp* on plasmid **(B)**, and fixed high-*lrp* on plasmid **(C)** were used as gating standard. The gating standard was applied to wild type low-Lrp colonies **(D)** and high-Lrp colonies **(E)** from a heterogeneous (HET) population, as well as a wild type high-Lrpcolonies **(F)** from a homogeneous (HOM) high-Lrp population.

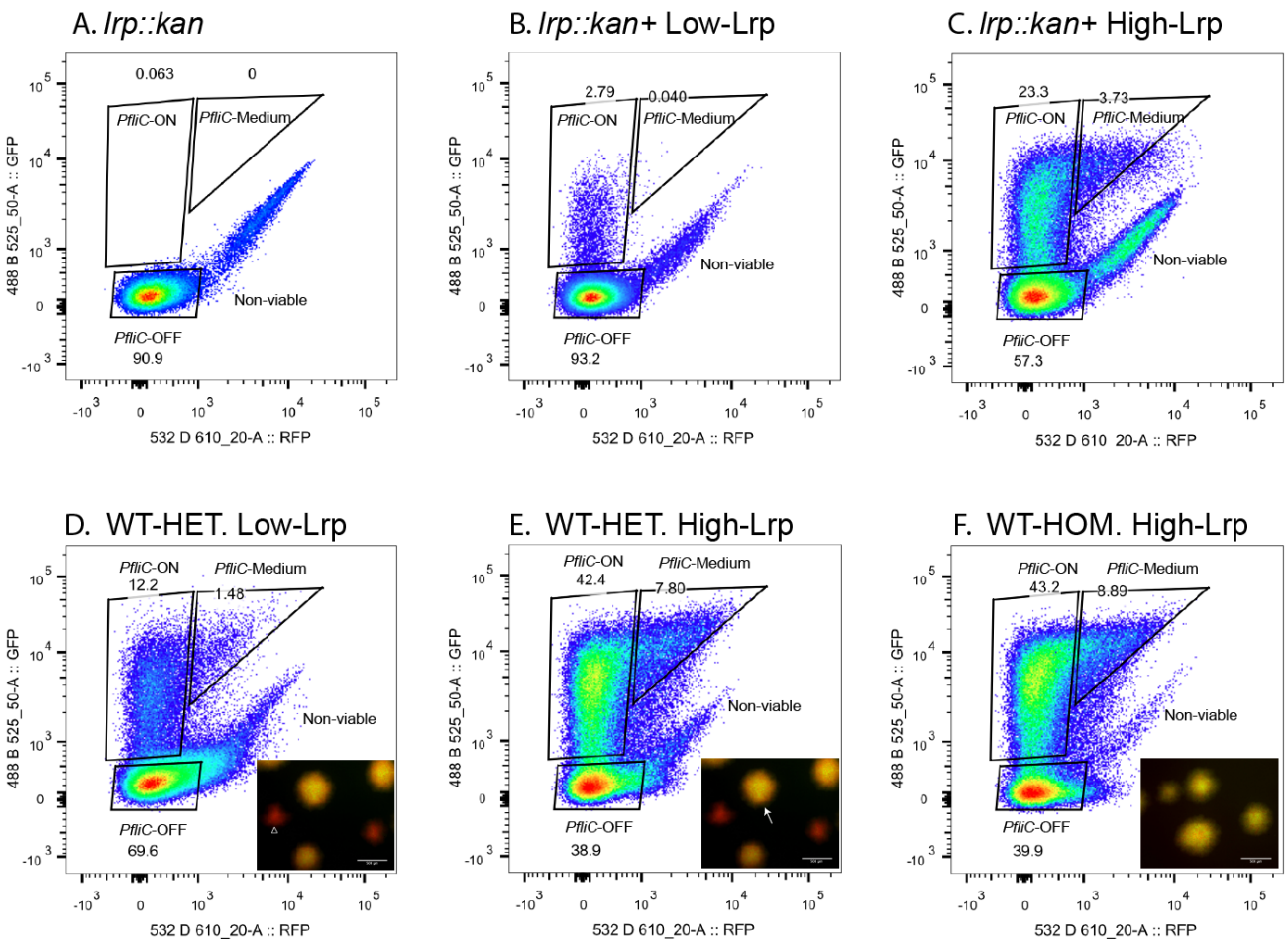
A. lrp::kan
0.063
0
PfliC-ON
PfliC-Medium
Non-viable
PfliC-OFF
90.9
B. lrp::kan+ Low-Lrp
2.79
0.040
PfliC-ON
PfliC-Medium
Non-viable
PfliC-OFF
93.2
C. lrp::kan+ High-Lrp
23.3
3.73
PfliC-ON
PfliC-Medium
Non-viable
PfliC-OFF
57.3
D. WT-HET. Low-Lrp
PfliC-ON
12.2
PfliC-Medium
1.48
Non-viable
PfliC-OFF
69.6
E. WT-HET. High-Lrp
PfliC-ON
42.4
PfliC-Medium
7.80
Non-viable
PfliC-OFF
38.9
F. WT-HOM. High-Lrp
PfliC-ON
43.2
PfliC-Medium
8.89
Non-viable
PfliC-OFF
39.9
488 B 525_50-A :: GFP
532 D 610_20-A :: RFP

Figure 3.5: Quantitative analysis of colony compositions.

According to the gating method in Fig.3.4, *PfliC*-OFF (GFP-low/RFP-low), *PfliC*-ON (GFP-high/RFP-low), and *PfliC*-Medium (GFP-high/RFP-high) subpopulations from wild type low-Lrp and high-Lrp colonies were analyzed to calculate frequency **(A and B)** and averaged single cell fluorescence intensity ratio **(C and D)** in each subpopulation. **(A)** Subpopulation frequency was calculated by percent of cells in each subpopulation (gate) out of total number of cells analyzed in the bacterial population per colony. **(B)** A simplified model interpreting the data of subpopulation frequency in different colonies (from panel A): a low-Lrp colony has significantly lower frequency of *PfliC*-ON subpopulation than a high-Lrp colony. **(C)** Averaged single cell fluorescence intensity ratio was calculated by ratio of averaged GFP intensity divided by averaged RFP intensity among individual cells in each subpopulation (gate). **(D)** A simplified model interpreting the data of average *PfliC* expression in each subpopulation (from panel C): a low-Lrp colony has significantly lower *PfliC* expression from the *PfliC*-ON subpopulation. Three biological replicates were used per bacterial strain. Each biological replicate include analysis of more than 10^5 individual bacterial cells in one colony. One-way ANOVA test was used for statistical analysis followed by Tuckey's multiple comparison. Error bars indicate standard error among biological replicates.

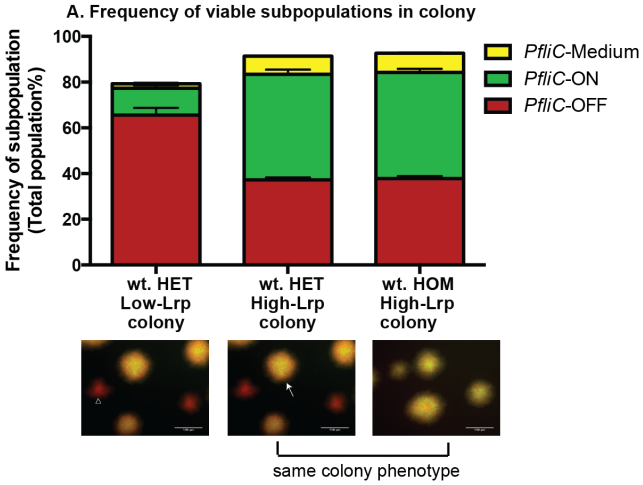
A. Frequency of viable subpopulations in colony
Frequency of subpopulation (Total population%)
100
80
60
40
20
0
PfliC-Medium
PfliC-ON
PfliC-OFF
wt. HET Low-Lrp colony
wt. HET High-Lrp colony
wt. HOM High-Lrp colony
same colony phenotype

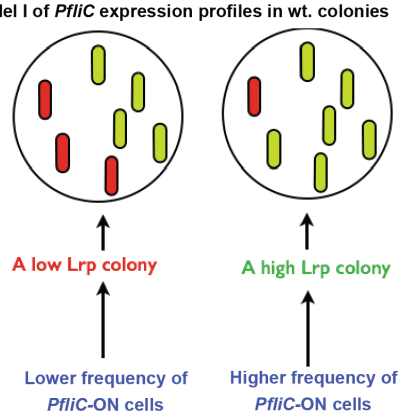
B. Model I of PfliC expression profiles in wt. colonies
A low Lrp colony
A high Lrp colony
Lower frequency of PfliC-ON cells
Higher frequency of PfliC-ON cells

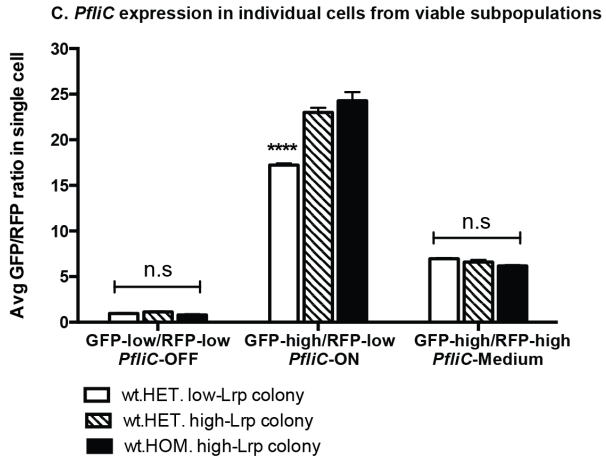
C. PfliC expression in individual cells from viable subpopulations
Avg GFP/RFP ratio in single cell
30
25
20
15
10
5
0
****
n.s
n.s
GFP-low/RFP-low PfliC-OFF
GFP-high/RFP-low PfliC-ON
GFP-high/RFP-high PfliC-Medium
wt.HET. low-Lrp colony
wt.HET. high-Lrp colony
wt.HOM. high-Lrp colony

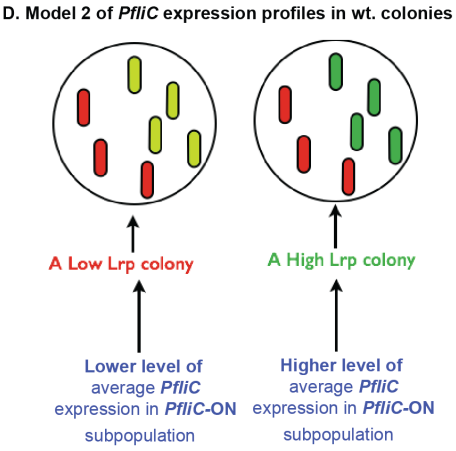
D. Model 2 of PfliC expression profiles in wt. colonies
A Low Lrp colony
A High Lrp colony
Lower level of average PfliC expression in PfliC-ON subpopulation
Higher level of average PfliC expression in PfliC-ON subpopulation

Figure 3.6. Low-Lrp colonies arise in wild type *X. nematophila* population under nutrient-limiting conditions.

A wild type bacterial frozen stock (carrying *PfliC-gfp/Plac-rfp* reporter inserted in *att*Tn7 site) was struck onto 100% strength LB **(A-C)**, 50% strength LB **(D-F)**, and 25% strength LB **(G-I)** agar. After 24 hours of incubation at 30°C, colonies were screened and imaged under epifluorescence scope using 200ms GFP exposure **(A, D, and G)** and 200ms RFP exposure **(B, E, and H)**. Images were overlaid in ImageJ **(C, F, and I)**, Scale bar =100 μm.

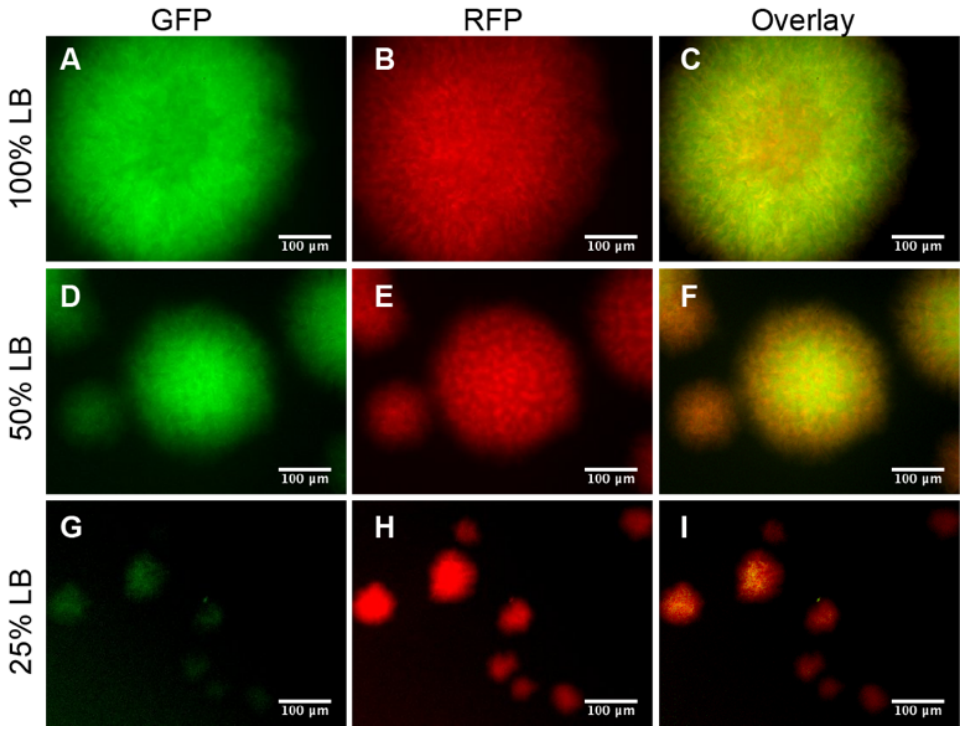
GFP
RFP
Overlay
100% LB
50% LB
25% LB
A
B
C
D
E
F
G
H
I
100 µm

Figure 3.7. The effects of casamino acids and glucose on Lrp-dependent population heterogeneity in wild type bacteria under nutrient-limiting conditions.

(A and B) Wild type bacteria were inoculated into LB from frozen stock, grew overnight, washed, and subcultured into minimal medium supplemented with either casamino acids **(A)** or glucose **(B).** Bacteria were grown in defined media for 3 days, and then subcultured into fresh LB medium for overnight growth. **(C)** Bacteria were inoculated from frozen stocks into LB medium, incubated overnight, washed, and subcultured into minimal medium supplemented with both casamino acids and glucose, then grew overnight to stationary phase (~10^9 cfu/mL). Each day of incubation, bacterial cultures were serially diluted, plated onto LB agar (5-6 dilutions, 3 droplets of 10μL samples per dilution as technical replicates), grew for 16-20 hours at 30°C. Low-Lrp colonies were identified and counted using epifluorescence microscopy across several dilutions to determine the optimal dilution for counting (i.e. the optimal dilution that contains 10-30 low-Lrp colonies in each10μL of sample). Bacterial CFU were calculated and corrected to CFU/10μL of the optimal dilution. Percent low-Lrp is calculated by number of low-Lrp colonies divided by number of CFU in 10μL of optional dilution. The averaged low-Lrp% from 3 technical replicates were used in 1 biological replicate. A total six biological replicates per bacterial strain from 3 independent experiments are shown in the figure.

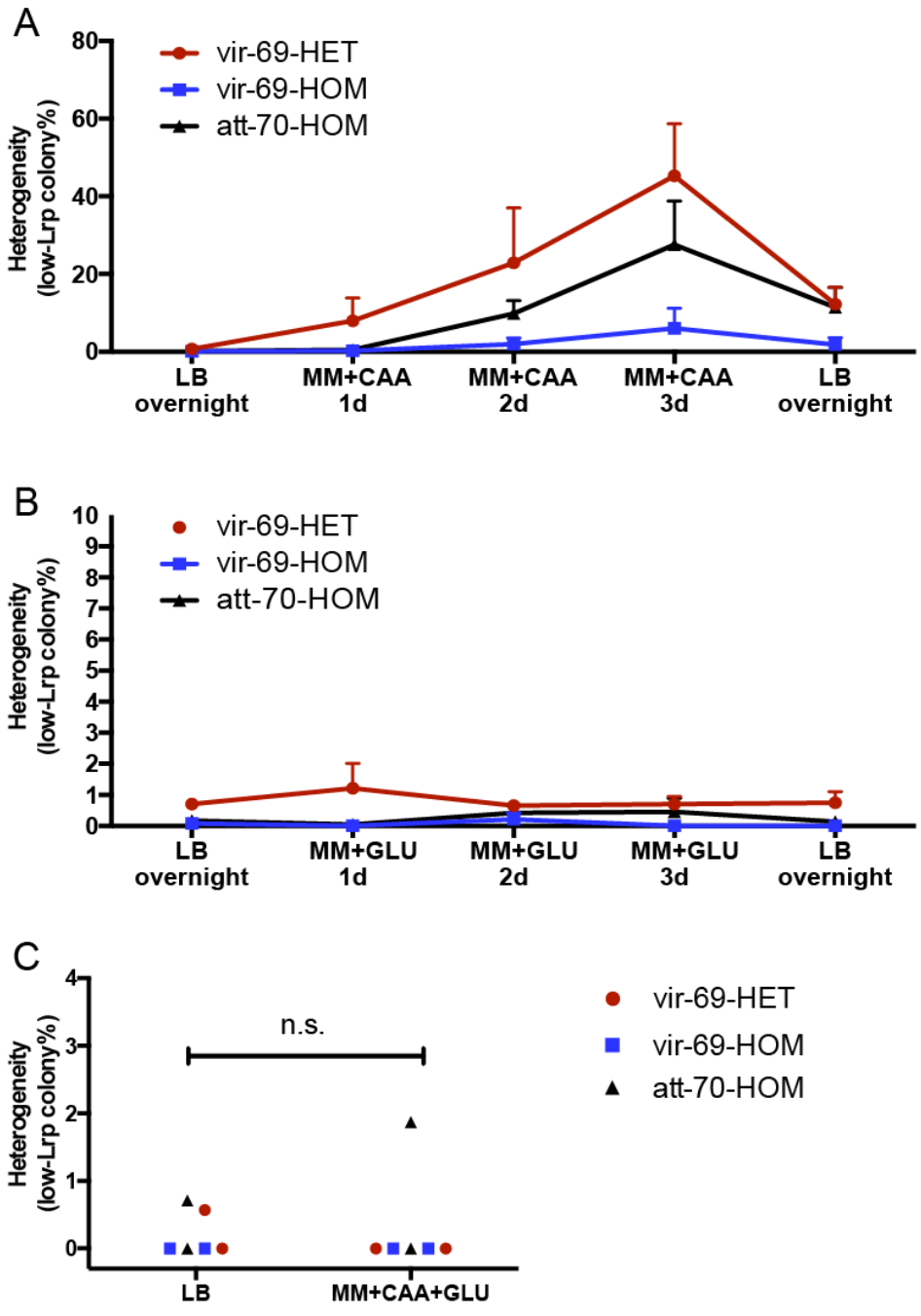
A
Heterogeneity (low-Lrp colony%)
80
60
40
20
0
vir-69-HET
vir-69-HOM
att-70-HOM
LB overnight
MM+CAA 1d
MM+CAA 2d
MM+CAA 3d
LB overnight
B
Heterogeneity (low-Lrp colony%)
10
9
8
7
6
5
4
3
2
1
0
vir-69-HET
vir-69-HOM
att-70-HOM
LB overnight
MM+GLU 1d
MM+GLU 2d
MM+GLU 3d
LB overnight
C
Heterogeneity (low-Lrp colony%)
4
3
2
1
0
n.s.
LB
MM+CAA+GLU
vir-69-HET
vir-69-HOM
att-70-HOM

Figure 3.8 The correlation of Lrp heterogeneity with the bacterial growth yield in glucose.

Vir-69-HET (red curves), vir-69-HOM (blue curves), and att-70-HOM (black curves) were grown in LB medium overnight, washed, and sub-cultured into minimal medium supplemented with glucose (MM+GLU) to approximate growth yield (left y-axis) and into minimal medium supplemented with casamino acids (MM+CAA) to approximate Lrp heterogeneity (low-Lrp colony%, right y-axis). According to the bacterial growth yield in MM+GLU, populations were categorized into high growth yield (>10^8 cfu/mL) **(A-C)**, low growth yield (10^5-10^8 cfu/mL) **(D-F)**, and no growth yield (<10^4 cfu/mL) **(G)**. Each curve represents an independent bacterial population. The same starting population used for inoculating MM+GLU (dashed line) and MM+CAA (solid line) were labeled with the same shape at each time point on the same graph. Data show 6 populations of each bacterial strain (6 biological replicates) from 3 independent experiments.

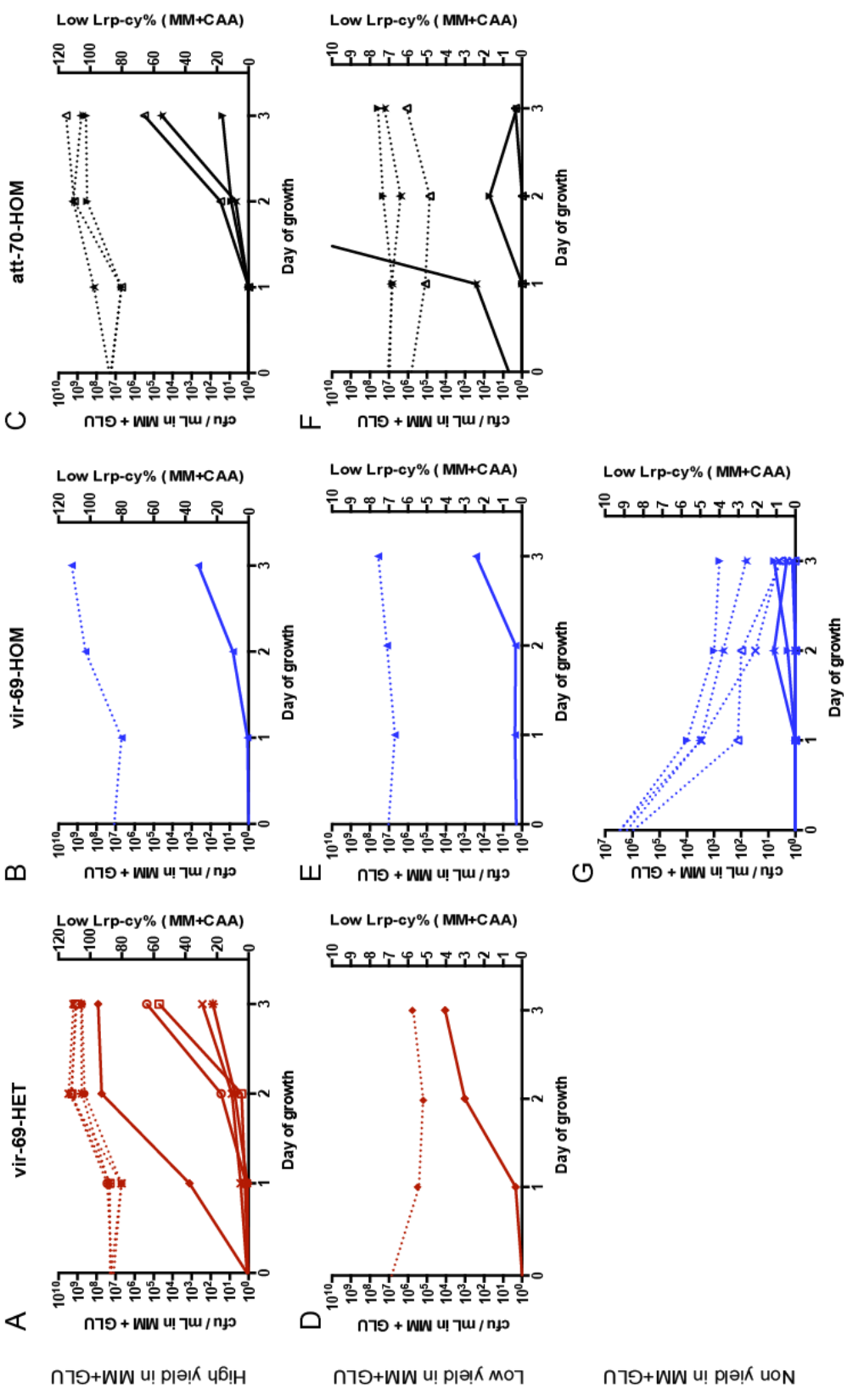
A
vir-69-HET
B
vir-69-HOM
C
att-70-HOM
D
E
F
G
Low Lrp-cy% (MM+CAA)
cfu / mL in MM + GLU
Day of growth
High yield in MM+GLU
Low yield in MM+GLU
Non yield in MM+GLU

Figure 3.9. Current model for Lrp-dependent phenotypic switch in *X. nematophila* life cycle.

I hypothesize that the nutrient shift when bacteria transit from insect to nematode host triggers the high-to-low Lrp switch in population. Such switch is promoted by either the presence of amino acids or the absence of glucose. The population heterogeneity serves as pre-adaptive responses to better confer the virulence in the upcoming infection stage. Another nutritional switch from IJ receptacle to the insect blood cavity, likely the presence of glucose, inhibits the growth of high-Lrp cells that are immunogenic (22)

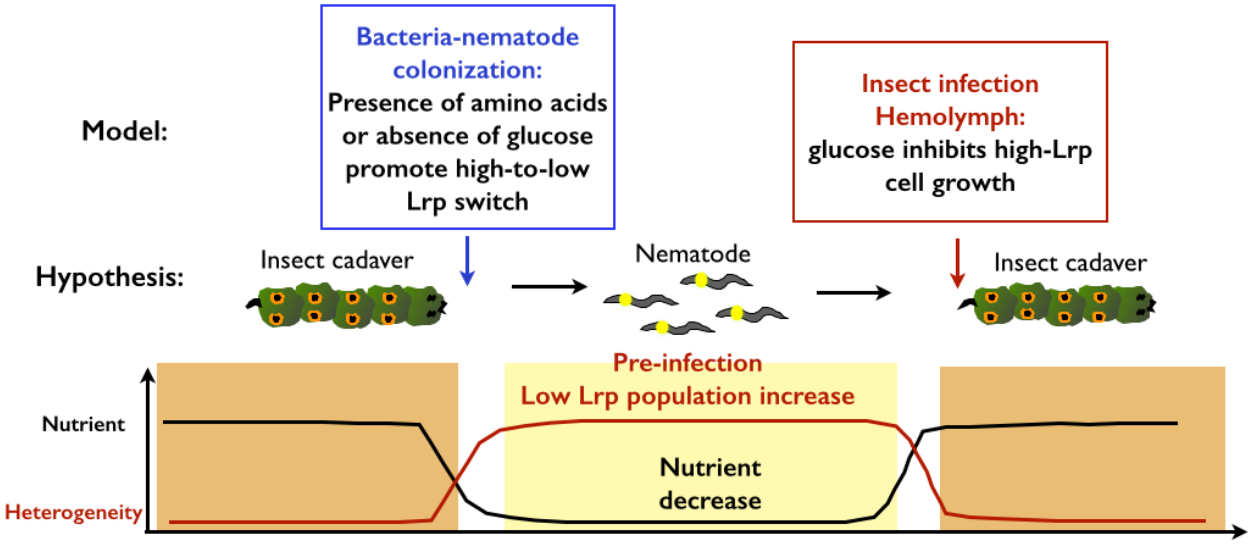
Model:
Bacteria-nematode colonization:
Presence of amino acids or absence of glucose promote high-to-low Lrp switch
Insect infection Hemolymph:
glucose inhibits high-Lrp cell growth
Hypothesis:
Insect cadaver
Nematode
Insect cadaver
Pre-infection
Low Lrp population increase
Nutrient
Heterogeneity
Nutrient decrease

Supplemental Figures for Chapter 3:

Figure S3.1: selected examples of diverse phenotypes of wild type *X. nematophila* colonies based on *PfliC-gfp/Plac-rfp* reporter.

Bacteria were inoculated from frozen stock directly into LB media, washed, and sub-cultured in minimal medium supplemented with casamino acids (with extra trace glutamate and aspartate) for 3 days, then plated onto LB agar and imaged using epifluorescence microscopy. These phenotypes include ‘green colonies’ (high GFP/RFP intensity), red colonies (low GFP/RFP intensity, but not SC), radiant colonies (concentric rings of alternating low and high GFP/RFP intensity), and sectored colonies (quarter, half, or full colonies with low or high GFP/RFP intensities). Note that the ‘low’ and ‘high’ GFP/RFP intensity were considered relative, with a range of GFP/RPG overlaid colors from ‘red’, ‘orange’, ‘yellow’, to ‘green’.

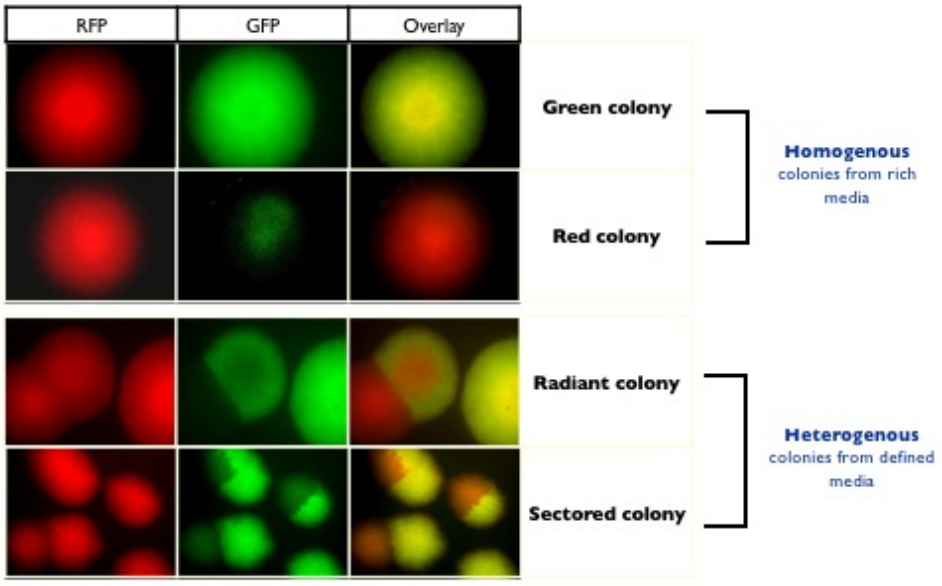

Figure S3.2: Lrp-dependent reporters showing the number of low-Lrp sectors per colony on minimal medium supplemented with casamino acids agar plate over time.

The number of low-Lrp sectors per colony was assessed using either *PfliC-gfp/Plac-rfp* reporter (low GFP/RFP, left Y-axis) or *PXNC1_2826-gfp/Plac-rfp* reporter (high GFP/RFP, right Y-axis) over 4 days of incubation on minimal medium supplemented with casamino acids. Wild type bacteria carrying either *PfliC-gfp/Plac-rfp* or *PXNC1_2826-gfp/Plac-rfp* were directly inoculated in LB liquid medium from frozen stock and incubated overnight. Overnight cultures were washed in 1XPBS and serially diluted. Three droplets of 10μL samples from each of the five dilutions were spotted onto MM+CAA agar for and incubated for 4 days. Colonies were counted to estimate the CFU/10μL at each dilution. Every 24h post incubation on MM+CAA agar, low-Lrp sectors were screened using epifluorescence microscopy. The number of sectors per colony is estimated using total low-Lrp sectors per spot divided by total CFU of the same spot. Each biological replicate represents the average of three technical replicates at each time point (3 spots of 10μL sample). Each data point and error bars represents the average and SEM from two biological replicates in one experiment.

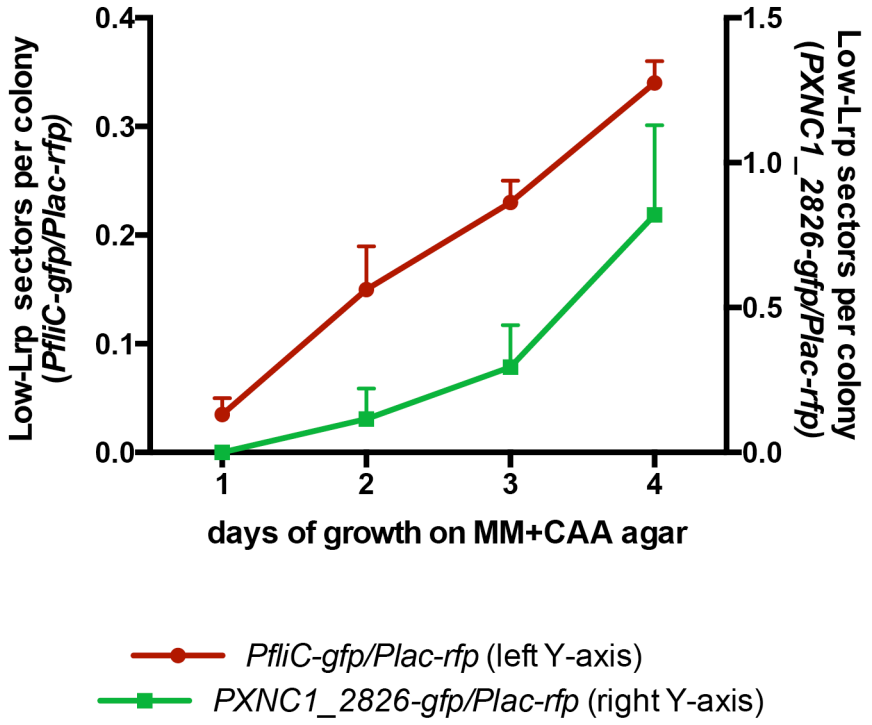
Low-Lrp sectors per colony
(PfliC-gfp/Plac-rfp)
0.4
0.3
0.2
0.1
0.0
1.5
1.0
0.5
0.0
Low-Lrp sectors per colony
(PXNC1_2826-gfp/Plac-rfp)
1
2
3
4
days of growth on MM+CAA agar
PfliC-gfp/Plac-rfp (left Y-axis)
PXNC1_2826-gfp/Plac-rfp (right Y-axis)

Chapter 4:

The symbiotic bacterium *Xenorhabdus nematophila* shifts from a mutualistic to a pathogenic population when associated with the transmission stage of the nematode *Steinernema carpocapsae*

Mengyi Cao: hypotheses, perform experiments, data analysis, writing.

Heidi Goodrich-Blair: Writing and editing.

Abstract

The symbiotic bacterium *Xenorhabdus nematophila* alternates between two invertebrate hosts in its natural life cycle: it engages in a mutualistic interaction with the nematode *Steinernema carpocapsae,* and it is a pathogen of the insect prey that *S. carpocapsae* infects. *X. nematophila* exhibits a phenotypic variation phenomenon termed virulence modulation (VMO), in which wild type bacteria switch between these two symbiotic states depending on the expression levels of the transcription factor Lrp (leucine-responsive regulatory protein): bacteria expressing high levels of Lrp are mutualistic towards nematodes but attenuated in virulence towards insects; while low-Lrp expressing bacteria are virulent towards insects but defective in nematode mutualism (Chapter 1 and 2). Based on my previous chapter, I have proposed the hypothesis that Lrp high (mutualism)-to-low (pathogenesis) switch occurs during bacteria-nematode interactions (Chapter 3) prior to infection stage. In this Chapter, I investigated the influence of *X. nematophila* Lrp levels specific stages of bacteria-nematode interaction, including *X. nematophila* colonization of developing nematode juveniles and adults and of the infective juvenile (IJ) stage of the nematode that transmits it between insect hosts. By comparing fixed-Lrp strains to wild type bacteria, I estimated the Lrp expression levels of wild type bacteria at specific stage of host-symbiont interaction. My data show that high Lrp expression by *X. nematophila* is optimal for early stages of bacteria-nematode association: colonization initiates at a higher percent population in nematode adults, juveniles, and pre-IJs. Further, once IJs form and begin to emerge, the percentage of colonized IJs by high-Lrp cells in these nematodes maintains at high level over time of emergence, while percentage of colonized IJs by a low-Lrp cells drops significantly faster compared to those colonized by a high-Lrp expressing strain. In contrast, after IJ colonization and during bacterial outgrowth, low-Lrp expressing cells arise; a low-Lrp expressing strain exhibits a higher number of average bacterial CFU per IJ than does a high-Lrp strain. To examine if *X. nematophila* Lrp expression levels naturally vary during the IJ stage I used an Lrp-dependent fluorescence reporter to monitor

bacterial population heterogeneity in both aging IJs and IJs emerging from bacterial lawns over time. Fluorescence quantification revealed that low-Lrp subpopulations arise significantly during the IJ aging process, suggesting a population shift from nematode mutualistic (high-Lrp) to the insect pathogenic (low-Lrp) occurs when bacteria grow and persist in IJ nematodes.

Introduction

Xenorhabdus nematophila virulence modulation is a phenotypic variation phenomenon that is influenced by nutritional conditions

Phenotypic variation is a phenomenon that occurs in many symbiotic microbes that leads to population heterogeneity. A heterogeneous population is composed of subpopulations of different functions, with each subpopulation fits a possible environment in the bacterial life cycle. Such bet-hedging strategy benefits the bacterial population for better adaptive performance in randomly or predictably varying environments (1–3). Population heterogeneity usually occurs during the transitional stage when bacteria switch from one environment to the other, such as transmission among different hosts, colonizing different host niches, or changing in between free-living and host-associated states. For example, the malaria parasites (*Plasmodium spp.*) show phenotypic plasticity depending on the host environment of the life stage: an asexual reproduction state during within-host survival (virulent) and a sexual reproduction state for host-to-host transmission (virulence variation). Recent research provided empirical evidence showing that environmental signals during transmission stage (such as nutrient release from the host) could increase the rate of asexual-to-sexual reproduction conversion in *Plasmodium,* which increases the genetic variation among the progenies. Such population heterogeneity benefits the parasite adaptive performance by maintaining genetic diversity for both infection (virulence-on, reproduction-off) and transmission (virulence-off, reproduction-on) of the next stage in life cycle (4). During the life cycle of bacterial pathogen *Vibrio cholerae*, a short-term persistence state appears in the transition period that occurs when

bacteria are released from a mammalian host into the aquatic environment. *V. cholerae* exhibits population heterogeneity during this transition period, with the majority of the population forming biofilm-like aggregates (biofilm-on, virulence-off) and a minority of the population expressing virulence (biofilm-off, virulence-on). Population heterogeneity during the short-term persistence period is proposed to provide a bet-hedging opportunity for bacteria to either form a biofilm and associate with a chitinous surface for long-term persistence (biofilm-on, virulence-off); or to immediately infect another mammalian host if available (biofilm-off, virulence-on) (5–8). Another example is the association of *Yersinia pestis* with the flea, the invertebrate vector that transmits the bacteria among different mammalian hosts. The flea host environment induces certain *Y. pestis* genes, including those encoding toxins. These flea-induced transcriptional changes in *Y. perstis* are proposed to prepare the bacteria for success in the upcoming infection of mammalian host (9).

Another symbiont that undergoes phenotypic variation is *X. nematophila,* a bacterium with a life cycle that can be generally categorized into three stages: the infection of an insect host (pathogenic interaction), the reproductive stage in the insect cadaver (mutualistic interaction), and transmission through infective juvenile (IJ) nematodes (also considered a mutualistic interaction). During the transmission stage, *X. nematophila* is associated with the IJ nematode in an intestinal pocket, the receptacle. IJ nematodes in the soil seek and enter the insect host and release the symbiotic bacteria into the insect hemocoel, where the bacteria and nematode kill the insect host (10). The insect cadaver provides a nutrient-rich environment for the reproductive stage of the mutualistic pair. While nematodes feed on *X. nematophila* directly as food source (Cao and Foye *et al.,* unpublished data), the bacteria also produce exoenzymes to convert insect tissue into nutrients to support nematode reproduction. As nutrients are depleted in the insect cadaver, *S. carpocapsae* juvenile nematodes develop into IJs, re-associate with the bacteria in the receptacle, and enter the transmission stage to seek another insect host (10).

X. nematophila bacteria associate with *S. carpocapsae* nematodes in a species-specific manner at each developmental stage of the nematode life cycle (Fig. 4.1) (11, 12). During the reproductive phase of the bacteria-nematode symbiosis, *Steinernema* nematodes recover from the infective juvenile (IJ) state into J4 juveniles, which in turn develop into adults that go through sexual reproduction. Once hatched from eggs, the next generation of juvenile nematodes (J1-J4) can again develop to become reproductive adult nematodes. In these adult and juvenile nematodes, *X. nematophila* bacteria specifically localize to the anterior intestinal caecum (AIC), where they adhere to the epithelial cell surface. In response to nutrient depletion (such as less bacteria and less nutrients from insect cadaver) and increased nematodeor population density, J2 juvenile nematodes undergo an alternate developmental path becoming pre-IJs in which the intestinal lumen gradually collapses. In pre-IJs, one or few *Xenorhabdus* bacterial cells localize to an extracellular pocket formed by nematode host cells in the nematode pharyngeal intestinal valve (PIV), a region between the esophagus and the intestinal lumen (12). As pre-IJs develop into non-feeding IJs, a few individual *X. nematophila* bacterial cells initiate colonization of the intestinal lumen (possibly migrating from the PIV), in the immature, pre-migratory IJs (which have not yet emerged from the insect cadaver) (12, 13). As IJs mature, the bacteria then multiply into a nearly clonal population (a process termed ‘bacterial outgrowth) (13). After emergence from the cadaver the mature IJs retain their bacterial symbionts as they age in the soil before finding a new insect host (14–16).

Previously a *X. nematophila* phenotypic variation phenomenon termed virulence modulation (VMO) was discovered, in which bacteria switch in between at least two phenotypic states depending on the expression level of global transcription factor leucine-responsive regulatory protein (Lrp). Bacterial cells expressing relatively high levels of Lrp are mutualistic towards nematodes during the reproductive stage, but are attenuated for virulence towards insects during the infection stage. In contrast, the bacterial cells expressing relatively low levels of Lrp are virulent towards insects but are defective in supporting nematode reproduction

(Chapter 2) (17–20). As yet, the impact of phenotypic variation on *X. nematophila* colonization of nematodes during each stage of the life cycle had not been explicitly investigated and is the focus of the experiments presented in this chapter. Previously, I have shown that Lrp high-to-low switch occurs during nutrient-limiting condition, creating a heterogeneous population that facilitates bacterial virulence (Chapter 3). Based on these data, I hypothesized that the mutualistic (high-Lrp) to pathogenic (low-Lrp) population shift occurs during bacteria-nematode association when host environment is limited in nutrients, facilitating the bacterial virulence for the upcoming infection stage. In this chapter, I will also present evidence to support this hypothetical model.

Results

X. nematophila bacterial lawn expressing fixed high levels of Lrp associate with early developmental stages of *S. carpocapsae* with a high frequency (Figure 4.2)

In the previous chapter I demonstrated that bacteria expressing high levels of Lrp better promote nematode reproduction and form more robust biofilms than their low-Lrp counterparts (Chapter 2). Based on these findings, I hypothesize that relative to low-Lrp expressing cells, high-Lrp expressing cells better associate with reproductive stage of nematodes (juveniles and adults) by forming biofilm-like adherent at AIC. To test this, I grew aposymbiotic nematodes on lawns of *X. nematophila* expressing no-*lrp,* low-*lrp,* and high-*lrp* in vitro and examined colonization phenotypes as nematodes developed. Using constitutively expressed green fluorescent protein to visualize the bacteria within nematodes, I screened by microscopy adult and juvenile nematodes for the presence of bacteria at the AIC (Fig. 4.2) and estimated AIC colonization frequency. My data show that both adult and juvenile nematodes cultivated with high-Lrp expressing bacteria are more frequently colonized at the AIC region than are nematodes cultivated with either low-Lrp or no-Lrp strains (Fig. 4.2).

Next I investigated if Lrp expression levels in *X. nematophila* affect pre-IJ PIV colonization. I identified pre-IJs within the developing nematode population by virtue of the presence of bacterial localization at PIV, either with an open or a collapsed intestine. I found that when associated with high-Lrp expressors, pre-IJ nematodes with either open or closed intestine were more frequently colonized at the PIV than were pre-IJs associated with low-Lrp or no-Lrp strains (Fig.4.2). Also as expected, immature IJs are more frequently colonized in the receptacle if they developed in the presence of high-Lrp expressers than with low- or no-Lrp expressers (Fig. 4.2). These data show that in comparison to low-Lrp or no-Lrp expressers, *X. nematophila* expressing high levels of Lrp have better ability to attach to AIC of reproductive stage of nematodes, to occupy the PIV in pre-IJs, and to enter the IJ receptacle. These findings support our hypothesis that high-Lrp expressers are adapted for mutualism with the nematode, including supporting nematode fecundity (Chapter 2) and associating with nematode tissues (this chapter). High Lrp expressers are also adapted to initiate colonization of the nematode IJ, ensuring their transmission to the next generation.

X. nematophila expressing either fixed high or fixed low levels of Lrp showed wild type level outgrowth rate in the immature IJs (Figure 4.3)

Following initiation of colonization, *X. nematophila* cells multiply in the receptacle of a maturing IJ (Fig. 4.3A) (12, 13). I investigated next if Lrp expression levels affect this outgrowth process (Fig. 4.3). I isolated immature IJs away from all other nematode developmental stages developing on bacterial lawns expressing no-, low-, high- Lrp, and a wild type strain (see Materials and Methods for strain description), and assessed bacterial outgrowth in the IJ receptacle by estimating CFU per colonized IJ every 12 hours for 5 days (Fig. 4.3B). Consistent with previous research, the *lrp* mutant (no-Lrp strain) had a defect in bacterial outgrowth (21). However, bacteria expressing either high- or low- levels of Lrp showed wild-type levels of outgrowth in the immature IJ receptacle. Thus, while *lrp* is important for outgrowth in the

nutrient-limiting IJ receptacle, the levels of Lrp expressed by individual bacterial cells was not critical.

X. nematophila expressing fixed low levels of Lrp colonize mature IJs at higher levels than their high-Lrp counterparts (Figure 4.4)

I next investigated if Lrp expression levels impact bacterial colonization of mature IJs emerging from bacterial lawns into water traps (Fig. 4.4). Previously, I have shown that in a pool of cumulative IJs (emerged in two weeks post water trap), high-Lrp expressors associate with nematodes at a higher percentage population than low-Lrp expressors (Chapter 2). To test if the timing of nematode emergence affects Lrp-dependent colonization, I harvested emerging IJs at various days after trapping and assessed the colonization frequency of IJs by the presence of GFP-expressing bacteria in the IJ receptacle among 150 IJs per water trap per time point (Fig. 4.4A). My data show that over time, nematodes emerging from lawns of bacteria expressing no-Lrp or low- levels of Lrp exhibit decreasing frequencies of colonization, while the high-Lrp expressers maintained higher colonization frequency among later-emerging IJs (Fig. 4.4A), suggesting high-Lrp expression is important for maintaining high level of colonization frequency in the later-emerged IJs.

The data presented above indicate that a nematodes cultivated with a low-Lrp expresser is less likely to be colonized. Next, I determined if, once an IJ is colonized there is any difference in the final bacterial population size depending on the Lrp expression level of the bacterial cells. To also test if timing of nematode emergence affect symbiont carriage, I used colonization frequency and average CFU/IJ calculations to estimated the average bacterial carriage per individual colonized IJ over 6 days of IJ emergence(Fig. 4.4B). My data showed a trend that low-Lrp expressers have a higher number of CFU per colonized IJ in all nematode populations regardless of day of emergence (Fig.4.4B). In addition, Low-Lrp expressers showed wild type level bacterial carriage on day 1, 2, 4, and 6 of emergence. However, only nematodes

emerged from low-Lrp bacterial lawns on earlier days (especially on day 2) post water trap showed significantly higher CFU per colonized IJ in comparison to those associated with high-Lrp bacteria. These data suggest that once colonized, low-Lrp bacteria maintain higher symbiont loads in mature IJs , particularly in earlier emerging IJs.

Based on my data (Fig. 4.4), I further explore the how Lrp affect symbiont load in cumulative mature IJs. To exclude the possibility that the Lrp-dependent association with nematodes (Fig. 4.2-4.4) is specific to the particular *gfp* reporter (*purr225*) I used in the previous experiments, I used a *Plac-rfp* based fluorescence screen to assess bacterial colonization frequency (Fig. 4.5). My data show that wild type bacteria and fixed high-Lrp expressers have a significantly higher colonization frequency in the initiation of IJ colonization in comparison to no- or low- Lrp fixed strains (Fig. 4.5A). In contrast, low-Lrp expressers showed significantly higher CFU per colonized IJ than high-Lrp and no-Lrp bacteria. Wild type bacteria (which presumably have heterogeneous populations with respect to Lrp expression levels) exhibited an intermediate level of CFU per colonized IJ that is not significantly different from either fixed high-Lrp or low-Lrp expressers. These data further confirmed the statistical differences in high- and low- Lrp expressing cells in bacterial carriage in mature IJ receptacle, suggesting that high-to-low Lrp population shift occurs in the mature IJs.

Wild type *X. nemaotphila* population shift from high-Lrp to low-Lrp in aging IJs (Figure 4.6)

In the previous chapter (Chapter 3), experiments using laboratory culture showed that population heterogeneity, characterized by a rise in low-Lrp expressing cells among the starting population of high-Lrp expressing cells, increases when populations are moved from a nutrient rich environment to a nutrient limiting environment, except when glucose is present in the latter. In addition, populations with heterogeneous Lrp expression are more virulent than homogeneous populations that contain only high-Lrp colonies. Based on these data, I hypothesized that *X. nematophila* cells switch from high- to low-Lrp states when they transition

from a nutrient-rich insect cadaver to the nutrient-limiting nematode host (22). The data described above indicated that within the receptacle of mature IJs, low-Lrp expressers multiply to higher numbers than do high-Lrp expressers, suggesting that this stage of the *X. nematophila* life cycle may be the one in which cells switch from the high-Lrp (mutualistic) to the low-Lrp (pathogenic) state, or that the latter cell type is selected (Fig. 4.7). Consistent with this idea, nutrient limitation during growth in laboratory medium promotes a shift from high-Lrp to low-Lrp expression in wild type populations, and after outgrowth the IJ receptacle is likely to be nutrient limiting.

To determine if *X. nematophila* cells in a mature IJ nematode are switching from high-Lrp to low-Lrp expression levels I used wild type *X. nematophila* expressing a *PfliC-gfp/Plac-rfp* reporter of Lrp levels to assess the frequency of high-Lrp and low-Lrp expressers in vivo. For this experiment I used several different wild type backgrounds as in Chapter 3: (i) vir-69-HET: a heterogeneous (high-Lrp and low-Lrp CFU) wild type population derived from a virulent parent; (ii) vir-69-HOM: a homogeneous wild type (high-Lrp colonies only) population derived from a virulent parental strain; and (iii) att-70-HOM: a homogeneous high-Lrp wild type population derived from a virulence-attenuated parental strain (Fig. 4.6).

Since I have observed the timing of IJ emergence could affect mature IJ colonization, I hypothesized that the switch from high-to-low Lrp expression occurs as IJs age, or that the switch occurs in later-emerging IJs in response to signals from nutrient-depletion in the agar or from the dense nematode population. To test these hypotheses, I assessed population heterogeneity (percentage of low-Lrp colonies) of bacteria grown in lamino acids and glucose as described in Chapter 3 (Fig. 4.6A and B) or isolated from aging IJ nematodes (Fig. 4.6C and D). For *X. nematophila* extracted from the aging IJ nematodes (Fig.4.6C), the low-Lrp colony frequency increased over the time course of IJ aging (4 weeks). The level of heterogeneity is strain-dependent: comparing to the other two wild type strains vir-69-HET and att-70-HOM, vir-69-HOM that showed significantly lower population heterogeneity (i.e. less switching from high-

Lrp to low-Lrp expression) in vitro (Fig. 4.6A) is consistent with the phenotype in vivo, showing a significantly lower heterogeneity compared to other strains when aged in the mature IJs (Fig. 4.6A). These data support the hypothetical model that MM+CAA may be mimicking the nutritional conditions encountered by *X. nematophila* within the aging IJ receptacle that induces a population switch from high-to-low Lrp expression and promotes a conversion of populations toward pathogenic phenotype. In contrast, similar to bacteria grown in MM+glucose as a negative control (Fig.4.6B), bacteria extracted from IJs emerged from later weeks did not show a significant high-to-low Lrp switch (Fig.4.6D), suggesting the timing of IJ emergence does not significantly affect high-to-low Lrp population conversion. Together, my data have that the bi-stable expression of Lrp (high-Lrp colony + low-Lrp colony) could be induced under laboratory conditions both in vitro and in vivo. Such population heterogeneity contributes to Lrp-dependent virulence modulation during bacteria-nematode association at transmission stage of the symbiotic life cycle.

Discussion

Lrp regulates early stage of *Steinernema-Xenorhabdus* colonization events

In this chapter, our data show that Lrp expression levels regulate the bacteria-nematode association frequencies in multiple stages of *S. carpocapsae* lifecycle. *X. nematophila* expressing high levels of Lrp promotes the colonization frequency with all developmental stages of nematodes up to immature IJ (Fig. 4.2), raising the question on what molecular mechanisms regulates Lrp-dependent bacteria-nematode association. The species-specific association in between *X. nematophila* and *S. carpocapsae* is regulated by *nilABC* genes located in the the SR1 (symbiosis region 1) in the bacterial genome. Our previous research showed that SR1 in *X. nematophila* is necessary and sufficient for the species-specific association in this particular symbiotic pair (11, 23), including the early stage colonization, such as the AIC localization in adults and juveniles, as well as PIV in pre-IJs (12). One possible model to explain how Lrp

regulates bacteria-nematode association is via *nil* genes expression. Indeed, previous research showed that *nilABC* gene expression is cooperatively and negatively regulated by both *lrp* (24)and *nilR* (25), another regulatory protein that controls *nilABC* expression. However, these research only investigated the presence of *lrp* (comparison of wild type and *lrp* mutant), leaving an open question of if Lrp expression levels control and optimize *nil* gene expressions for colonization. The data in this supports a hypothesis that among bacteria expressing various levels of Lrp, high-*lrp* expression promotes an optimal gene expression of Sr1, which best facilitate bacterial colonization in early stages of nematodes. Future work should test if Lrp regulates colonization of early developmental stages of nematodes through optimizing the expression of *nil* genes. Experiments such as assessing *nil* genes transcription (qPCR) and promoter activities (ß-galactocidase activity assay of *Pnil-lacZ* fusions) in fixed Lrp strains will help elucidate the regulatory effects of Lrp levels on bacterial colonization. In addition, identification and quantification of optimal *nil* genes activity during colonization *in vivo* would be important to understand the molecular mechanisms of Lrp affected early colonization events.

Alternatively, our data in this chapter also pointed out the possibility that high-Lrp expression in *X. nematophila* supports better transitions if bacteria move among different tropism/niche of the nematode hosts (such as AIC, PIV, and IJ-receptacle). The eukaryotic host, with its complicity in physical structures could provide various host niches with different nutritional conditions. For instance, the intestinal cells in *C. elegans* were found to maintain a highly heterogeneous and compartmentalized cellular distribution of metal ions (26). In another example, different structures in the mammalian GI tract, such as the apical surface vs. the colonic crypt, could provide different species of polysaccharides that facilitate distinct host-microbe associations (27). It is not yet clear if *S. carpocapsae* nematode provide tissue-specific nutritional niches, such that different tissues of the host (such as intestinal lumen, AIC, PIV, and receptacle) are associated with different species or concentrations of sugar or other molecules

(metal ion, amino acids, proteins, etc.). In the future research, it would be intriguing to investigate if *lrp* plays a role in bacterial localization and growth at different host niches.

Lrp-dependent mutualism-to-pathogenesis switch occurs in the IJ nematodes.

The data shown in this chapter suggest that an Lrp-dependent bacterial population switch occurs in the aging IJ nematode, raising questions such as: what molecules could induce the Lrp-dependent switch and population shift in the host environment? My in-vitro experiments show that minimal media supplemented with amino acids could increase the population heterogeneity in a similar manner as aging IJs, suggesting the amino acids present in the IJ receptacle might play an important role as as a nutrient signal for Lrp-dependent switch. In an alternative model, it could be the IJ receptacle environment that selects low-Lrp cells (high-Lrp cells die faster) rather then promoting high-to-low Lrp switch. To distinguish the former (inducible model) vs. the latter (selection model), it requires the development of tools to track individual living IJ nematodes and fluorescence reporters that could report Lrp switch in IJ receptacle. In the following chapter, I will be describing one solution/design that I used to develop such tools.

Materials and Methods

Bacterial strain, media, and growth conditions

The bacterial strains and plasmids used in this study are listed in Table 4.1. Bacteria were grown in lysogeny broth (LB) culture media (28) at either 30°C (for *X. nematophila*) or 37°C (for *E. coli*). The medium was either stored in the dark or supplemented with 0.1% sodium pyruvate (29). *Xenorhabdus* bacteria carrying plasmids were grown in the culture medium supplemented with 7.5 μg/ml of tetracycline in order to maintain plasmids. Other antibiotics were used as indicated at the following concentrations: ampicillin (Amp), 150 μg/ml; chloramphenicol

(Cm), 15 μg/ml (*X. nematophila*) and 30 μg/ml (*E. coli*); kanamycin (Kan), 50 μg/ml; and erythromycin (Erm), 200 μg/ml, and tetracycline (Tet), 75 μg/ml.

Bacterial strain construction

kefA::*Plac-gfp* with fixed-*lrp* on plasmids strains: to create fixed-*lrp X. nematophila* strains with bright *gfp* reporter, I inserted plasmid pJMC1 at *kefA* gene of an *lrp* mutant strain (HGB 1059) via by parental conjugation, creating *lrp::kan/kefA:: Plac-gfp* (12). Then I extracted plasmids pKV69 (vector), pEH54 (low-*lrp* plasmids), and pEH56 (high-*lrp* plasmids), transferred them into *lrp::kan/Plac-gfp* strain via previously described methods for transformation (18, 29), using tetracycline to select for transformants.

*kefA::*fixed-*lrp/* attTn7::KR-*gfp* strains: to create in-genome fixed low-*lrp* and high-*lrp* strains carrying bright *gfp* reporter for visualization and quantification of bacterial growth and persistence in IJ nematodes, I first inserted plasmids pMYC4 (*kefA::*low-*lrp*) and pMYC5 (*kefA::* high-*lrp*) (19) into the genome of and *lrp-2::* Kan mutant (HGB1059) via bi-parental conjugation, resulting *kefA::*low-*lrp* strain (MC-B6-C5) and *kerfA::*high-*lrp* strain (MC-B6-G5). To create the GFP-expressing *X. nematophila* strain (MC-B6-A10, MC-B7-A1, MC-B7-F1, and HGB 2110), I inserted the *gfp* in plasmid pURR25 (mini-Tn7-KS-GFP) (30, 31) from *E. coli* donor strain (HGB 1262) into the attTn7 site in the genome of recipient *Xenorhabdus nematophila lrp* mutant (HGB1059), *kefA::*low-*lrp* (MC-B6-C5), *kefA::* high-*lrp* (MC-B6-G5), and a wild type bacterial strain (HGB 1969, vector plasmid cured) using tri-parental conjugation with pUX-BF13 (HGB 283) as a helper plasmid. The site-specific insertion at attTn7 was confirmed by antibiotic resistance, sensitivity, and PCR amplification using primers mTn7-befKanR (GTCGACTGCAGGCCAACCAGATAAGT) and AttTn7-ext (TGTTGGTTTCACATCC) yielding positive a band of ~500 base pairs.

Nematode maintenance

Conventional nematodes were propagated through *Galleria mellonella* larvae (Grubco, Hamilton, OH) and used for generating aposymbiotic nematodes. A new batch of conventional nematodes was used for each biological replicate. Aposymbiotic nematodes were generated from standard axenic egg preparation from conventional nematodes (31). To generate aposymbiotic IJs, axenic eggs were then reared on *X. nematophila* colonization-deficient *rpoS* mutant lawns and aposymbiotic nematodes were water-trapped, surface-sterilized, and confirmed by grinding and plating on LB agar. Axenic nematodes were surfaced-sterilized right before adding to bacterial lawns in colonization assays (32)

Nematode colonization assay

X. nematophila overnight culture were grown at 30°C and spread onto lipid agar (15ml per plate), incubated at 25°C for 48 hours to create bacterial lawns. In the experiments using *X. nematophila* that carry multicopy plasmids (such as HGB2108, 2109, 2190, see Table 4.1), tetracycline (7.5 μg/ml) was supplemented in overnight culture and lipid agar to maintain plasmids during bacterial growth. In the experiments using *X. nematophila* strains with in-genome insertions no antibiotics were used when growing bacteria. Approximately 5000 aposymtiotic IJs were surface-sterilized and seeded on the bacterial lawns.

Colonization at AIC, PIV, and immature IJ initiation: I modified a previously published method (12) to monitor and assess *X. nematophila* colonization at AIC in adults and juveniles, PIV in pre-IJs, and immature IJs (Data shown in Fig.4.2). Nematodes of various developmental stages were sampled from agar plates on days 4, 6, 8, 10, 12, 14, 17 after seeding the aposymbitic IJs. On each day, samples were taken by scrapping gently using a toothpick and washed in 1XPBS for 3-5 times. Nematode population was screened using epifluorescence microscopy on Nikon Eclipse TE300 inverted microscope (Nikon, Melville, NY, USA). For each category (developmental stage, such as adults, juveniles, pre-IJs-open intestine, per-IJs closed

intestine, and immature IJs), 150-250 nematodes were screened from each biological replicate on each day. The total colonized and non-colonized nematodes in each category were pooled together after 17 days of sampling for colonization frequency estimation and statistical analysis (total nematode counts: 4606 nematodes for high-*lrp* strain, 4529 nematodes for low-*lrp* strain; 4560 nematodes for no-*lrp* strain). Colonization frequency was estimated by percentage colonized nematodes out of the total number nematode of its category. Statistical analysis was performed using One-way ANOVA followed by Tuckey's multiple comparison. Three biological replicates were used, each came from a different batch of conventional nematodes. Within each biological replicate (each day of sampling), three technical replicates were used each represents nematode samples from one agar plate.

Immature IJ bacterial outgrowth: Immature IJs were isolated using a modified method from previous research (13) from lipid agar plates 6 days post seeding the the aposymbiotic nematodes (data shown in Fig. 4.3). I sampled nematodes from the bacterial lawn and examined them by microscopy to confirm the formation of immature IJs. Immature IJs were isolated by flooding the nematode population from the bacterial lawns using sterile deionized water, collected by sedimentation in water, re-suspended in sterile water, and treated with a 1% SDS aqueous solution for 20 min with shaking by hand (13). The SDS solution kills nematodes in other developmental stages except for IJ, which we recovered and washed by centrifugation (10 min at 3000rpm) for 3 times and resuspending in sterile water. The isolated immature IJs were stored in sterile water at room temperature in dark. At each time point (every 12 hours for 5 days), 100-200 immature IJs are taken from each sample pool (one sample pool per biological replicate per bacterial strain) and estimate for colonization frequency using epifluorescence microscopy (percent colonized IJ out of total number of IJs). Another 100-200 immature IJs from each sample pool were surface-sterilized (32) by treating samples with 1% bleach for 2 min, spun down the samples in microfuge tubes, and washed with sterile water for 4 times. Surface-sterilized nematodes were grinded in 1XPBS using a hand-grinding pellet

pestle motor (Kontes) (33), serially diluted in 1XPBS, plated onto LB agar plates, and colony forming units per colonized IJ. Three biological replicates were used, each from a different batch of conventional IJ nematodes.

Colonization of mature IJs. After 7 days post adding aposymbiotic nematodes onto bacterial lawns, water traps were set up to collect mature IJs. For mature IJ emerged on each day (day 1, 2, 3-4, 5-6 in Fig.4.4), nematode samples were taken from the water-trap that only contain the nematode that emerged from these specific days. For instance, mature IJs emerged on day 1 were sampled after which the nematode population were pooled into a different flask. A new water-trap was set up to collect IJ nematodes that only emerge on day 2 post trapping. For cumulative mature IJ colonization assessment (data shown on Fig.4.5), cumulative nematodes collected for 2 weeks post water-trap were examined on the same day. To assess colonization frequency in mature IJs, epifluorescence microscopy was used to count colonized and un-colonized IJs. To assess the bacterial carriage per colonized IJs, 100-150 mature IJs were surface-sterilized and grinded to extract bacterial symbionts. Bacteria were diluted and CFU were counted to determine CFU per colonized IJ.

Bacterial carriage in aging IJ and later-emerged IJs: to track bacterial symbionts from aging IJs, mature IJ nematodes trapped after 7 days (water-trap set up 7 days post adding aposymbiotic nematodes onto bacterial lawn) were collected in sterile culture flasks (Falcon) in dark. At each time point, 100-150 aging IJs (0, 1, 2, and 4 weeks after storage) were taken out of the pool of IJs to assess wild type bacterial population heterogeneity. For later emerged IJs, IJs collected in the first week of water-trapping were taken to assess symbiotic bacteria population heterogeneity. The IJs collected from previous week(s) were removed from water trap, and sample pool only represent the IJs emerged from one (or two) specific week(s).

Bacterial population heterogeneity was determined using the fluorescence screening methods modified from Chapter 3. In particular, 100-200 IJs were surface-sterilized and grinded; bacterial symbionts were serially diluted and plated onto LB agar. After 16h-18h incubation at

30°C, epifluorescence microscopy was used to determine colony phenotype (either low-Lrp or high-Lrp colonies) under GFP and RFP channels. The percentage of low-Lrp colonies were estimated and used to assess population heterogeneity.

Acknowledgements

I would like to thank Dr. Kristen Murfin for her time and efforts training me on nematode sample preparation and identification of AIC, PIV colonization of *X. nematophila* in different developmental stages of *S. carpocapsae.*

References

1. **van der Woude MW**, **Bäumler AJ**. 2004. Phase and antigenic variation in bacteria. Clin Microbiol Rev **17**:581–611.
2. **Veening J-W**, **Smits WK**, **Kuipers OP**. 2008. Bistability, Epigenetics, and Bet-Hedging in Bacteria. Annu Rev Microbiol **62**:193–210.
3. **Cao M**, **Goodrich-Blair H**. 2017. Ready or Not: Microbial Adaptive Responses in Dynamic Symbiosis Environments. J Bacteriol JB.00883-16.
4. **Birget PLG**, **Repton C**, **O 'donnell AJ**, **Schneider P**, **Reece SE**. 2017. Phenotypic plasticity in reproductive effort: malaria parasites respond to resource availability. Proc R Soc B Biol Sci **284**.
5. **Tischler AD**, **Camilli A**. 2004. Cyclic diguanylate (c-di-GMP) regulates *Vibrio cholerae* biofilm formation. Mol Microbiol **53**:857–869.
6. **Tischler AD**, **Camilli A**. 2005. Cyclic diguanylate regulates *Vibrio cholerae* virulence gene expression. Infect Immun **73**:5873–5882.
7. **Schild S**, **Tamayo R**, **Nelson EJ**, **Qadri F**, **Calderwood SB**, **Camilli A**. 2007. Genes Induced Late in Infection Increase Fitness of *Vibrio cholerae* after Release into the Environment. Cell Host Microbe **2**:264–277.
8. **Nielsen AT**, **Dolganov NA**, **Rasmussen T**, **Otto G**, **Miller MC**, **Felt SA**, **Torreilles S**, **Schoolnik GK**. 2010. A bistable switch and anatomical site control *Vibrio cholerae* virulence gene expression in the intestine. PLoS Pathog **6**:e1001102.
9. **Vadyvaloo V**, **Jarrett C**, **Sturdevant DE**, **Sebbane F**, **Hinnebusch BJ**. 2010. Transit through the flea vector induces a pretransmission innate immunity resistance phenotype in *Yersinia pestis*. PLoS Pathog **6**:e1000783.
10. **Richards GR**, **Goodrich-Blair H**. 2009. Masters of conquest and pillage: *Xenorhabdus nematophila* global regulators control transitions from virulence to nutrient acquisition. Cell Microbiol **11**:1025–1033.

11. **Cowles CE**, **Goodrich-Blair H**. 2008. The *Xenorhabdus nematophila nilABC* genes confer the ability of *Xenorhabdus* spp. to colonize *Steinernema carpocapsae* nematodes. J Bacteriol **190**:4121–4128.

12. **Chaston JM**, **Murfin KE**, **Heath-Heckman EA**, **Goodrich-Blair H**. 2013. Previously unrecognized stages of species-specific colonization in the mutualism between *Xenorhabdus* bacteria and *Steinernema* nematodes. Cell Microbiol **15**:1545–1559.

13. **Martens EC**, **Heungens K**, **Goodrich-Blair H**. 2003. Early Colonization Events in the Mutualistic Association between *Steinernema carpocapsae* Nematodes and *Xenorhabdus nematophila* Bacteria. J Bacteriol **185**:3147–3154.

14. **Kung SP**, **Gaugler R**, **Kaya HK**. 1990. Influence of Soil pH and Oxygen on Persistence of *Steinernema* spp. J Nematol **22**:440–5.

15. **Kung S-P**, **Gaugler R**, **Kaya HK**. 1990. Soil type and entomopathogenic nematode persistence. J Invertebr Pathol **55**:401–406.

16. **Kung S-P**, **Gaugler R**, **Kaya HK**. 1991. Effects of soil temperature, moisture, and relative humidity on entomopathogenic nematode persistence. J Invertebr Pathol **57**:242–249.

17. **Park Y**, **Herbert EE**, **Cowles CE**, **Cowles KN**, **Menard ML**, **Orchard SS**, **Goodrich-Blair H**. 2007. Clonal variation in *Xenorhabdus nematophila* virulence and suppression of *Manduca sexta* immunity. Cell Microbiol **9**:645–656.

18. **Hussa EA**, **Casanova-Torres ÁM**, **Goodrich-Blair H**. 2015. The global transcription factor Lrp controls virulence modulation in *Xenorhabdus nematophila*. J Bacteriol **197**:3015–3025.

19. **Cao M**, **Patel T**, **Goodrich-Blair H**, **Hussa EA**. 2017. High levels of Xenorhabdus nematophila transcription factor Lrp promote mutualism with *Steinernema carpocapsae* nematode hosts. Appl Environ Microbiol **83**:17.

20. **Casanova-Torres ÁM**, **Shokal U**, **Morag N**, **Eleftherianos I**, **Goodrich-Blair H**. 2017. The global transcription factor Lrp is both essential for and inhibitory to *Xenorhabdus*

nematophila insecticidal activity. Appl Environ Microbiol AEM.00185-17.

21. **Cowles KN**, **Cowles CE**, **Richards GR**, **Martens EC**, **Goodrich-Blair H**. 2007. The global regulator Lrp contributes to mutualism, pathogenesis and phenotypic variation in the bacterium *Xenorhabdus nematophila*. Cell Microbiol **9**:1311–1323.
22. **Martens EC**, **Russell FM**, **Goodrich-Blair H**. 2005. Analysis of *Xenorhabdus nematophila* metabolic mutants yields insight into stages of *Steinernema carpocapsae* nematode intestinal colonization. Mol Microbiol **58**:28–45.
23. **Heungens K**, **Cowles CE**, **Goodrich-Blair H**. 2002. Identification of *Xenorhabdus nematophila* genes required for mutualistic colonization of *Steinernema carpocapsae* nematodes. Mol Microbiol **45**:1337–1353.
24. **Cowles CE**, **Goodrich-Blair H**. 2004. Characterization of a lipoprotein, NilC, required by *Xenorhabdus nematophila* for mutualism with its nematode host. Mol Microbiol **54**:464–477.
25. **Cowles CE**, **Goodrich-Blair H**. 2006. *nilR* is necessary for co-ordinate repression of *Xenorhabdus nematophila* mutualism genes. Mol Microbiol **62**:760–771.
26. **McColl G**, **James SA**, **Mayo S**, **Howard DL**, **Ryan CG**, **Kirkham R**, **Moorhead GF**, **Paterson D**, **de Jonge MD**, **Bush AI**. 2012. Caenorhabditis elegans Maintains Highly Compartmentalized Cellular Distribution of Metals and Steep Concentration Gradients of Manganese. PLoS One **7**:e32685.
27. **Lee SM**, **Donaldson GP**, **Mikulski Z**, **Boyajian S**, **Ley K**, **Mazmanian SK**. 2013. Bacterial colonization factors control specificity and stability of the gut microbiota. Nature **501**:426–429.
28. **Miller JH**. 1972. Experiments in molecular genetics. Cold Spring Harb Lab Press Cold Spring Harb NY **433**:352–355.
29. **Xu J**, **Hurlbert RE**. 1990. Toxicity of Irradiated Media for *Xenorhabdus* spp. Appl Environ Microbiol **56**:815–8.

30. **Lambertsen L**, **Sternberg C**, **Molin S**. 2004. Mini-Tn7 transposons for site-specific tagging of bacteria with fluorescent proteins. Environ Microbiol **6**:726–732.

31. **Murfin KE**, **Chaston J**, **Goodrich-Blair H**. 2012. Visualizing bacteria in nematodes using fluorescent microscopy. J Vis Exp.

32. **Vivas EI**, **Goodrich-Blair H**. 2001. *Xenorhabdus nematophilus* as a model for host-bacterium interactions: *rpoS* is necessary for mutualism with nematodes. J Bacteriol **183**:4687–93.

33. **Murfin KE**, **Lee MM**, **Klassen JL**, **McDonald BR**, **Larget B**, **Forst S**, **Stock SP**, **Currie CR**, **Goodrich-Blair H**. 2015. *Xenorhabdus bovienii* strain diversity impacts coevolution and symbiotic maintenance with *Steinernema* spp. nematode hosts. MBio **6**:1–10.

34. **Teal TK**, **Lies DP**, **Wold BJ**, **Newman DK**. 2006. Spatiometabolic stratification of *Shewanella oneidensis* biofilms. Appl Environ Microbiol **72**:7324–7330.

35. **Visick KL**, **Skoufos LM**. 2001. Two-component sensor required for normal symbiotic colonization of *Euprymna scolopes* by *Vibrio fischeri*. J Bacteriol **183**:835–42.

Tables and Figures

Table 4.1. Bacterial strains used in Chapter 4.

Strain or plasmids	Relevant genetic characteristic(s)	Source/references
HGB1059	*X. nematophila* HGB800 *lrp-2::kan*	(21)
HGB2261	HGB1059 attTn7*::PfliC-gfp/Plac-rfp*	(19) Chapter 2
HGB2262	HGB2261 *kefA*::pMYC4 (low Lrp); attTn7*::PfliC-gfp/Plac-rfp*	(19) Chapter 2
HGB2263	HGB2261 *kefA*::pMYC5 (high Lrp); attTn7*::PfliC-gfp/Plac-rfp*	(19) Chapter 2
HGB1262	*E. coli* carrying plasmid purr25-mini Tn7/KR-*gfp*	(12, 34)
MC-B6-A10[4]	HGB 1059 attTn7*::*KR-*gfp*	This study
MC-B7-A1	*X. nematophila kefA*::pMYC4 (low Lrp); attTn7::KR-*gfp*	This study
MC-B7-F1	*X. nematophila kefA*::pMYC5 (high Lrp); attTn7::KR-*gfp*	This study
HGB1783	*E. coli* S17-*lpir* carrying plasmid pJMC001	(12)
HGB2108	*X. nematophila lrp-2*::kan, *kefA*::*Plac-gfp*; plus pEH54 (low Lrp plasmid)	This study
HGB2109	*X. nematophila lrp-2::kan*, *kefA*::*Plac-gfp*; plus pEH56 (high Lrp plasmid)	This study
HGB2190	*X. nematophila lrp-2::kan, kefA::Plac-gfp;* plus pKV69 (vector)	This study
HGB1969	*X. nematophlia* wild type virulent strain plus pKV69 (vector)	(18)
HGB1970	*X. nematophlia* wild type virulence-attenuated strain plus pKV69 (vector)	(18)
HGB2110	HGB1969, vector cured, attTn7::KR-*gfp*	This study
MC-B6-E3[5] (HGB2264)	HGB1969, vector cured, attTn7:: *PfliC-gfp/Plac-rfp*; heterogeneous population	Chapter 3
MC-B6-I3 (HGB2265)	HGB1969, vector cured, attTn7:: *PfliC-gfp/Plac-rfp*; homogeneous population	Chapter 3
MC-B6-I4 (HGB2266)	HGB1970, vector cured, attTn7:: *PfliC-gfp/Plac-rfp*; homogeneous population	Chapter 3
Plasmids		
purr25-mini Tn7/KR-GFP	plasmid that inserts *Plac-gfp* at attTn7, Cm^R, Kan^R	(12, 34)
pJMC1	Plasmid carries *Plac-gfp* that integrates at *kefA,* CmR	(12)
pKV69	Multicopy mobilizable vector; Cm^R, Tet^R	(35)
pEH54	pKV69 with *lrp* in oppositie orientation relative to P*lac*	(18)
pEH56	pKV69 with *lrp* under control of P*lac*	(18)

[4] Yellow highlights: strains that have not been frozen down in the HGB laboratory strain collection. Nomenclature for the strain name is based on the strain location in MC box: MC-B6-A10 represents MC-Box 6- Position A10.

[5] Blue highlights: strains that have been frozen down in MC-Boxes as multiple isolates. Here present the matching isolates in MC-Boxes and HGB box.

Figure 4.1: Life cycle of bacterium *Xenorhabdus nematophila* and developmental stages of *Steinernema carpocapsae* in a species-specific manner.

In the insect cadaver, adult and juvenile nematodes are colonized by symbiotic bacteria at AIC (anterior intenstinal ceacum). In pre-IJ nematodes, bacteria are localized at PIV (pharyngeal intestinal valve). In the immature IJs (pre-migratory), *X. nematophila* enter the nematode receptacle. While immature IJ further develop into mature IJs and emerge from the insect cadaver, the few symbiotic bacteria grow into a nearly clonal population, termed bacterial outgrowth.

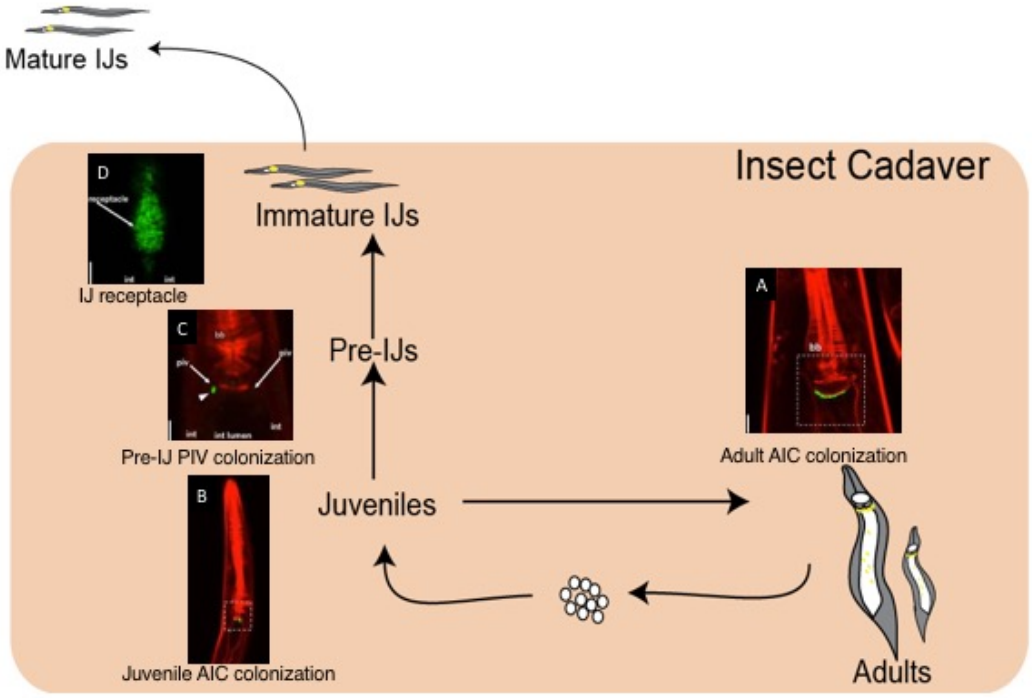
Mature IJs
Insect Cadaver
Immature IJs
D
IJ receptacle
C
Pre-IJ PIV colonization
Pre-IJs
A
Adult AIC colonization
B
Juvenile AIC colonization
Juveniles
Adults

Figure 4.2. *X. nematophila* expressing fixed high levels of Lrp has a high colonization frequency relative to fixed low-Lrp expressers with early stages of nematode development including AIC, PIV, and immature IJ colonization initiation.

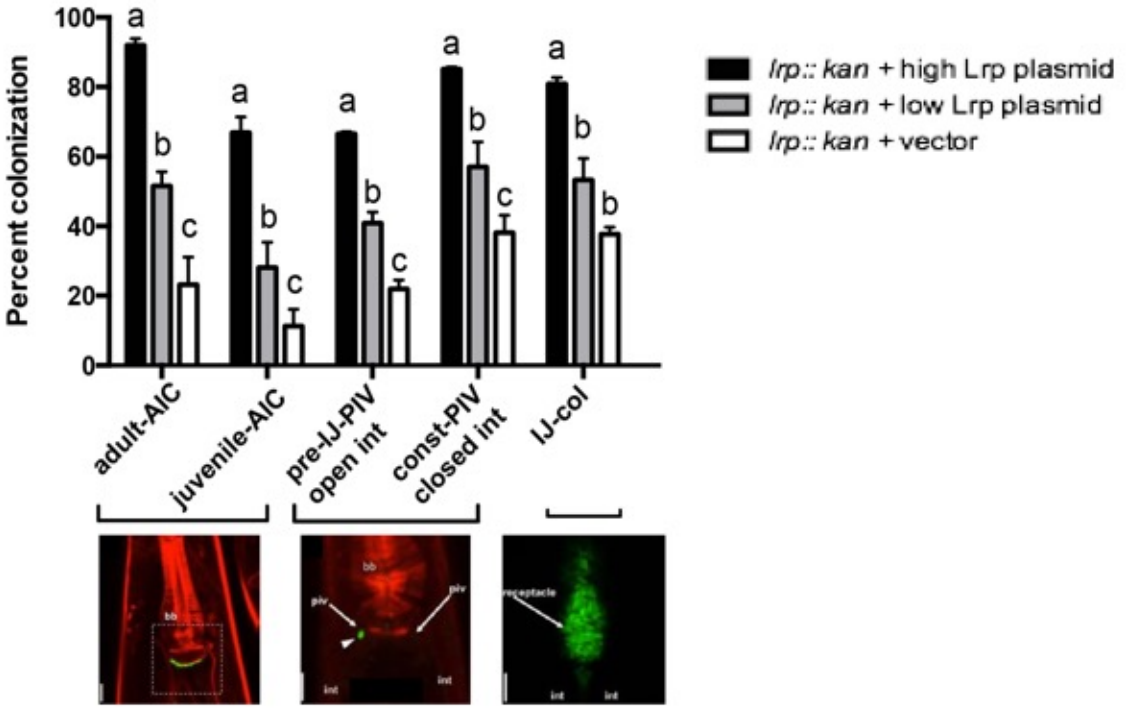

Figure 4.3. *X. nematophila* expressing fixed high and fixed low levels of Lrp show similar growth rate in the immature nematode receptacle.

(A): Current model of bacterial outgrowth in the IJ receptacle **(B):** CFU per colonized immature IJ during 120h post isolation. Immature IJs were isolated from bacterial lawns. At each time point, immature IJs were surface-sterilized, grounded, and colonized bacteria were plated onto LB agar to approximate CFU per immature IJ. N=3 (biological replicates), error bars show SEM. Statistical analysis was performed by two-way ANOVA followed by Tukey's multiple comparison, (***, $P \leq 0.001$).

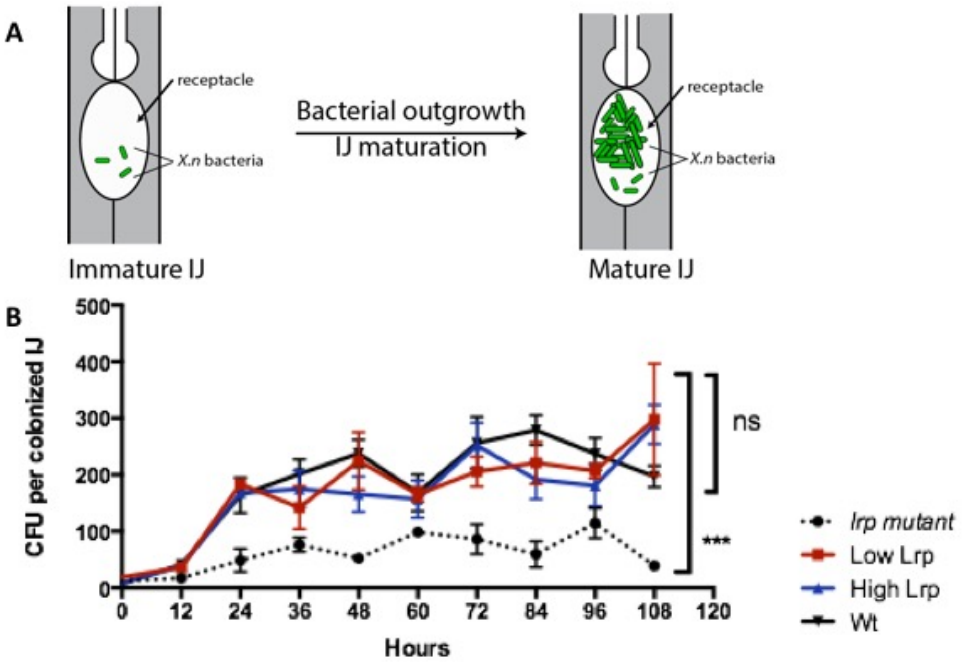
A
receptacle
X.n bacteria
Bacterial outgrowth
IJ maturation
receptacle
X.n bacteria
Immature IJ
Mature IJ
B
CFU per colonized IJ
500
400
300
200
100
0
0
12
24
36
48
60
72
84
96
108
120
Hours
ns
***
lrp mutant
Low Lrp
High Lrp
Wt

Figure 4.4. Lrp-dependent colonization in mature IJs on varying days of emergence.

Aposymbiotic IJs were co-cultured with bacteria carrying *Plac-gfp* in genome on agar plates. Newly emerged mature IJs were removed from water-trap on day 1, 2, 4, and 6 post trap, and used for screening the frequency and level of colonization. **(A):** Percent mature IJ colonized by *X. nematophila* expressing no, low high levels of Lrp and wild type. Mature IJs emerged on day 1, 2, 4, and 6 post trap were screened, n=3 biological replicates. **(B)**: CFU per colonized mature IJ emerged on day 1, 2, 4, and 6 post trapping, n=3 biological replicates. ANOVA test was used for statistical analysis followed by Tuckey's multiple comparisons. On each day of emergence, different letters indicate different statistical groups.

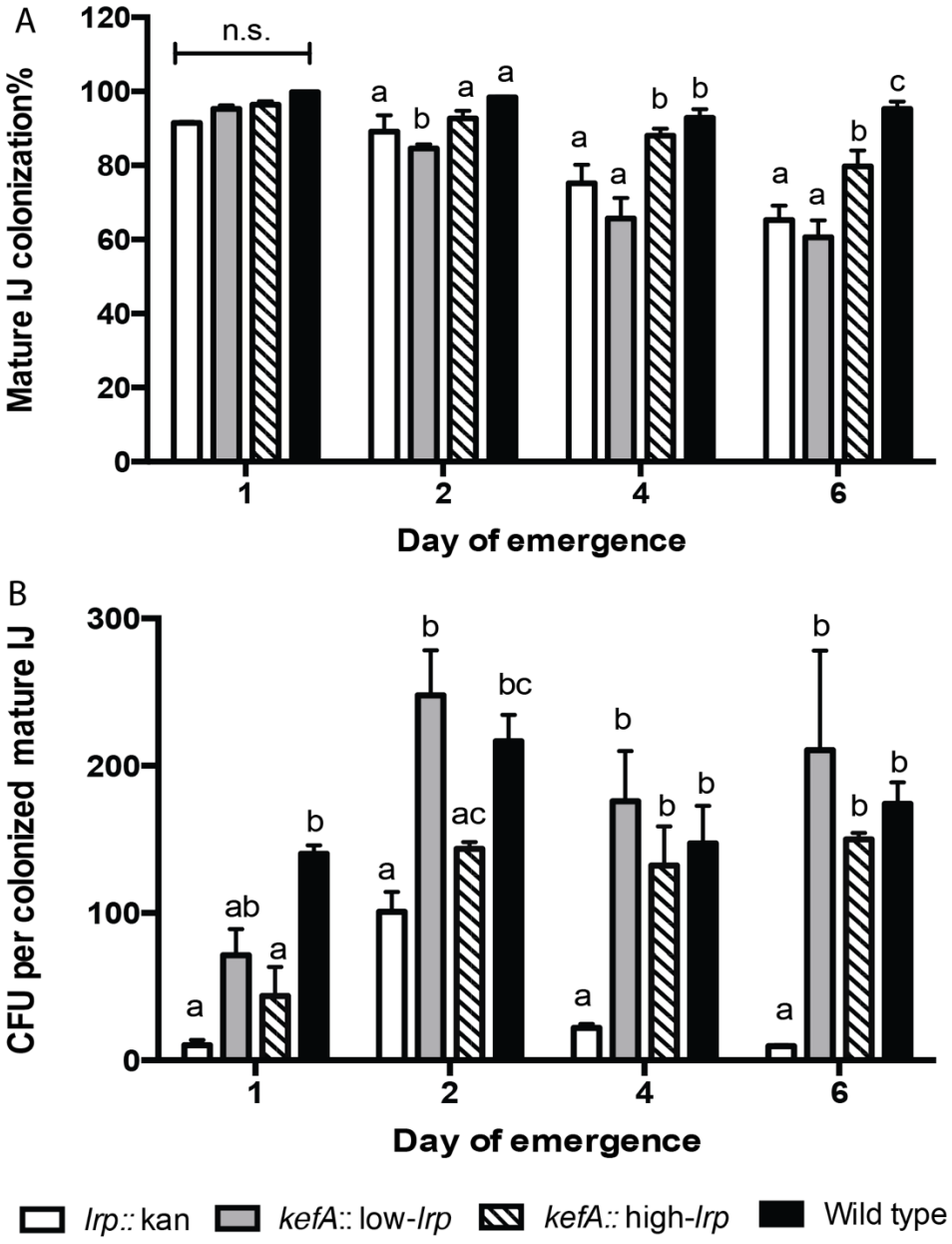
A
Mature IJ colonization%
120
100
80
60
40
20
0
n.s.
a
b
a
a
a
a
b
b
a
a
b
c
1
2
4
6
Day of emergence
B
CFU per colonized mature IJ
300
200
100
0
a
ab
a
b
a
b
ac
bc
a
b
b
b
a
b
b
b
1
2
4
6
Day of emergence
lrp:: kan
kefA:: low-lrp
kefA:: high-lrp
Wild type

Figure 4.5. Lrp-dependent colonization in cumulative mature IJs.

Aposymbiotic IJs were co-cultured with bacteria carrying *PfliC-gfp/Plac-rfp* (see Chapter 2 and 3) on agar plates. Accumulative mature IJs were collected 14 days post trap and screened for percentage colonization and CFU per nematode. **(A):** Percent colonization of *X. nematophila* expressing no-, low-, high- levels of Lrp and wild type, n=5 biological replicates. **(B):** CFU per colonized IJ emerged from *X. nematophila* expressing no-, low-, high- levels of Lrp and wild type, n=3. Statistical analysis was done by One-Way ANOVA followed by Tukey's multiple comparison.

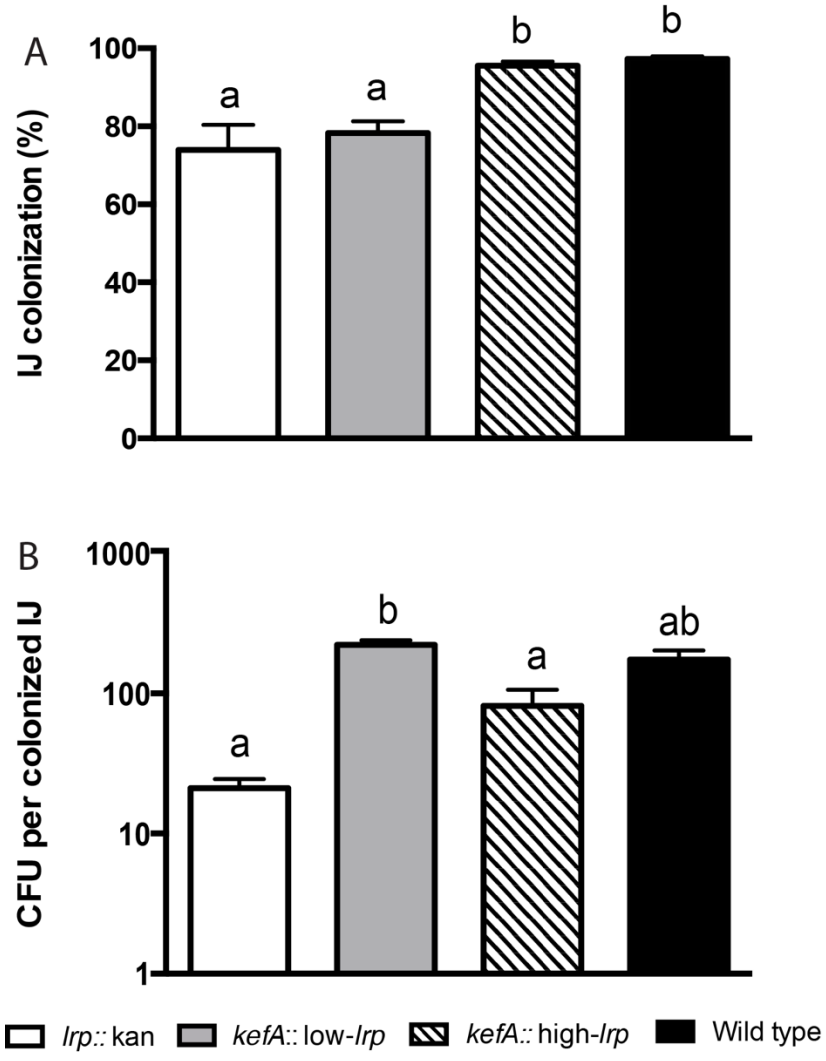
A
IJ colonization (%)
100
80
60
40
20
0
a
a
b
b
B
CFU per colonized IJ
1000
100
10
1
a
b
a
ab
lrp:: kan
kefA:: low-lrp
kefA:: high-lrp
Wild type

Figure 4.6. Comparison of *X. nematophila* population switch to low-Lrp expressing subpopulations in vitro and in vivo.

Three wild type *X. nematophila* strains carrying *PfliC-gfp/Plac-rfp* in genome (see Chapter 3 for details) were assessed for Lrp high-to-low switch. Bacteria were extracted from culture in vitro (A and B) or from nematodes (C and D), serially diluated and plated onto LB agar. After 16-18 hours' incubation, bacterial colonies were screened using epifluorescence microscopy under GFP and RFP channels. Low-Lrp colonies (red colonies) were counted and calculated as percent low-Lrp colony out of the total number of colonies. Bacteria grown in minimal media supplemented with casamino acids (A) or glucose (B) for 3 days. Bacteria were serially diluted and plated onto LB agar for fluorescence screen. (C): Bacteria were extracted from mature IJ nematodes aged for 1-4 weeks. (D): Bacteria were extracted from IJ nematodes emerged in week 0-1, week 1-2, and week 2-4. (C and D): Symbiotic bacteria from 100-200 surface-sterilized IJs were extracted, serially diluted, and plated onto LB agar. Six biological replicates from two independent experiments are shown for each bacterial strain.

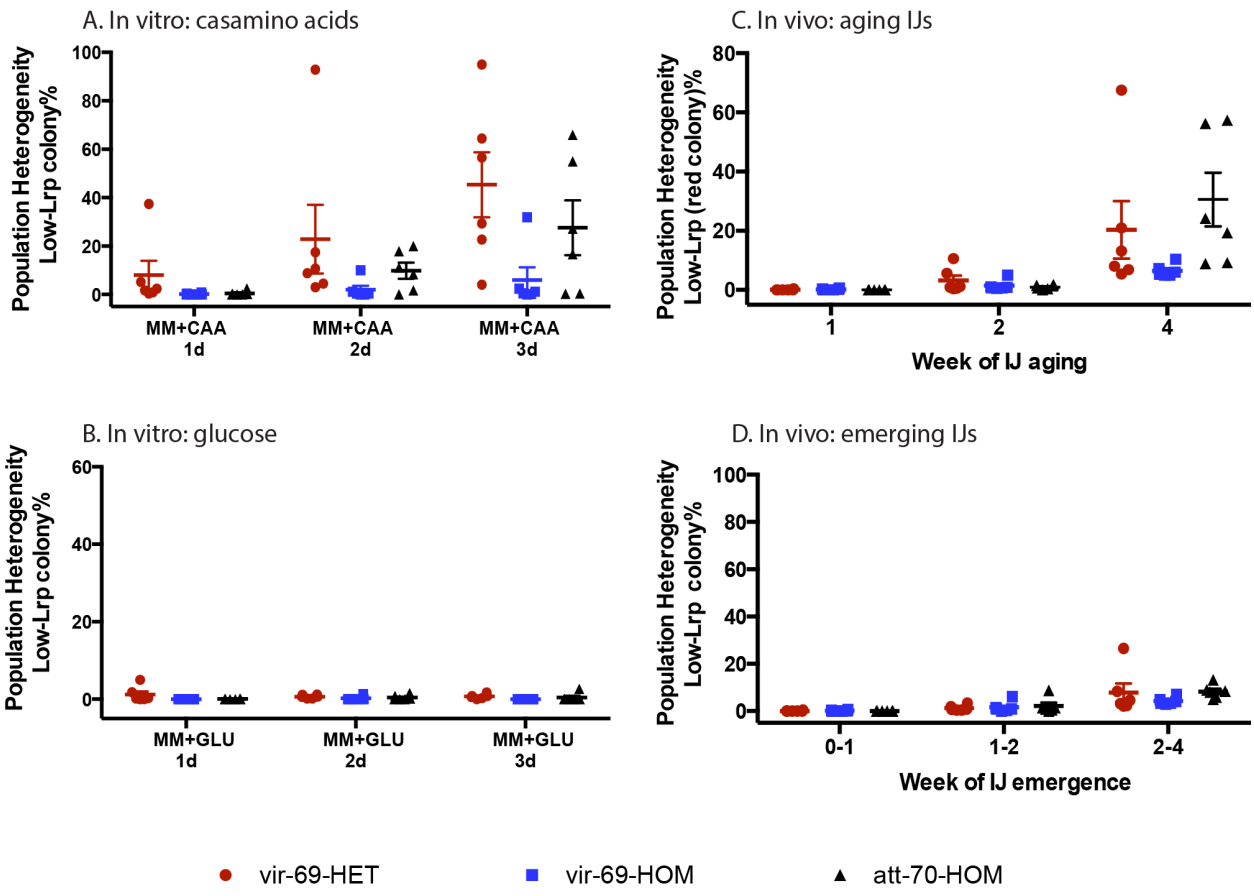
A. In vitro: casamino acids
Population Heterogeneity
Low-Lrp colony%
100
80
60
40
20
0
MM+CAA
1d
MM+CAA
2d
MM+CAA
3d
C. In vivo: aging IJs
Population Heterogeneity
Low-Lrp (red colony)%
80
60
40
20
0
1
2
4
Week of IJ aging
B. In vitro: glucose
Population Heterogeneity
Low-Lrp colony%
60
40
20
0
MM+GLU
1d
MM+GLU
2d
MM+GLU
3d
D. In vivo: emerging IJs
Population Heterogeneity
Low-Lrp colony%
100
80
60
40
20
0
0-1
1-2
2-4
Week of IJ emergence
vir-69-HET
vir-69-HOM
att-70-HOM

Figure 4.7. Current model of VMO switch in *X. nematophila* life cycle.

In comparison to low-Lrp expressing cells, bacteria expressing high levels of Lrp have higher frequency associating with early developmental stages of nematodes including adult, juveniles, pre-IJ, and IJs. During the immature IJ stage, bacterial growth is not significantly different in between low-Lrp and high-Lrp cells. Low-Lrp expressing cells better persist in the mature IJs. Bacteria high-to-low Lrp switch occurs during IJ aging process.

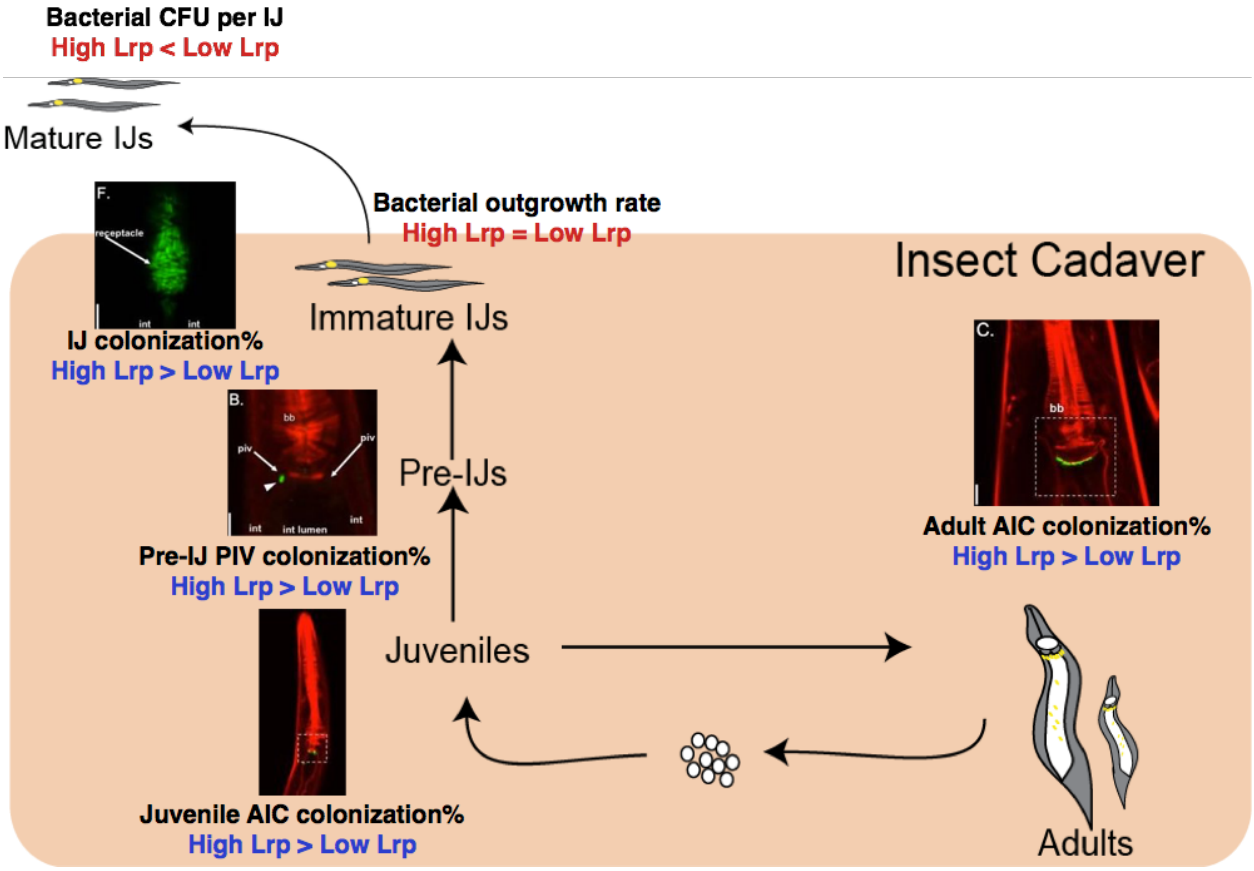
Bacterial CFU per IJ
High Lrp < Low Lrp
Mature IJs
Bacterial outgrowth rate
High Lrp = Low Lrp
Insect Cadaver
Immature IJs
IJ colonization%
High Lrp > Low Lrp
Pre-IJs
Pre-IJ PIV colonization%
High Lrp > Low Lrp
Adult AIC colonization%
High Lrp > Low Lrp
Juveniles
Juvenile AIC colonization%
High Lrp > Low Lrp
Adults

Chapter 5:

Studying the symbiotic bacterium *Xenorhabdus nematophila* in individual, living *Steinernema carpocapsae* nematodes using microfluidic systems

This Chapter is in preparation for submission for *mSphere*:
Matthew Stilwell*, **Mengyi Cao*,** Douglas Weibel, Heidi Goodrich-Blair; Using microfluidic devices to study symbiotic bacteria population dynamics in the individual nematode hosts.
***denotes equal contribution as co-first authors**.

Mengyi Cao: Hypothesis, experimental design, nematode cultivation, perform experiments, data analysis, writing manuscript. (Biological perspective)

Heidi Goodrich-Blair: rationale, writing and editing of manuscript (Biological perspective)

Abstract

Animal-microbe symbioses are ubiquitous in nature and are scientifically important in diverse areas including ecology, medicine, and agriculture. *Steinernema* nematodes and *Xenorhabdus* bacteria are an established, successful model system for investigating microbial pathogenesis and mutualism, the two extremes of symbiotic relationships. The bacterium *Xenorhabdus nematophila* is a species-specific mutualist of insect-infecting *Steinernema carpocapsae* nematodes. As part of this relationship, the bacterium colonizes a specialized intestinal pocket within the infective stage of the nematodes, which transports the bacteria between insects that are then killed and consumed by the pair for reproduction. Current understanding of the interaction between the infective stage nematode and its bacterial colonizers is based largely on population level, snap-shot time point studies in these organisms. This is because investigating temporal dynamics of the bacterium within the nematode is impeded by the difficulty of isolating and maintaining individual living nematodes and tracking colonizing bacterial cells over time. To overcome this challenge, we developed a microfluidic system that enables us to spatially isolate and microscopically observe individual, living *Steinernema* nematodes, keep them alive and in focus on a microscope for weeks, and image the growth and development of *X. nematophila* bacterial communities—starting from a single cell or few cell—over this time scale. Our data demonstrate the first direct, temporal, *in vivo* analysis of a bacteria-nematode symbiosis and the application of this system to reveal continuous dynamics of symbiont population in the individual living host animal.

IMPORTANCE

This paper describes an experimental system for directly investigating population dynamics of a symbiotic bacterium (*Xenorhabdus nematophila*) in its host—the infective stage of entomopathogenic nematode *Steinernema carpocapsae.* Tracking individual and groups of bacteria in individual host nematodes over days and weeks yielded insight into dynamic growth

and topology changes of symbiotic bacterial populations within infective juvenile nematodes. Our approach for studying symbioses between bacterium and nematode provides a system to investigate long-term host-microbe interactions in individual nematodes and extrapolate the lessons learned to other bacteria-animal interactions.

Introduction

Microbes form symbiotic relationships with organisms in every kingdom of life and in every ecosystem, ranging from mutualism (all partners benefit) to parasitism (some partners benefit, others are harmed or killed). Many bacterial species are obligate mutualists or obligate pathogens, however others can switch between these two extremes depending on aspects of their external environment, such as host identity, abiotic parameters (e.g. temperature), or microbial community partners. Microbial symbioses are important in a wide and growing range of areas—including in medicine and agriculture—as these relationships play a crucial role in host health, development, and nutrition. An understanding of the processes underlying the initiation and maintenance of microbial symbioses is important in predicting conditions in which they may emerge, as well as strategies to control, prevent, or engineer them. Insights into these processes requires surpassing the limitations of traditional microbiology approaches that rely heavily on the *in vitro* growth of microbes in synthetic conditions; techniques that make it possible to study microbes *in situ* within the complex and dynamic host environment could have an important impact on the symbiosis field. To bypass the logistic, technical, and ethical constraints associated with studying symbiosis in vertebrate mammals, numerous labs have developed model systems centered on invertebrate animals to investigate principles of symbiosis.

Invertebrate animals (e.g., nematodes, ants, squid, and coral) and their microbial symbionts provide tractable model systems for studying basic mechanisms and dynamics in host-microbe interactions. These model organisms have yielded insights into signaling, recognition, persistence, host development, and nutrient exchange between hosts and symbionts (1). Nematodes are particularly useful model organisms for studying bacterial symbiosis, as they are small, transparent, relatively simple in terms of multicellular organisms, and occupy diverse environmental niches. Several bacteria-nematode model systems have been developed to explore basic mechanisms of host-microbe symbiotic interactions, including:

terrestrial entomopathogenic nematodes associated with gamma-proteobacteria; *Laxus oneistus* marine nematodes with surface-colonizing thiotrophic bacteria; and filarial nematodes interacting with their intracellular symbiotic bacteria, *Wolbachia* (2). Also, recent studies have explored microbial symbiosis in the model nematode *Caenorhabditis elegans* in the context of recognizing its association with diverse microbes in its natural environment (2, 3).

A well-characterized model of nematode-bacterium symbiosis is the soil dwelling and entomopathogenic *Steinernema* nematode species and their *Xenorhabdus* bacterial partners. These mutually beneficial symbionts have co-adapted, co-evolved, and use molecular mechanisms to promote transmission and maintenance of their species-specific pairings (4). Among this family of organisms, the *Steinernema carpocapsae* nematode and *Xenorhabdus nematophila* bacterium symbiotic pair and their insect prey has been established for decades as a tractable system to investigate pathogenesis and mutualism in microbial symbiosis and a relatively simple model to investigate animal-microbe interactions *in vivo* (5–7).

X. nematophila cells occupy an intestinal pocket called the receptacle in the non-feeding, developmentally arrested stage of nematodes referred to as infective juveniles (IJs). As they hunt and prey on insects, *S. carpocapsae* IJ nematodes transport bacteria housed in the receptacle. Upon entering the insect hemocoel (literally ‘bag of blood’), *S. carpocapsae* nematodes release the population of *X. nematophila* and together the nematode and bacteria kill the insect and use it as a nutrient source for reproduction. IJ nematodes grow into adults, mate sexually, and produce eggs, which hatch into juvenile nematodes. With sufficient nutrients, juvenile nematodes develop into adults and start the next round of the reproductive cycle. A high density of nematodes and depletion of nutrients within the insect cadaver triggers the formation of pre-IJ nematodes, a transient developmental stage that leads to the formation of colonized IJs. Immature IJs leave the cadaver guided by chemical attractants stimulating dispersal behavior, become mature IJs, and seek a new insect host (see Fig. 5.1).

Entomopathogenic nematodes can be raised and propagated in the laboratory using inexpensive and straightforward techniques (8). The transparency and hardiness of *S. carpocapsae* nematodes makes them amenable to optical microscopy to study the anatomical structures of bacterial localization. This is further facilitated by the fact that *X. nematophila* can be genetically manipulated and *X. nematophila* strains exist that stably express fluorescent proteins, making them visible within nematodes (Fig. 5.1) (9). Studies using such tools have revealed discrete stages of bacterial colonization of nematodes in juvenile, adult, pre-IJ, and IJ forms (10) and have demonstrated that these colonization events are species-specific, such that only *X. nematophila* and not other *Xenorhabdus* species associate with *S. carpocapsae* nematodes (11). Previous research also revealed that the final population of bacterial cells in the IJ nematode is clonal and that a period of outgrowth occurs, in which the bacterial population expands to fill the receptacle (12). In contrast to the smooth exponential growth of *X. nematophila* in laboratory medium, outgrowth in the IJ receptacle appears to result from periodic increases and decreases in population size over time (12). Based on these observations, a colonization bottleneck has been proposed in which entry into the receptacle is limited to one or two cells, or in which cells within the receptacle compete during outgrowth resulting in a single dominant clonal type (10, 12).

The studies described above relied on destructive sampling from nematode populations: bacteria are extracted by grinding from hundreds of IJs, and bacterial colony forming units (CFU) are quantified to calculate an average CFU per IJ across the population of nematodes. Alternatively, bacteria are observed within individual nematodes but only at discrete stages, since the process of sample preparation (e.g. paralysis) and dehydration ultimately leads to nematode death. As such, as yet studies have not achieved the direct visualization and quantification of bacterial population dynamics in individual, living host nematodes over the course of days or weeks, necessary to examine the continuing progression of bacterial colonization events and persistence.

To bridge this methodological gap in the study of host-microbe interactions we developed a microfluidic system. Microfluidic channels have characteristic dimensions of ~1-100s of microns that enable the precise manipulation of small volumes of fluids to create controlled chemical environments. Microfluidic systems have been designed for the isolation of individual nematodes and encompass a range of architectures and mechanisms for isolating individual nematodes, including: (i) trapping in droplets of liquid; (ii) isolating in tapered channels; and (iii) concentrating in straight channels sealed with valves. However, these designs are typically used to study the adult stage of *C. elegans*, which is ~10-100X larger in body size than the dauer larval stage, a developmentally arrested phase similar to IJs of entomopathogenic nematodes. These microfluidic devices usually keep whole-organisms alive for a relatively short time period—from minutes to hours. Much longer time frames—from days to weeks—are required to study the processes underlying the establishment and persistence of long-term microbial symbioses. Thus, tools to study individual dauer or IJ stages of nematodes remain at-large.

This Chapter describes an experimental system for exploring symbiosis between bacteria and nematodes and its application to studying the relationship between *X. nematophila* and *S. carpocapsae*. Individual nematodes are confined within single microfluidic chambers in which a flow of cold water is periodically applied to temporarily immobilize worms while imaging by optical microscopy; many parallel chambers enable multiple nematodes to be studied simultaneously. The system is simple to operate, does not require chemically induced paralysis (e.g., using levamisole or CO_2), and eliminate the impact of these reagents and conditions on the population of symbiotic bacteria. We describe using our microfluidic design to isolate, maintain, and track individual, living nematodes for the study of host-microbe interaction experiments over days and weeks.

Results

We focused our investigation on a key stage of mutualism between *X. nematophila* and *S. carpocapsae*—the nematode IJ stage that acts as a vector from the infection of one insect to another. To investigate *X. nematophila* colonization of and outgrowth in individual IJ receptacles, we fabricated a microfluidic device to isolate and maintain multiple IJ nematodes in individual chambers (referred to as traps) that enabled us to image by microscopy bacteria and nematodes (Fig. 5.2). We used several criteria in the design of the traps. First, each trap should contain an individual IJ. Second, the devices need to maintain IJ viability for weeks to enable long-term observations of the colonization process. Third, the IJs have to be immobilized without the use of chemical paralyzing agents that could impact the colonization process and obscure biological data. Fourth, the system should be simple to operate. The design we developed to meet these criteria isolates individual nematodes in traps and flows room temperature water throughout the device to keep the IJ nematodes hydrated. To immobilize the IJs for imaging, we temporarily flow cold water through the device prior to and during the imaging process.

Device design and operation

We designed and fabricated a microfluidic system in the transparent silicone elastomer, poly(dimethylsiloxane) (PDMS) using soft lithography. We used a previous design for cell bending experiments as a starting point and revamped it for this study. The system consists of one inlet (through which nematodes and fluids are introduced) connected to an outlet through a straight, primary channel, with traps connected to each side of the primary channel that are attached to a set of filtering channels and terminate in a second outlet that serves as a vacuum port used to apply a negative source of pressure to the channels and traps (Fig. 5.2). We designed the height of all channels (including the traps) to be 25 μm, the width of the primary channel was 500 μm, the distance between the inlet and outlet was 8 mm, and the device

contained 38 traps that all fit within the field of view of the microscope we used to image when loading nematodes into the system. Different numbers of traps can be designed into this system for other applications. The entire system was 15 x 20 mm long and 3 mm tall and fit on the stage of a standard inverted microscope. To facilitate nematode loading, we introduced an arc into the channel entrances to the traps. Since the body width of IJ nematodes varies with age, we used traps with variable entrance widths, ranging from 10 to 25 μm for experiments with immature IJs or mature IJs, respectively (see Table 5.1). The traps became wider at the region where the nematodes would be positioned and the diameter was adjusted to ensure that water could flow around them during the course of the experiment. The length of each microfluidic trap was 600-μm long (~1.5x longer than the average body length of mature IJ nematodes) and 25-μm wide (~1.5-2x wider than the nematode body; (13)). The width of the traps can be chosen such that the device does not restrict the nematodes natural sigmoidal movement or energy expenditure, which may impact the nutritional conditions of the symbionts. The traps we designed then narrow to 10 μm and connect to the vacuum port via a set of filtering channels.

We loaded IJ nematodes—isolated and prepared as described in the next section—in the inlet of the device using a hand-held syringe connected to Tygon tubing and attached to the inlet. As we pushed a suspension of the nematodes in liquid using the syringe into the primary channel with the hand-held syringe, we applied a source of negative pressure using another syringe connected by tubing to the vacuum port that pulled nematodes into the traps. After trapping the nematodes, we relieved the source of negative pressure and connected the inlet to a syringe through a section of tubing; the syringe was loaded on a syringe pump that perfused the traps with water at room temperature to keep the IJ nematodes hydrated (see Fig. 5.2). The flow of water mimics the experimental conditions in previous research using populations of nematodes in which nematodes are stored in water between experiments measuring bacterial

colonization (9, 12). Since *Steinernema* nematodes are soil dwelling, we also reduced light exposure by covering the entire system with foil except while imaging.

Preparation of colonized IJs and survival in microfluidic traps

To facilitate direct observation of bacteria within the IJ receptacle using microscopy, we cultivated nematodes colonized with *X. nematophila* cells engineered to express GFP from a constitutive lac promoter. On an *X. nematophila* lawn, *S. carpocapsae* nematodes go through reproductive cycles and develop into IJs similar to those in the insect cadaver. Previous research has shown that the *X. nematophila* population exhibits the most drastic changes during the outgrowth process in which few bacterial cells in newly formed, pre-migratory immature IJs grow into a population of tens to hundreds of bacterial cells during an IJ maturation process that lasts ~5 days (12). To capture the bacterial population profile during the stages of initiation of colonization (one or few cells in the IJ receptacle), bacterial outgrowth (one or a few colonized bacteria grow into a population of tens to hundreds of cells), and bacterial persistence in the IJ receptacle, we isolated immature IJs from a mixed population of nematodes from a variety of developmental stages that included adults, juveniles, pre-IJs, and IJs (see Fig. 5.1) (10, 12). We isolated immature *S. carpocapsae* IJs by treating a population of nematodes with 1% SDS, which kills nematodes at all other developmental stages except for IJs that are protected by a double cuticle (12). We purified immature IJs directly following the SDS treatment by breaking down the tissues of nematode cadavers using bleach. A previous study reported that 1 h after SDS treatment of nematodes, the survival rate of *S. feltiae* IJs was 11%-82% (14).

As the conditions for isolating nematodes in our experiments and physical confinement (e.g., restricted space for growth and movement in microfluidic traps) may alter the physiology of IJs, we initially monitored the survival of immature IJs in the device over a 5-day period (Fig. 5.3). Nematode death is accompanied by a characteristic rigid, straight body posture that lacks movement (Fig. 5.3A) followed by tissue degradation (data not shown). We searched for this

phenotype by optical microscopy and counted the number of viable immature IJs in microfluidic traps at the end of a 5-day period. Out of the total number of *S. carpocapsae* IJs loaded in the traps at the beginning of the experiment (n=60), we found that by the end of the experiment (time=112 h), 60% of the trapped nematodes were viable (n=39), 20% were dead (n=11), and 20% had escaped from the traps (n=10) (Fig. 5.3B). Nematodes have a distribution of body sizes, with a subset of IJ nematodes with body widths <10 μm. As such, these slender nematodes were smaller than the smallest physical dimensions of the channels and traps and were able to escape. Reducing the width of the entrance to the traps reduces the number of nematodes that escape, however we found that it makes trapping nematodes more difficult, as many nematodes will now be wider than the entrance dimensions. Consequently, we decided to leave the design and dimensions as-is and accept the loss of 20% of the nematodes during our experiments (still leaving us with the ability to track the majority of nematodes per experiment). Our maintenance data demonstrates that this approach to nematode isolation allows *in vivo* studies of bacteria-nematode interactions.

Bacterial population dynamics within individual IJs

In a typical experiment, we simultaneously monitored the population dynamics of *X. nematophila* cells in 10-18 live nematodes isolated in parallel microfluidic traps over a 5-day period (Fig. 5.4). We imaged *X. nematophila* cells in the IJ receptacle using epifluorescence microscopy at 8 h intervals by vertically sectioning the entire structure in 9 x 1 μm steps (Fig. 5.4A displays images of a representative IJ nematode using this approach). Using a custom IgorPro script, we converted the total integrated fluorescence intensity signal of the receptacle to the approximate number of *X. nematophila* cells by quantifying the GFP intensity across each z-stack and dividing by the fluorescence intensity for a single cell (Fig. 5.4B). Single cell

fluorescence intensities were determined by analysis of early time point images containing few or single bacterial cells using ImageJ.

At the level of individual nematodes, we found that the number of *X. nematophila* cells per unit time increased and then decreased in all of the nematodes we studied (n=50; selected nematodes are shown in Fig. 5.4B). The number of *X. nematophila* cells per unit time varied between individual nematodes. These data are consistent with temporally fluctuating bacterial population sizes observed in past studies based on destructive nematode sampling and ensemble averaging [(12), also see Fig. 5.5AB]. In these previously published experiments (presented here as Fig. 5.5AB), each data point was assessed by traditional microbiological CFU counting from grinding and plating a subpopulation of nematodes. There are three key limitations with the CFU counting approach. (i) Combining different subsets of the nematode population for each time point is likely to increase variability in the CFU/IJ calculation, since both the number of nematodes in the sample and the colony growth conditions can vary. (ii) Culture based methods underestimate cell counts, as they do not accurately represent non-culturable or slow-growing cells such as persisters (15). (iii) Sample-to-sample variation in the formation of colonies from cells isolated from the nematode gut and plated on synthetic culture conditions may misrepresent the actual bacterial load. As such, variations in CFU counts may suggest fluctuations in bacterial physiology yet miss bacterial persistence in the IJ, which is an important phenotype in other microbial structures (1).These previous experiments were unable to distinguish between two models of bacterial population outgrowth dynamics: (i) a fluctuation in the number of *X. nematophila* cells during outgrowth caused by differences in the number of bacterial cells colonizing individual nematodes; or (ii) a fluctuation caused by an increase or decrease in the population of *X. nematophila* cells within individual nematodes. We compared previous data on bacterial outgrowth (Fig. 5.5AB, republished from (12)) and our data using fluorescence quantification (Fig. 5.5C). As expected, our direct, fluorescence microscopy measurements quantifying *X. nematophila* cells in *S. carpocapsae* nematodes provided larger

numbers of cells than by CFU counting. The comparison between the two techniques also reveals more variance in bacterial cell numbers when using bacterial CFU counts (Fig. 5.5). We found striking differences in the number of bacterial cells colonizing different IJ nematodes and observed that the number of bacterial cells within a single nematode increased and decreased over time, showing that the *X. nematophila* population may have periods of growth and death inside the nematode receptacle.

Another method previously applied to assess the bacterial colonization of IJ nematodes is to qualitatively describe the cross-sectional area of colonization within the receptacle visible by microscopy and categorize the colonization level phenotype as full (receptacle filled), half full (bacteria occupying half the receptacle), >1/3 full, oligo-colonized (<10 bacterial cells), or single-cell colonization (10, 12, 16). This method is highly subjective, as researchers screen a population of IJs under the microscope, count the number of nematodes that fall within subjectively assigned categories. Using this method, a population of immature IJ nematodes displayed an increase in the number of IJs with fully colonized receptacles over time; the number of IJs categorized as having no visible colonization decreased over time, while the number categorized as having full receptacles increased over time. These observations suggested that bacterial population size increases within IJs over time. However the reliance of the technique on qualitative, subjective, and destructive sampling limits the confidence with which conclusions can be made. As such, we chose to address a similar question using individual IJs trapped within the microfluidic chamber. We quantified the approximate area of colonization by measuring the area of fluorescence in each IJ receptacle (Fig. 5.4C). Consistent with bacterial number approximation (Fig. 5.4B), the colonization area also increases and decreases in individual nematodes, with some exceptions (Fig. 5.4B & C), confirming the previously published data.

Growth rates of the bacterial population in the nematode receptacle provide an approximate indication of community health. To our knowledge, there has been only one study

that measured the growth rate of *X. nematophila* in *Steinernema* nematodes, although another study has measured the growth rate in synthetic media. Using a value for the average of individual *X. nematophila* growth curves from each experiment, and averaging the three independent experiments, we calculated a growth rate of 0.085 ± 0.060 doublings/h (mean ± standard deviation). This value is in good agreement with previous *in vivo* measurements (0.1 doublings/h in the IJ receptacle) and slower than the values measured in synthetic media (0.62 doublings/h in LB) or insect hemolymph (0.41 doublings/h) (5, 12, 17). One advantage of our system compared to the traditional nematode grinding experiments is that a growth rate can be calculated for each individual nematode and is not limited to a population-based measurement.

We applied our microfluidic device to study the bacterial colonization of nematode hosts at single-cell resolution. For these experiments, we reduced the widths and heights of the microfluidic traps to ~10 μm to further restrict the movement of nematodes, enabling us to perform confocal microscopy on *X. nematophila* cells and recreate the topology of the community in 3D. As in the epifluorescence measurements, we cooled liquid to <4 °C for 30 min before imaging to further reduce nematode movements while shielding them from ambient light. Using this method, we imaged bacterial populations at single-cell resolution in the nematode receptacle over 21 days. We optically 'sectioned' the bacterial population in the receptacle in 1 μm steps once per day for the first five days, and once a week thereafter; during this incubation time, we only cooled samples for 30 min before each imaging step, and incubated at 25°C the rest of the time. Fig. 5.6 shows a 3D reconstruction of the bacterial population within a nematode receptacle over time. 3D reconstructions of the confocal images revealed bacterial population topology changes in the IJ receptacle over weeks, especially during week 3-4.

Discussion

In this Chapter, we describe a microfluidic system that enables fundamental questions of host-microbe interactions to be addressed at the level of individual nematode hosts and individual bacterial cells. The data we acquired using this method are generally consistent with those published using traditional, culture-based microbiological methods, yet expand on earlier observations. First, by tracking individual nematodes, our data are consistent with the previously established model that one or very few 'founder cells' initiate IJ colonization. Second, our data demonstrate increases and decreases of a population of *X. nematophila* cells in a single nematode over time, which to the best of our knowledge has not previously been reported. Microfluidic traps also enabled us to isolate and study many parallel host-symbiont interactions at the level of single nematodes, including temporal changes in the spatial distribution of bacterial colonization in the nematode receptacle and symbiont population density. Combining microfluidic traps with confocal microscopy, we imaged individual living nematodes and their symbionts for >3 weeks and reconstructed the structure of the bacterial population (and approximated the number of cells) over time. These experiments demonstrate a unique new capability for pushing the boundary of host-microbe interaction studies to new level of resolution.

The sharp and repeated increases and decreases in the symbiont population of every nematode in our study is an intriguing phenomenon. We propose several hypothetical models to explain periodic changes in the symbiont population. In model 1, physiological changes—e.g., internal patterns created by a circadian rhythm or the nematode's physical movement—trigger nutrient influx to the receptacle that affects bacterial metabolism. Rhythmic physiological changes in other organisms have been shown to affect bacterial symbionts (18), however this area has not yet been studied in *S. carpocapsae* nematodes. Nematode movement may stimulate peristalsis in the gut, facilitate mixing and diffusion within this organ, and alter bacterial growth and structures in the receptacle. It is unknown whether the nematode host continuously

provides nutrients for the bacteria during long-term colonization. This microfluidic device facilitates future investigations into the nutritional state of the receptacle in individual nematodes.

In model 2, during bacterial outgrowth in the IJ receptacle, subpopulations of bacteria compete with and kill each other, subsequently causing increases and decreases on the population level. The *X. nematophila* genome encodes genes for the Type VI secretion system, which is known for interspecies competition. However, future experiments will be necessary to determine whether *X. nematophila* exhibits competition among subpopulations. The microfluidic system enables direct visualization of the nematode receptacle over long timescales to help provide insight into this phenomenon.

In model 3, population growth and death may arise due to phenotypic switching. *X. nematophila* exhibits a phenotypic variation phenomenon termed virulence modulation (VMO), in which cells switch between mutualistic and pathogenic states (19–21). As the IJ life stage is intermediate between *X. nematophila* displaying mutualistic phenotypes (insect cadaver) and pathogenic phenotypes (next insect blood cavity) (Fig. 5.1), it is the hypothetical host environment for the symbiont population to switch from the mutualistic to the pathogenic state to (pre)-adapt to an upcoming infection stage (Cao and Goodrich-Blair*.,* In press). An intriguing question is whether repeated growth and death of the bacteria in the IJs is involved in the mutualistic-to-pathogenic phenotypic switch. The development of tools for tracking individual nematode host and monitoring their bacterial symbiont population and physiology has the potential to reveal the mechanism of symbiont VMO *in situ*, facilitating the visualization and quantification of phenotypic switching in the single-cell level in the living host environment. Since VMO is a switch in between mutualistic and pathogenic behaviors, the two extreme relationships of symbiosis, understanding the phenotypic vairation at single-cell level in a naturally occurring system of *Steinernema-Xenorhabdus* would contribute to our understanding of fundamental question in this microbial symbiosis.

The physiology of IJ nematodes is unique in the nematode life cycle and awaits investigation. The composition of nutrients, growth factors, and other molecules in IJ receptacles has not been elucidated in entirety. *X. nematophila* symbionts can survive for months in the IJ nematode receptacle. This niche is thought to be nutrient-limited since *X. nematophila* grows slowly within it (as we have reaffirmed here), relative to nutrient-rich media (7, 16, 22–24). A previous study observed a decline in average CFU per IJs during long-term IJ storage, suggesting a decline in nutritional conditions and altered host-microbe interactions during long-term association (23). This microfluidic device may help decipher the chemical environment of the IJ receptacle in greater detail by tracking and analyzing various *X. nematophlia* metabolic mutant population topology and dynamics in the individual living nematodes during bacterial persistence.

The microfluidic device we present in this Chapter is the first to isolate individual, living *S. carpocapsae* nematodes for the study of host-symbiont dynamics. Our device restricts the movement of the nematodes without the use of chemically induced paralysis, avoiding any negative effects these chemicals may have on host-symbiont interactions. Many microfluidic devices have been published that isolate individual nematodes, however the majority of these require microfluidics expertise to use. Our goal was to provide the field with a tool that was simple enough that microbiology or nematology laboratories could perform long timescale, single nematode studies. Consequently, the number of accoutrements required to operate the systems are kept minimal: disposable syringes, needles, and tubing. We provide a link to download the CAD file in the SI; using this file, laboratories can purchase a device ‘master’ and fabricate their own microfluidic devices (see Supplemental Materials for device design downloads). The device operation is easy to operate and we anticipate that non-experts may find the device approachable and useful for their studies. We believe these devices will be of great use to microbiology and nematology labs and we hope that the device will be adapted for single organism studies with other model systems.

We envision several ways this device can be improved upon for future experiments. To rapidly and efficiently cool and immobilize the nematodes before imaging, Peltier coolers can be incorporated into a layer of the device either above or below the traps. Alterations of the trap dimensions will enable the isolation of other organisms with a range of sizes for long-term studies.

Microfluidics provides one approach to mobilize and maintain individual nematodes and has been successfully applied to neuroscience and behavioral studies of *C. elegans* (25, 26). Most of the systems used for experiments studying individual *C. elegans* were designed for adult nematodes, which are ~10x larger than IJ *Steinernema* nematodes. The IJ stage of *Steinernema* nematodes provides an opportunity to study intriguing questions regarding symbiont and host physiology—that are not currently known in *C. elegans*—however the small body size of nematodes and the technical demands for long-term time course experiments are not compatible with previous microfluidic systems for nematode studies. Redesign, testing, and optimization led us to a new microfluidic platform that is compatible with the constraints of loading, maintaining, and immobilizing IJ *Steinernema* nematodes and imaging their symbiotic bacteria. The design also serves as a template for more complicated experiments or experiments with other organisms, which may facilitate the study of microbes that cannot be grown with traditional microbiology methods and for studying microbiomes. Understanding the colonization, survival, growth and persistence of microbial symbionts in host animals is central to the health and function of these organisms, and will be unraveled with the aid of new tools, such as the microfluidic system we describe in this Chapter.

Materials and Methods

Bacterial strain construction and growth

We created the GFP-expressing *X. nematophila* strain HGB 2110 inserting the *gfp* in plasmid pURR25 (mini-Tn7-KS-GFP) (9, 27) from *E. coli* donor strain (HGB 1262) into the attTn7 site in

the genome of recipient *Xenorhabdus nematophila* wild type bacterial strain (HGB 1969) using tri-parental conjugation with pUX-BF13 (HGB 283) as a helper plasmid. The site-specific insertion at attTn7 was confirmed by antibiotic resistance, sensitivity, and PCR amplification using primers mTn7-befKanR (GTCGACTGCAGGCCAACCAGATAAGT) and AttTn7-ext (TGTTGGTTTCACATCC) yielding positive a band of ~500 base pairs.

We streaked bacteria on LB agar supplemented with 1 g/L sodium pyruvate (28). Overnight cultures were grown in LB liquid media incubated at 30 °C with rotation on a cell roller. Agar or liquid media were supplemented with the appropriate concentration of antibiotics: kanamycin: 50 μg/mL; chloramphenicol: 30 μg/mL for *E. coli*, or 15 μg/mL for *X. nematophila*. We incubated bacteria growing in liquid media or on agar infused with liquid media at 30 °C in the dark.

Nematode propagation and aposymbiotic IJ preparation

S. carpocapsae nematodes were propagated through *Galleria mellonella* insect larvae (Grubco) and stored in water at room temperature. Conventional nematodes produced from three independent rounds of propagations were used to prepare independent batches of axenic eggs and aposymbiotic nematodes, each used in one independent experiment.

Nematode colonization assay and immature IJ isolation

We grew bacterial lawns by plating 600 μl of overnight culture of *X. nematophila* onto each lipid agar plate, incubated at 25 °C for 48 h in dark. For each replicate, 5000 aposymbiotic IJs (500 μL) were surface-sterilized, added to the bacterial lawn, and incubated at 25 °C in the dark. 6 days later, we sampled nematodes from the bacterial lawn and examined under them by microscopy to confirm the formation of immature IJs. Immature IJs were isolated by flooding the nematode population from the bacterial lawns (using sterile deionized water), collected by

sedimentation in water, re-suspended in sterile water, and treated with a 1% SDS solution (in water) for 20 min with shaking (12). The SDS solution kills nematodes in other developmental stages except for IJ, which we recovered and washed by centrifugation (10 min at 3000rpm) and resuspending in sterile water. After immature IJs are isolated and washed, we performed a modified surface-sterilization protocol (29) by treating samples with 0.5% bleach for 2 min, then filter the bleach solution and wash nematodes for 3 times with sterile water using vacuum aspiration. This bleaching treatment removed cadavers of dead nematodes (mostly non-IJs) in the sample, facilitating the loading of immature IJ nematodes into microfluidic device.

Microfluidic device fabrication and operation

We fabricated microfluidic device masters using standard soft lithography techniques. Briefly, we created masters by transferring a pattern from a CAD computer file into SU-8 3025 photoresist (Microchem, Newton, MA, USA) on silicon wafers using photolithography. We used a benchtop spincoater (Laurell Technologies Corp., New Wales, PA, USA) to deposit a thin layer of SU-8 3025 onto a clean wafer at 3000 RPM for 30 s, followed by a post-exposure bake step, and UV exposure to transfer the pattern into photoresist. To transfer the pattern into SU-8 3025, we used negative photomasks (CAD/Art Services Inc., Bandon, OR, USA) and a custom aligner and UV light source. Excess photoresist was removed using SU-8 developer (Microchem, Newton, MA, USA). Microfluidic channels had a height of 25 μm and microfluidic elements had the dimensions described in the paper. We silanized masters with a vapor of (tridecafluoro-1,1,2,2-tetrahydrooctyl) trichlorosilane (Gelest Inc., Morristown, NJ, USA) to facilitate removal of cured layers of poly(dimethylsiloxane) (PDMS) from the master. We cast PDMS (10:1 ratio of base to crosslinking agent; Sylgard 184, Dow Corning, Midland, MI, USA) on the masters to a depth of ~ 4mm, then cured the polymer at 120°C for >2 h. We peeled cured PDMS layers embossed with microfluidic designs from the master and trimmed them with a razor to a suitable size for bonding to a glass slide. A 1-mm diameter tissue bore was used to

punch inlets and outlets in the PDMS device. We cleaned the surface of PDMS devices with frosted scotch tape, immersed the PDMS layers in a container with acetone placed in a sonicating water bath for 20-30 min, then dried them using YYY. Glass coverslips and clean, dry PDMS devices were exposed to an oxygen plasma for 1 min and pressed into conformal contact to create the final microfluidic device. Connections to the microfluidic device were created using 19 gauge needles, trimmed to size, and Tygon Micro Bore PVC tubing (0.030" ID, 0.090" OD, 0.030" Wall).

We diluted nematodes to a concentration of <10 nematodes per μL and introduced them into the device with a 1 mL Luer lock syringe. Simultaneously, we applied a vacuum to pull nematodes into the chamber with a 5 mL Luer lock syringe. Once nematodes were loaded, we used a syringe pump to flow water into the device at a rate of 1000 μL/h to maintain the hydration of the nematodes.

Symbiotic bacteria imaging in vivo

All epifluorescence images were acquired using an Eclipse Ti inverted microscope (Nikon, Tokyo, Japan) equipped with a CoolSNAP HQ^2 camera (Photometrics, Munich, Germany). Images were taken using a Nikon S Plan Fluor ELWD 40X objective. Each nematode was imaged with 9 x 1 μm steps to construct a z-stack to capture the depth of the receptacle. All confocal images were taken using a Nikon A1R-Si+ confocal microscope (Nikon, Tokyo, Japan) equipped with high sensitivity GaAsP detectors.

Data acquisition and analysis

Quantitative analysis of fluorescently labeled bacterial cells was performed using a custom script in IgorPro. Briefly, cells were detected using the ImageThreshold function, and then a mask was created in the area of detected cells. The pixel intensities were combined to produce

an integrated fluorescence intensity. The number of pixels was counted and converted to an area measurement based on a pixel-to-micron conversion. The integrated fluorescence intensity was converted to an approximate bacterial cell number by dividing the integrated intensity by the integrated intensity of a single cell. Single cell images were collected at the beginning of experiments and analyzed in ImageJ.

Acknowledgements:

We thank Piercen M. Oliver for discussions on microfluidic device designs. I also acknowledge the Weibel lab members for various support they offered for this work.

References

1. **Edward G. Ruby**. 2008. Symbiotic conversations are revealed under genetic interrogation. Nat Rev Microbiol **6**:752–762.
2. **Murfin KE**, **Dillman AR**, **Foster JM**, **Bulgheresi S**, **Slatko BE**, **Sternberg PW**, **Goodrich-Blair H**. 2012. Nematode-bacterium symbioses-cooperation and conflict revealed in the “Omics” age. Biol Bull **223**:85–102.
3. **Tan M-W**, **Shapira M**. 2011. Genetic and molecular analysis of nematode-microbe interactions. Cell Microbiol **13**:497–507.
4. **Murfin KE**, **Lee MM**, **Klassen JL**, **McDonald BR**, **Larget B**, **Forst S**, **Stock SP**, **Currie CR**, **Goodrich-Blair H**. 2015. *Xenorhabdus bovienii* strain diversity impacts coevolution and symbiotic maintenance with *Steinernema* spp. nematode hosts. MBio **6**:1–10.
5. **Herbert EE**, **Goodrich-Blair H**. 2007. Friend and foe: the two faces of *Xenorhabdus nematophila*. Nat Rev Microbiol **5**:634–646.
6. **Richards GR**, **Goodrich-Blair H**. 2009. Masters of conquest and pillage: *Xenorhabdus nematophila* global regulators control transitions from virulence to nutrient acquisition. Cell Microbiol **11**:1025–1033.
7. **Bird AF**, **Akhurst RJ**. 1983. The nature of the intestinal vesicle in nematodes of the family steinernematidae. Int J Parasitol **13**:599–606.
8. **Kaya HK**, **Gaugler R**. 1993. Entomopathogenic Nematodes. Annu Rev Entomol **38**:181–206.
9. **Murfin KE**, **Chaston J**, **Goodrich-Blair H**. 2012. Visualizing bacteria in nematodes using fluorescent microscopy. J Vis Exp.
10. **Chaston JM**, **Murfin KE**, **Heath-Heckman EA**, **Goodrich-Blair H**. 2013. Previously unrecognized stages of species-specific colonization in the mutualism between *Xenorhabdus* bacteria and *Steinernema* nematodes. Cell Microbiol **15**:1545–1559.
11. **Cowles CE**, **Goodrich-Blair H**. 2008. The *Xenorhabdus nematophila nilABC* genes

confer the ability of *Xenorhabdus* spp. to colonize *Steinernema carpocapsae* nematodes. J Bacteriol **190**:4121–4128.

12. **Martens EC**, **Heungens K**, **Goodrich-Blair H**. 2003. Early Colonization Events in the Mutualistic Association between *Steinernema carpocapsae* Nematodes and *Xenorhabdus nematophila* Bacteria. J Bacteriol **185**:3147–3154.
13. 2002. ENTOMOPATHOGENIC NEMATOLOGY. CABI, New York.
14. **Rolston AN**, **Griffin CT**, **Downes MJ**. 2006. Emergence and Dispersal Patterns of Two Isolates of the Entomopathogenic Nematode Steinernema feltiae. J Nematol **38**:221–228.
15. **Keren I**, **Shah D**, **Spoering A**, **Kaldalu N**, **Lewis K**. 2004. Specialized Persister Cells and the Mechanism of Multidrug Tolerance in Escherichia coli **186**:8172–8180.
16. **Martens EC**, **Russell FM**, **Goodrich-Blair H**. 2005. Analysis of *Xenorhabdus nematophila* metabolic mutants yields insight into stages of *Steinernema carpocapsae* nematode intestinal colonization. Mol Microbiol **58**:28–45.
17. **Orchard SS**, **Goodrich-Blair H**. 2004. Identification and functional characterization of a *Xenorhabdus nematophila* oligopeptide permease. Appl Environ Microbiol **70**:5621–7.
18. **Heath-Heckman EAC**. 2016. The Metronome of Symbiosis: Interactions Between Microbes and the Host Circadian Clock. Integr Comp Biol **56**:776–783.
19. **Park Y**, **Herbert EE**, **Cowles CE**, **Cowles KN**, **Menard ML**, **Orchard SS**, **Goodrich-Blair H**. 2007. Clonal variation in *Xenorhabdus nematophila* virulence and suppression of *Manduca sexta* immunity. Cell Microbiol **9**:645–656.
20. **Hussa EA**, **Casanova-Torres ÁM**, **Goodrich-Blair H**. 2015. The global transcription factor Lrp controls virulence modulation in *Xenorhabdus nematophila*. J Bacteriol **197**:3015–3025.
21. **Cao M**, **Patel T**, **Goodrich-Blair H**, **Hussa EA**. 2017. High levels of Xenorhabdus nematophila transcription factor Lrp promote mutualism with *Steinernema carpocapsae* nematode hosts. Appl Environ Microbiol **83**:17.

22. **Flores-Lara Y**, **Renneckar D**, **Forst S**, **Goodrich-Blair H**, **Stock P**. 2007. Influence of nematode age and culture conditions on morphological and physiological parameters in the bacterial vesicle of *Steinernema carpocapsae* (Nematoda: Steinernematidae). J Invertebr Pathol **95**:110–118.

23. **Goetsch M**, **Owen H**, **Goldman B**, **Forst S**. 2006. Analysis of the PixA inclusion body protein of *Xenorhabdus nematophila*. J Bacteriol **188**:2706–2710.

24. **Martens EC**. 2005. Initiation and maintenance of *Steinernema carpocapsae* nematode colonization by *Xenorhabdus nematophila* bacteria *(Doctoal Thesis)* . University of Wisconsin-Madison.

25. **Chung K**, **Zhan M**, **Srinivasan J**, **Sternberg PW**, **Gong E**, **Schroeder FC**, **Lu H**. 2011. Microfluidic chamber arrays for whole-organism behavior-based chemical screening. Lab Chip **11**:3689–97.

26. **Chung K**, **Crane MM**, **Lu H**. 2008. Automated on-chip rapid microscopy, phenotyping and sorting of C. elegans. Nat Methods **5**:637–643.

27. **Lambertsen L**, **Sternberg C**, **Molin S**. 2004. Mini-Tn7 transposons for site-specific tagging of bacteria with fluorescent proteins. Environ Microbiol **6**:726–732.

28. **Xu J**, **Hurlbert RE**. 1990. Toxicity of Irradiated Media for *Xenorhabdus* spp. Appl Environ Microbiol **56**:815–8.

29. **Vivas EI**, **Goodrich-Blair H**. 2001. *Xenorhabdus nematophilus* as a model for host-bacterium interactions: *rpoS* is necessary for mutualism with nematodes. J Bacteriol **183**:4687–93.

Tables and Figures

Table 5.1. Parameter values in design of microfluidic devices.

		Epifluorescence[2]		Confocal[3]			
Parameter[1]	Description	E1 (μm)	E2 (μm)	C1 (μm)	C2 (μm)	C3 (μm)	C4 (μm)
a	Entrance radius	75	75	75	75	75	75
b	Connection (w/l)	15/200	10/200	10/200	10/200	10/200	15/200
c	Trap (w/l)	25/600	25/600	25/600	10/600	15/600	20/600

[1]Various combination parameter a, b, and c values (see Fig. 5.2C for details) are used for designs of microfluidic devices of different devices to fit various sizes of nematodes in either epifluorescence microscopy or confocal microscopy experiments. Parameter a = radius of the circular arc used for the entrance of the side chambers; Parameter b= dimensions of the connection between entrance and trapping chamber (shown in width/length); Parameter c= dimension of the trapping chamber (shown in width/length).

[2]The combination of parameter values used for the device designs in epifluorescence microscopy experiments (E1= epifluorescence design 1 and E2= epifluorescence design 2) are listed.

[3]The combination of parameter values used for the device designs in confocal microscopy experiments (C1-C4= Confocal design 1-4) are listed.

Figure 5.1. The mutualistic relationship between *Xenorhabdus nematophila* bacteria and *Steinernema carpocapsae* nematodes.

(A) A cartoon depicting the tripartite life cycle of *S. carpocapsae* nematodes. Infective juveniles (IJs) infect an insect prey and release *X. nematophila* cells to evade the host immune system and kill the host. Both species use the cadaver's nutrients for reproduction; upon nutrient depletion, both organisms re-associate and enter the soil to begin the cycle again. B-D) Micrographs of the IJ stage of an *S. carpocapsae* nematode carrying GFP-expressing *X. nematophila* cells in the intestinal receptacle.

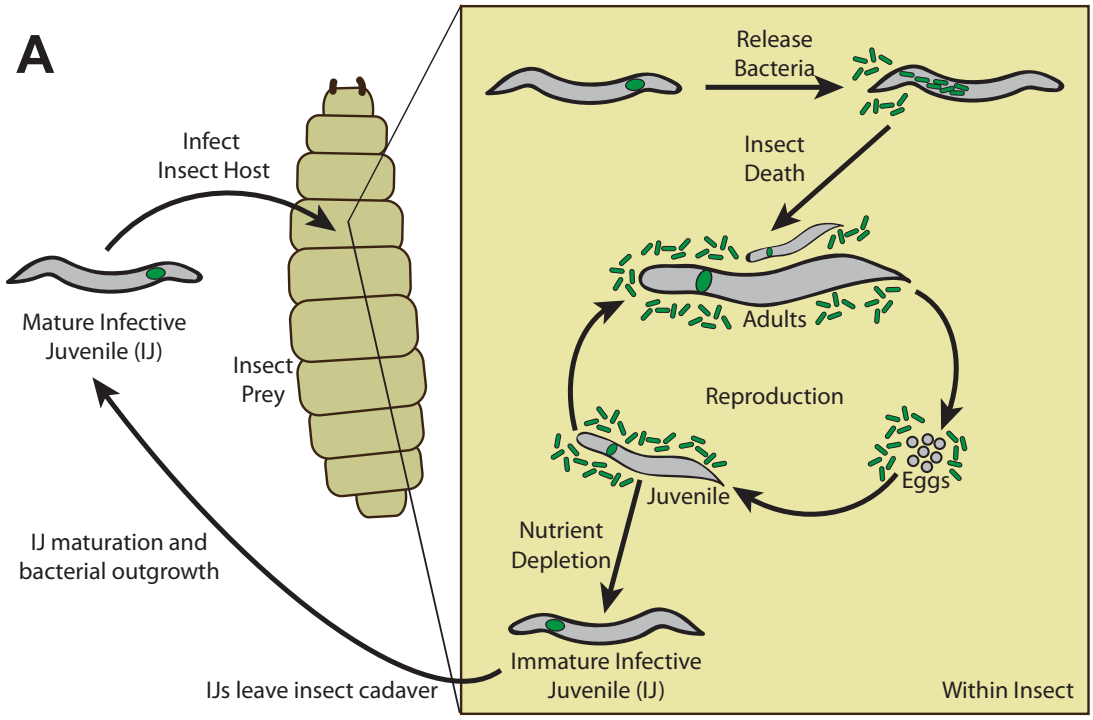
A
Infect
Insect Host
Mature Infective
Juvenile (IJ)
Insect
Prey
IJ maturation and
bacterial outgrowth
IJs leave insect cadaver
Release
Bacteria
Insect
Death
Adults
Reproduction
Eggs
Juvenile
Nutrient
Depletion
Immature Infective
Juvenile (IJ)
Within Insect

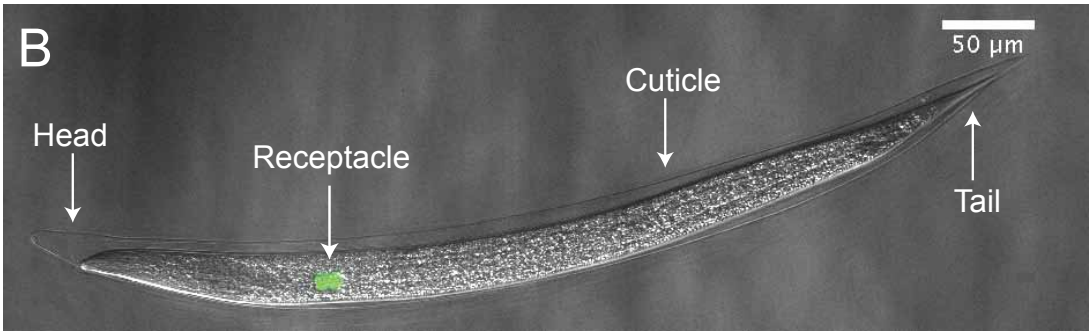
B
50 µm
Head
Receptacle
Cuticle
Tail

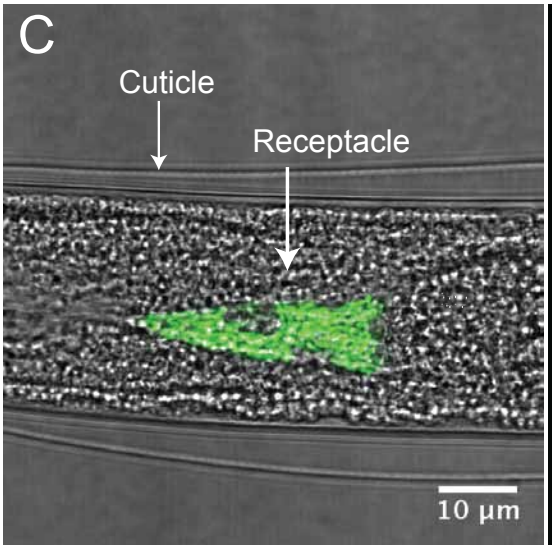
C
Cuticle
Receptacle
10 µm

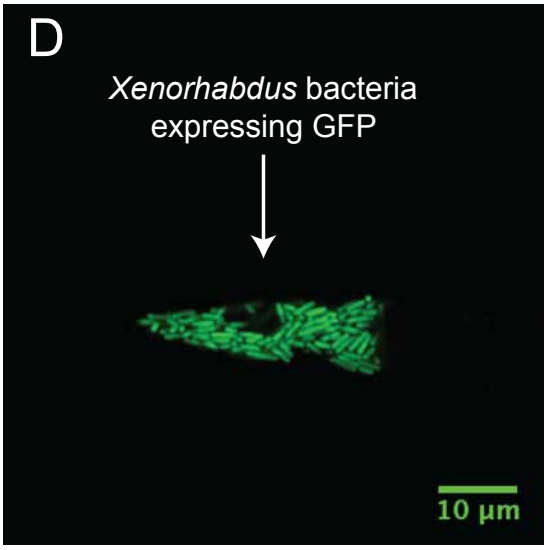
D
Xenorhabdus bacteria
expressing GFP
10 µm

Figure 5.2. Schematic of microfluidic device for *S. carpocapsae* nematode isolation and maintenance.

(A) Device schematic. Nematodes are introduced through the inlet and pushed through the primary channel. (B) Nematodes in the primary channel are pulled into traps with the aid of negative pressure from the vacuum. (C) Physical dimensions of the nematode traps. For more detail on the trap dimensions, see Table 5.1.

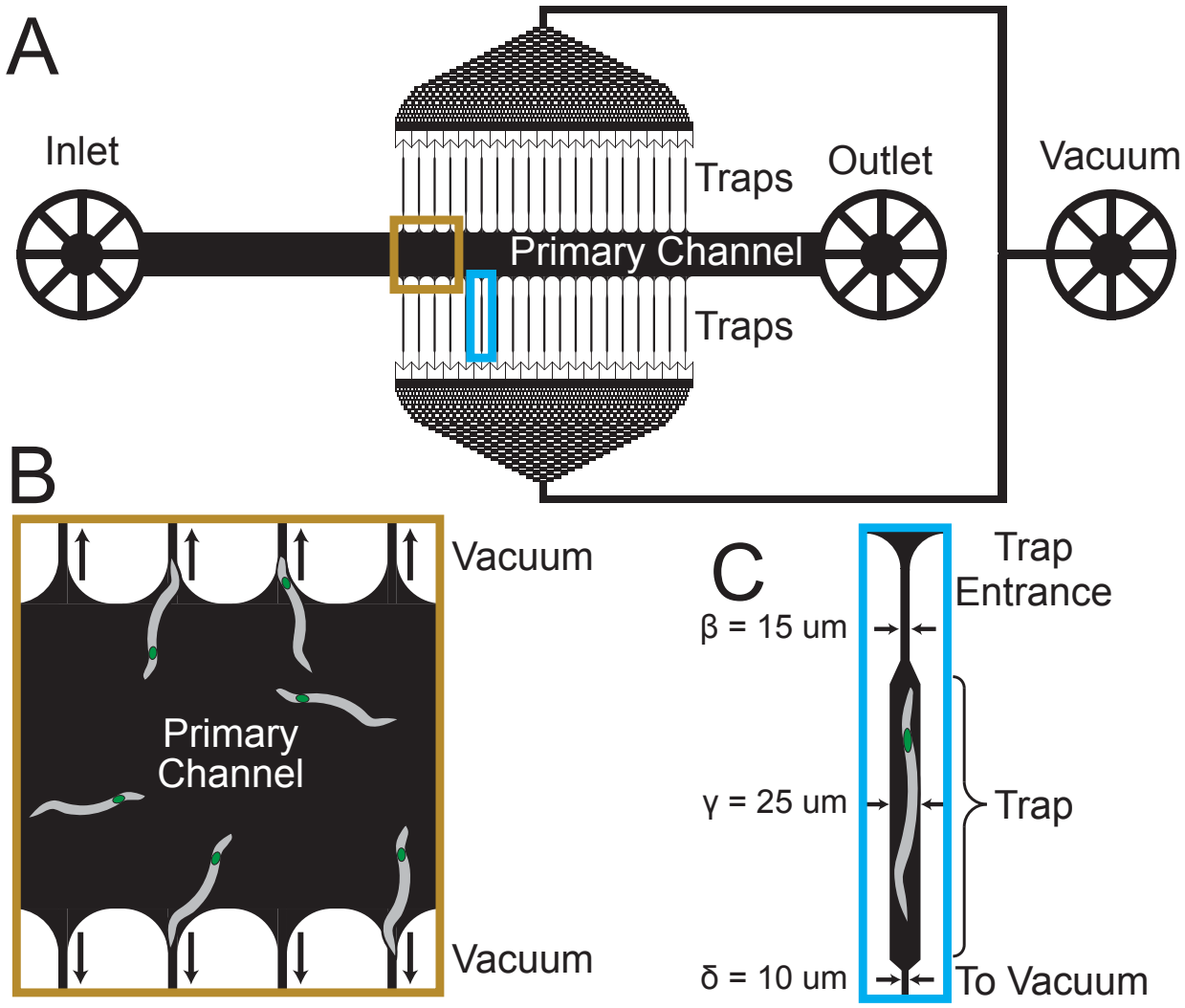
A
Inlet
Traps
Outlet
Vacuum
Primary Channel
Traps
B
Vacuum
Primary
Channel
Vacuum
C
Trap
Entrance
β = 15 um
γ = 25 um
Trap
δ = 10 um
To Vacuum

Figure 5.3. Nematode survival and maintenance in the microfluidic device.

(A) A confocal micrograph of 4 *S. carpocapsae* nematodes isolated in adjacent microfluidic traps. Living nematodes (highlighted with black arrows) have characteristic body curvature and movements of healthy nematodes; dead nematodes (highlighted with white arrow) are identified by a straight body and disintegration of tissues. *X. nematophila* bacteria constitutively expressing GFP are colonized in the nematode receptacles. (B) Percentage of nematodes in the microfluidic device isolated and alive (circle), escaped (square), or dead (triangle) over the course of 112 h at room temperature. The average of three independent experiments is indicated; total numbers of nematodes trapped in the device were 18, 22, and 20 respectively. Error bars indicate standard error (SEM).

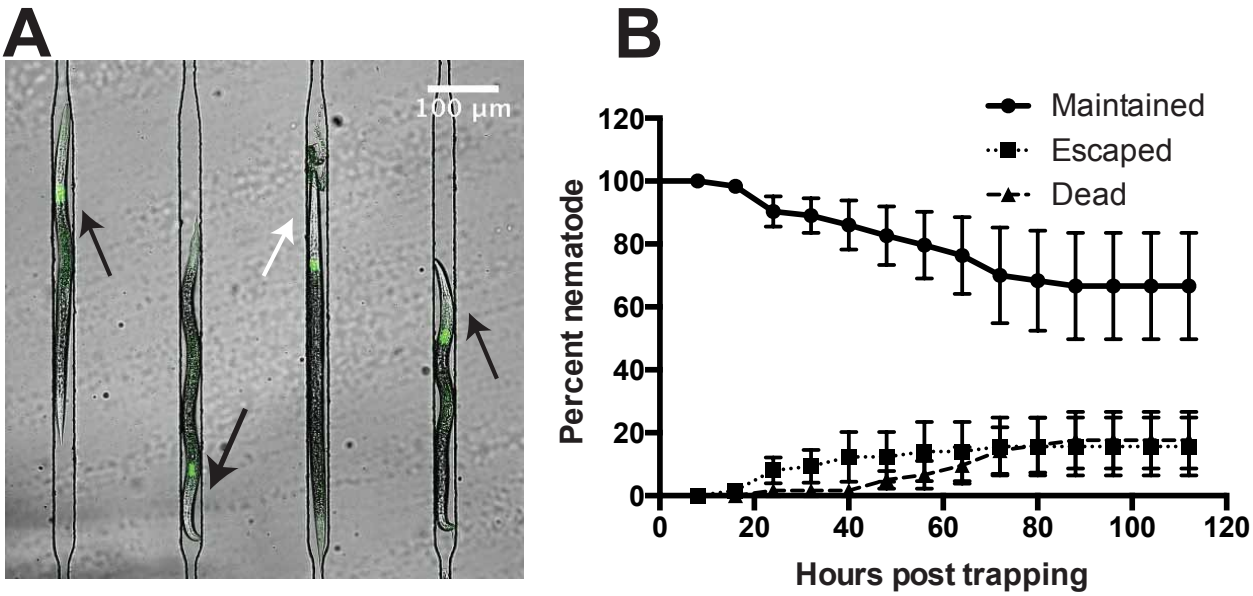
A
100 µm
B
Maintained
Escaped
Dead
Percent nematode
Hours post trapping
0
20
40
60
80
100
120

Figure 5.4. Qualitative and quantitative analysis of bacterial populations in individual, living IJ nematodes.

(A) Epifluorescence micrographs of a living, immature IJ nematode receptacle at 0 h -112 h post-trapping in microfluidic device. (B) Bacterial cell numbers and fluorescence intensity as measured in five individual nematode receptacles. Green trace represents data for bacterial cells in A. (C) Colonization cross-sectional area in the same five nematodes. Green trace represents cells from A.

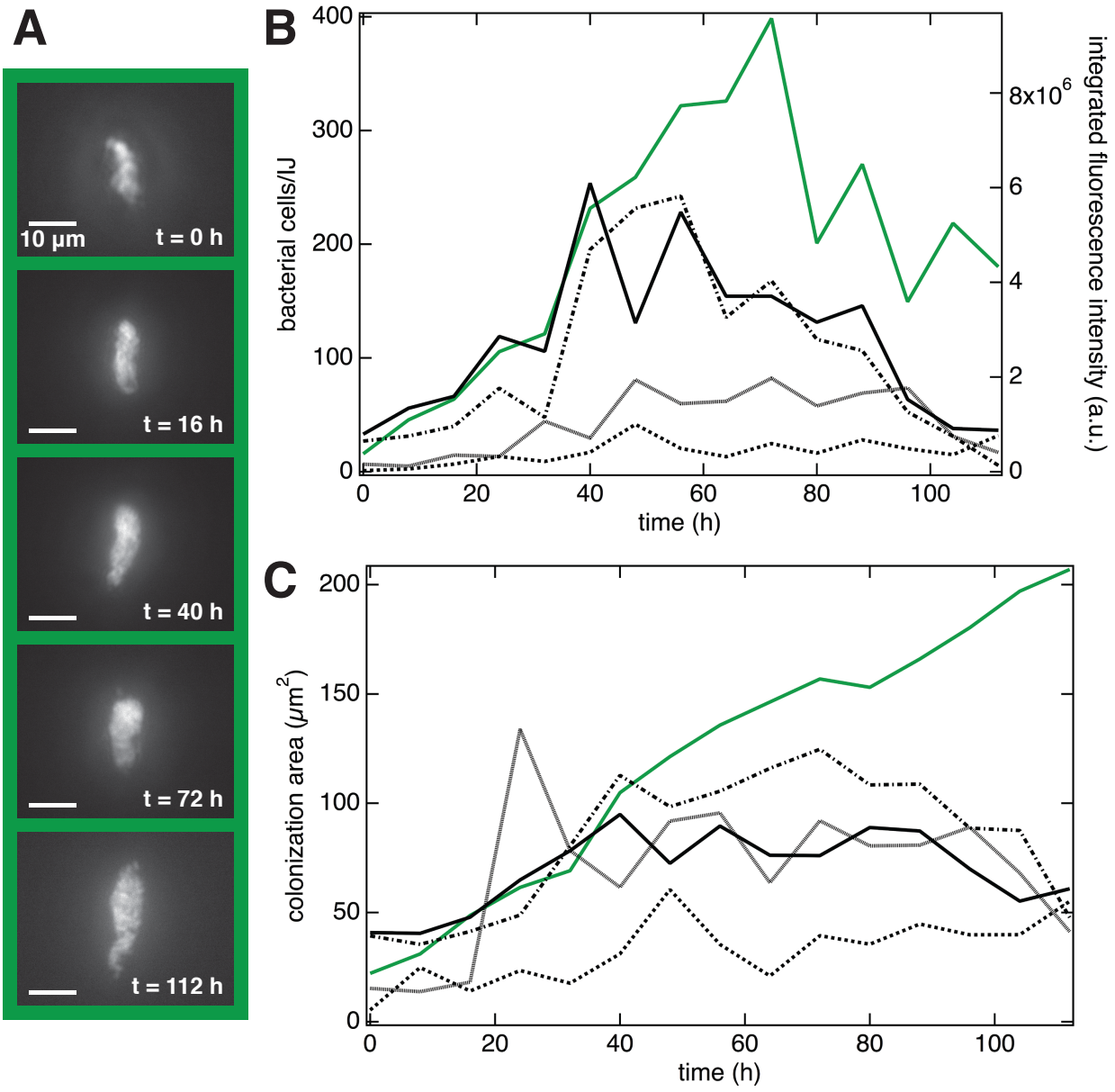
A
10 µm
t = 0 h
t = 16 h
t = 40 h
t = 72 h
t = 112 h
B
bacterial cells/IJ
integrated fluorescence intensity (a.u.)
8x10^6
time (h)
C
colonization area (µm^2)
time (h)

Figure 5.5. Comparison of traditional grinding experiments to microfluidic device experiments for quantification of *X. nematophila* bacterial population dynamics in *S. carpocapsae* nematodes.

(A, B) Traditional grinding experiments include surface-sterilization, grinding a subpopulation of nematodes, plating on synthetic media and performing bacterial CFU counts. Subpopulations of immature IJs were isolated and assayed every 4-8h. A and B show two replicates each from two separate experiments, each point is the average result for three individual assays. (C) Analysis of epifluorescence micrographs of GFP-expressing *X. nematophila* in individual *S. carpocapsae* trapped in a microfluidic device. Each plot represents the average of all living nematodes in experiment. Error bars indicate standard error (SEM). (A and B are re-published from Martens et al., 2003 Figure 5.3 A and B, with permission).

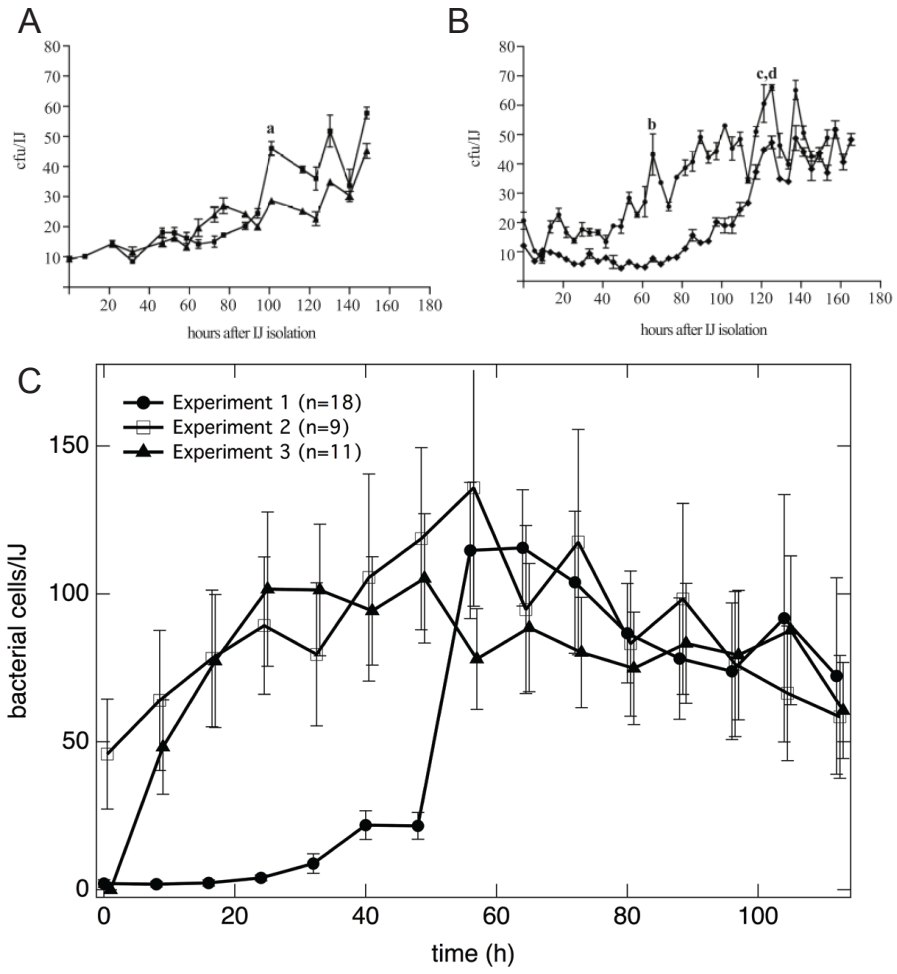
A
cfu/IJ
a
hours after IJ isolation
B
cfu/IJ
b
c,d
hours after IJ isolation
C
Experiment 1 (n=18)
Experiment 2 (n=9)
Experiment 3 (n=11)
bacterial cells/IJ
time (h)

Figure 5.6. Confocal micrographs of a bacterial population in a receptacle over the course of 3 weeks.

An individual living immature IJ nematode (head towards the top) was maintained in the microfluidic device and the receptacle was imaged on day 1 (A and E), 7 (B and F), 14 (C and G), and 21(D and H) post-trapping. The GFP expressing bacteria population are shown in the host nematode (A, B, C, D) as well as in 3D reconstruction of z-stack images (E, F, G, H).

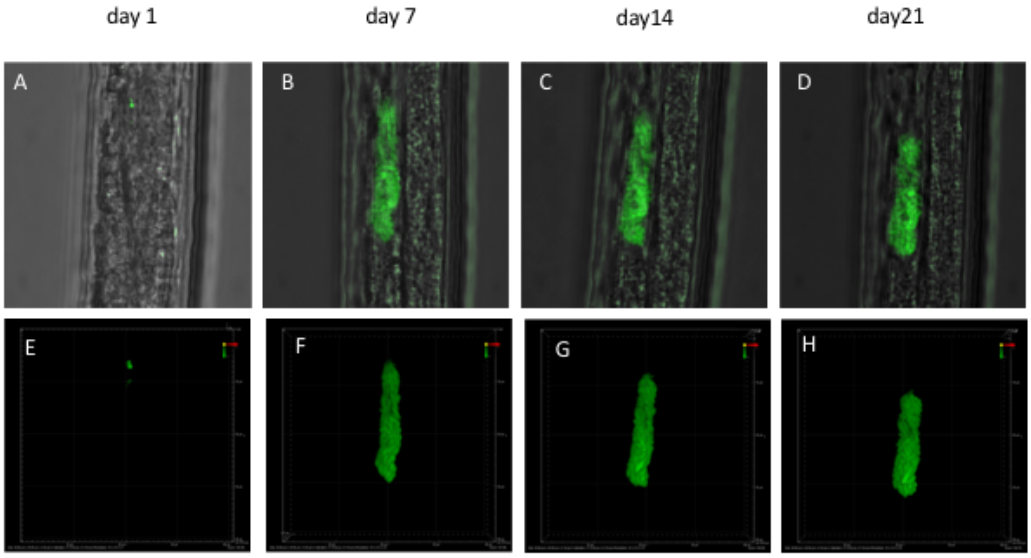
day 1
day 7
day14
day21
A
B
C
D
E
F
G
H

Chapter 6:

Summary and future directions

This Chapter has been partially adapted from manuscript **'Mengyi Cao and Heidi Goodrich-Blair;** Ready or Not: Microbial Adaptive Responses in Dynamic Symbiosis Environments. In revision, *Journal of Bacteriology,* special issue conference proceedings.'

Mengyi Cao**:** Outlined, wrote, and revised the manuscript. Arts for Figures.

Heidi Goodrich-Blair**:** Edited and revised the manuscript. Arts for Figures.

Abstract:

In Chapters 2-5, I presented my research work on an Lrp-dependent phenotypic switch, termed VMO, that controls the switch between mutualism (with nematode) and pathogenesis (with insect) phenotypes in the symbiotic bacterium *X. nematophila*. This chapter will provide a brief summary of my thesis research work on the VMO switch and bacterial adaptive fitness during the symbiotic life cycle (summarized in Table 6.1). I will also discuss the current working models based on my data, and future directions for the research.

I. From IJ to insect: *X. nematophila* populations with heterogeneous expression of high and low Lrp are more virulent during infection than those expressing homogeneously high Lrp levels

The development of an Lrp-dependent reporter facilitated the visualization and quantification of population heterogeneity in wild type *X. nematophila* populations (Chapter 3). Heterogeneous populations of bacteria, consisting of bi-stable expression of high-Lrp and low-Lrp expressing colonies, are significantly more virulent than homogeneous populations predominantly composed of high-Lrp colonies (Chapter 3). A switch from high to low Lrp expression, resulting in population heterogeneity, occurs within minimal medium supplemented with amino acids, and within aging IJ nematodes (Chapter 4). These data suggest that the IJ receptacle environment promotes the formation of an *X. nematophila* population that is prepared for virulence in the upcoming infection stage.

I propose that two nutritional shifts during the IJ-to-insect transition could signal a change in Lrp levels from high to low: (i) the nutrient composition (likely the presence of amino acids) of the IJ receptacle promotes population heterogeneity and the rise of low-Lrp-expressing cells (Chapter 3 and 4); (ii) Once released into insect blood cavity, the presence of glucose in the insect hemolymph inhibits growth of high-Lrp cells (Chapter 3). This would be an adaptive benefit for *X. nematophila* populations, since high-Lrp cells are immunogenic (1). Further, homogeneously high-Lrp wild type populations that are either defective in switching to

heterogeneous populations, or defective in growing in the presence of glucose, showed virulence-attenuated phenotypes (Chapter 3). This indicates that both the ability to convert to a low-Lrp-expressing state and the ability to inhibit growth of high-Lrp expressers are important for *X. nematophila* virulence success in insects. These two hypothesized nutritional shifts in the IJ receptacle and insect hemolymph brought my attention to a particular event, the IJ recovery (or release of bacteria from IJ nematodes into the insect blood cavity), that is connecting bacterial persistence in transmission stage of IJ nematodes and insect infection (2). So far, if the Lrp switch or the inhibition of the switch occur particularly when bacteria are released from recovery IJs have not been explicitly investigated (table 6.1). Future work will focus on Lrp regulated adaptive response in glucose metabolism, as well as Lrp switch during the IJ recovery and insect infection stage. Using the Lrp-fixed strains (Chapter 2) and wild type strains with Lrp-dependent reporters (Chapter 3), future experiment could test the hypothesis if low-Lrp expressing cells, but not high-Lrp expressing cells are exclusively released from a recovery IJ nematode. In addition, it would be intriguing to explore the mechanisms by which the growth of high-Lrp cells is inhibited by glucose.

II. From virulence to feeding: a switch from low-Lrp to high-Lrp expression provides adaptive fitness in mutualistic symbiosis in the insect cadaver**.**

In contrary to the insect infection stage in which virulent and immuno-suppressive low-Lrp expressing bacteria have an advantage (1, 3), in the insect cadaver *X. nematophila* expressing high-Lrp are more capable of supporting reproduction of the nematode (4). This indirectly increases the fitness of *X. nematophila* by ensuring the IJ emergence and symbiont transmission for the next round of its life cycle (Chapter 2). I have observed a low-to-high Lrp switch occurring in nutrient-rich media in vitro (Chapter 3), indicating the nutrient release from insect tissue could up-regulate or select for high-Lrp expressing bacteria. However, the specific

nutrients (lipids, amino acids, or sugar) that may trigger a population-wide Lrp switch have not been identified. One possibility suggested from my work is glucose, which inhibits a switch from high Lrp to low Lrp *in vitro* (Chapter 3). Glucose in the insect hemolymph (during the infection stage) or released from dead hemocytes and tissues (during the cadaver stage) (5) might select against low Lrp expressers, thereby increasing the success of high-Lrp expressers that are (pre)-adaptive for the upcoming reproductive stage in the nutrient-rich insect cadaver. In the previous section, I discussed the hypothetical model that glucose inhibits high-Lrp expressers to grow in the insect hemolymph. Taken these observations (glucose inhibits high-Lrp cells growth and high-to-low Lrp switch), I hypothesize that the insect hemolymph selects or promotes the bacterial population to express intermediate level of Lrp, which doesn't trigger immuoresponse in the infection stage, but could subsequently pre-adapted for high-Lrp expression in the upcoming reproductive stage of life cycle (Fig. 6.1, rectangles). Alternatively, different temporal levels of glucose in different environments (such as hemolymph exposure, hemocytes lysis, etc) could either inhibit high-Lrp expressers growth or inhibit the high-to-low Lrp switch. Future experiments could test these hypotheses by FACS analysis of population dynamics change during infection. It would also be interesting to test bacterial population response to different glucose concentrations. These models awaits future investigations and testing.

III. From spent cadaver to IJ: high-Lrp expressing bacterial cells are adapted for early colonization events

The 'early colonization events' in which *X. nematophila* bacteria associate with adult, juvenile, pre-IJ, and immature IJ stage nematodes all occur in the insect cadaver (6, 7). At all developmental stages of nematodes up to the initiation of colonization of IJ nematodes, high-Lrp expressing bacteria displayed a slightly higher colonization frequency (20-50% more colonized nematode out of the total number of nematodes in each developmental stage) than low-Lrp counterparts (Chapter 4). The molecular mechanisms underlying Lrp-dependent colonization

with different developmental stages of nematodes are not elucidated yet. I predict that Lrp, as a transcription factor (8, 9), regulates expression of a suite of gene products that are involved in direct interactions with the nematode hosts. My data indicate that these products are expressed at optimal levels when Lrp levels are high. Alternatively, it may be that some gene products expressed in low-Lrp cells are inhibitory to colonization. In either case, an analysis of transcriptional profiles of cells constitutively expressing either high or low levels of Lrp may reveal specific genes necessary for or inhibitory to colonization, respectively. In addition, it will be interesting to investigate host cell-surface molecules that may be interacting with *X. nematophila* These molecules, which may include glycans or lectins could be responsible for physical interactions with *X. nematophila* Lrp-dependent factors (10, 11).

Instead of regulating bacteria-nematode association by small molecule production, Lrp could also regulate bacterial colonization via nutritional adaptation. As *X. nematophila* colonizes different tissues over the course of nematode development (e.g. from AIC in a J2 juvenile to PIV in a pre-IJ) it may encounter a series of nutritional shifts to which it responds in an Lrp-dependent manner. For instance, different species (or concentrations of) of glycans might associate with different tissues of the host (12), such as AIC, PIV, and IJ receptacle, that bacterial cells expressing high levels of Lrp are more adaptive when transitioning from one tissue (associated with glycan 1) to another (associated with glycan 2). Since these tissue-specific molecules associated at AIC/PIV/IJ receptacle might dictate species-specific interactions among *Xenorhabdus* bacteria and *Steinernema* nematode, the answers to these questions are possibly hidden in the other *Steinernema-Xenorhabdus* symbiotic pairs that are co-evolved into species-specific recognition and localization at AIC, PIV, and IJ receptacle (13). For instance, future research could start to ask questions, such as: what species of glycans (and other molecules) are specifically associated with different tissues in the nematode? Do *Xenorhabdus* bacteria respond to specific series of glycans in the Lrp-dependent manner? Are the specific order of the glycans that *Xenorhabdus* bacteria are adaptive to also matching the

glycan species in their host nematodes? These questions could start to elucidate if Lrp plays a role in symbiont tissue specificity and bacterial adaptive response to different tropisms of varying developmental stages of the host nematode.

IV. Persistence in the IJ: nutrient limitation promotes Lrp heterogeneity through an increase in low-Lrp expressing cells

Using an Lrp-dependent fluorescence reporter, I observed that a switch from high- to low-Lrp expression is promoted by the presence of amino acids or the absence of glucose *in vitro* (Chapter 3). This may reflect the *X. nematophila* life history transition from the nutrient rich insect cadaver that supports growth of large bacterial populations (14) to colonization of the IJ receptacle, which is considered nutrient poor (7, 15, 16). In turn, this comparison predicts that low-Lrp expressers may arise in the IJ receptacle. My data support this idea, since low-Lrp expressers are more persistent, or arise in the nutrient-limiting IJ receptacle, compared to high-Lrp expressing cells (Chapter 4).

By tracking individual nematodes using microfluidic devices, I observed *X. nematophila* symbiont population dynamics in live IJ nematodes and found that the number of colonizing symbionts fluctuates sharply over time (Chapter 5). One model to explain such symbiont population dynamics is that the host animal provides nutrients in rhythmic cycles, such as circadian or diel changes in host physiology. I also observed bacterial population topological changes in individual IJ receptacles over 3-4 weeks of aging, suggesting nutrient composition or distribution might change significantly in the IJ receptacle during IJ aging process (Chapter 5). This particular timing (3-4 weeks aging) corresponds with a significant increase in low-Lrp expressers observed in aging IJs (Chapter 4) This drastic change in the symbiotic bacterial population indicate the specific timing of IJ aging might associate with a dramatic change in host physiology, such as stress response, secretion or synthesis of pheromones, or other signaling cascades that affect the nutrition transferred into the IJ receptacle. An intriguing question to

explore in the future research would be identifying the signaling molecules that are present or absent during IJ aging and how they trigger Lrp-dependent response in the symbiotic bacterial population . Since I have found that *in vitro,* the presence of amino acids or the absence of glucose could trigger similar Lrp-depdnent switch as it is in the aging IJ receptacle (Chapter 3 and 4), future research could start to investigate of glucose or particular amino acids play a role in the Lrp switch in the IJ receptacle. Such investigations might involve the development of new technologies such as nematode tissue-specific mass spectrometry to study the nutrient composition and distribution in the receptacle. The development of technologies such as nematode host transcriptomics or proteomics in aging IJs would also help identify the critical physiological responses in the aging IJs that could be associated with the symbiont population switch.

Lrp-dependent phenotypic variation in *X. nematophila:* a model to study anticipatory behavior in naturally occurring microbial symbiosis?

Anticipatory behavior, or the ability to learn from history, has been long known in vertebrates (17) and recently has been investigated in microbes. During the symbiotic life cycle, microbes often are exposed to and must adapt to predictable or indeterminate environmental changes in temporal and spatial manner, which could cause population heterogeneity and anticipatory behavior. Current experimental evidence of microbial anticipation in an animal host environment is limited to *E. coli.* In Chapter 1 (Introduction), I discussed multiple animal-microbes symbiosis models that hint at the possibility of anticipatory behavior contributing to the fitness and success of the microbial symbiont partner. Testing this concept will rely on the establishment of the signals that characterize the spatial and temporal environments encountered by symbionts, and testing the abilities of these signals to elicit pre-adaptive responses. The symbiosis between *Xenorhabdus* bacteria and *Steinernema* nematodes

provides a powerful system with which to approach this type of research, based on its predictability for both the bacterium and the investigator.

The findings of this thesis work have led to the idea that over the entire life history of *X. nematophila* the Lrp-dependent VMO switch gives rise to population heterogeneity with respect to host interactions and adaptive responses to environmental changes. Based on current knowledge of the phenotypes of high- and low-Lrp expressing cells, I have developed a working model of how Lrp-dependent phenotypic variation might be contributing to adaptive prediction if it occurs in *X. nematophila* (Fig. 6.1). Briefly, if adaptive prediction is occurring, each environment (Fig. 6.1 top row, open symbols) selects for either induction of a phenotypic switch or selection of a particular cell type that expresses the Lrp-dependent gene expression profile (Fig. 6.1 high- or hetero (for heterogeneous)-Lrp; bottom row, closed symbols) that is adaptive for the next environment that will be encountered. This model of adaptive prediction awaits testing, and is not mutually exclusive with the alternative, canonical model that the prevailing conditions elicit a gene expression response that is adaptive in that condition (not for a future condition). To begin to address these ideas, the next steps will be applying and expanding the tools developed in this thesis work, such as using microfluidic devices and fluorescence reporters to investigate the temporal and spatial Lrp-dependent population heterogeneity in individual bacterial cells over the span of the *X. nematophila* life cycle, and determine if this variability serves as a (pre)-adaptive mechanism for bacteria transitioning from the nematode to the insect host and back again. As a result of previous research and my thesis work, there is considerable knowledge about the stages, microenvironments, and regulatory processes of the *Xenorhabdus* life cycle. Together these provide a strong foundation for posing testable hypotheses about the triggers and outputs of possible anticipatory behaviors in symbiosis.

References

1. **Casanova-Torres ÁM**, **Shokal U**, **Morag N**, **Eleftherianos I**, **Goodrich-Blair H**. 2017. The global transcription factor Lrp is both essential for and inhibitory to *Xenorhabdus nematophila* insecticidal activity. Appl Environ Microbiol AEM.00185-17.
2. **Snyder H**, **Stock SP**, **Kim S-KK**, **Flores-Lara Y**, **Forst S**. 2007. New insights into the colonization and release processes of *Xenorhabdus nematophila* and the morphology and ultrastructure of the bacterial receptacle of its nematode host, *Steinernema carpocapsae*. Appl Environ Microbiol **73**:5338–5346.
3. **Hussa EA**, **Casanova-Torres ÁM**, **Goodrich-Blair H**. 2015. The global transcription factor Lrp controls virulence modulation in *Xenorhabdus nematophila*. J Bacteriol **197**:3015–3025.
4. **Cao M**, **Patel T**, **Goodrich-Blair H**, **Hussa EA**. 2017. High levels of Xenorhabdus nematophila transcription factor Lrp promote mutualism with *Steinernema carpocapsae* nematode hosts. Appl Environ Microbiol **83**:17.
5. **Phalaraksh C**, **Lenz EM**, **Lindon JC**, **Nicholson JK**, **Farrant RD**, **Reynolds SE**, **Wilson ID**, **Osborn D**, **Weeks JM**. 1999. NMR spectroscopic studies on the haemolymph of the tobacco hornworm, *Manduca sexta*: assignment of ^{1}H and ^{13}C NMR spectra. Insect Biochem Mol Biol **29**:795–805.
6. **Chaston JM**, **Murfin KE**, **Heath-Heckman EA**, **Goodrich-Blair H**. 2013. Previously unrecognized stages of species-specific colonization in the mutualism between *Xenorhabdus* bacteria and *Steinernema* nematodes. Cell Microbiol **15**:1545–1559.
7. **Martens EC**, **Heungens K**, **Goodrich-Blair H**. 2003. Early Colonization Events in the Mutualistic Association between *Steinernema carpocapsae* Nematodes and *Xenorhabdus nematophila* Bacteria. J Bacteriol **185**:3147–3154.
8. **Cowles KN**, **Cowles CE**, **Richards GR**, **Martens EC**, **Goodrich-Blair H**. 2007. The global regulator Lrp contributes to mutualism, pathogenesis and phenotypic variation in the bacterium *Xenorhabdus nematophila*. Cell Microbiol **9**:1311–1323.
9. **Engel Y**, **Windhorst C**, **Lu X**, **Goodrich-Blair H**, **Bode HB**. 2017. The Global Regulators

Lrp, LeuO, and HexA Control Secondary Metabolism in Entomopathogenic Bacteria. Front Microbiol **8**:209.

10. **Martens EC**, **Goodrich-Blair H**. 2005. The *Steinernema carpocapsae* intestinal vesicle contains a subcellular structure with which *Xenorhabdus nematophila* associates during colonization initiation. Cell Microbiol **7**:1723–1735.
11. **Bhasin A**, **Chaston JM**, **Goodrich-Blair H**. 2012. Mutational analyses reveal overall topology and functional regions of NilB, a bacterial outer membrane protein required for host association in a model of animal-microbe mutualism. J Bacteriol **194**:1763–76.
12. **Lee SM**, **Donaldson GP**, **Mikulski Z**, **Boyajian S**, **Ley K**, **Mazmanian SK**. 2013. Bacterial colonization factors control specificity and stability of the gut microbiota. Nature **501**:426–429.
13. **Murfin KE**, **Lee MM**, **Klassen JL**, **McDonald BR**, **Larget B**, **Forst S**, **Stock SP**, **Currie CR**, **Goodrich-Blair H**. 2015. *Xenorhabdus bovienii* strain diversity impacts coevolution and symbiotic maintenance with *Steinernema* spp. nematode hosts. MBio **6**:1–10.
14. **Jubelin G**, **Pagès S**, **Lanois A**, **Boyer M-H**, **Gaudriault S**, **Ferdy J-B**, **Givaudan A**. 2011. Studies of the dynamic expression of the *Xenorhabdus* FliAZ regulon reveal atypical iron-dependent regulation of the flagellin and haemolysin genes during insect infection. Environ Microbiol **13**:1271–1284.
15. **Martens EC**, **Russell FM**, **Goodrich-Blair H**. 2005. Analysis of *Xenorhabdus nematophila* metabolic mutants yields insight into stages of *Steinernema carpocapsae* nematode intestinal colonization. Mol Microbiol **58**:28–45.
16. **Herbert EE**, **Goodrich-Blair H**. 2007. Friend and foe: the two faces of *Xenorhabdus nematophila*. Nat Rev Microbiol **5**:634–646.
17. **Pavlov IP**. 1927. Conditioned reflexes: an investigation of the physiological activity of the cerebral cortex. Oxford Univ. Press, Oxford, England.

Tables and Figures

Table 6.1. A summary of Lrp-dependent VMO switch in the life cyle of *X. nematophila.*

Bacterial strains	IJ recovery*	Infection	Nematode reproduction	Nematode colonization in cadaver				Colonization during IJ Transmission		IJ fitness in the next generation (*Galleria*)
				adult AIC	Juv AIC	preIJ PIV	IJ init	Immature outgrow	Mature cfu carrg	
lrp::kan	NA[1]	-[3]	-	-/-	-/-	-/-	-/-	-	-	-
Low Lrp	NA	+	-	-	-	-	-	+	+	-
High Lrp	NA	-	+	+	+	+	+	+	-	+
Wild type	+[2]	+/-	+	+	+	+	+	+	+(HET)[4]	+

IJ recovery*: Lrp expression in bacterial cells have been observed during IJ recovery in two ways: (1) preliminary data from previous lab member indicated that *Plrp* was up-regulated during IJ recovery using the fluorescence reporter (Hussa, personal communication). Such up-regulation of *Plrp* promoter creates Lrp-heterogeneity among bacterial cells in the nematode intestine. (2) my preliminary data also showed that released *X. nematophila* cells (expressing *PfliC-gfp*) onto LB agar and observed colony-level heterogeneity. However, such heterogeneity could have pre-adapted from the aging IJ nematodes.

[1]NA: data not completed.

[2]+ normal phenotype (in comparison to wild type)

[3]- partial defect phenotype

[4](HET): Heterogeneous Lrp expression has been observed during IJ aging process

Figure 6.1: A working model of Lrp-dependent adaptive prediction as it may occur for *Xenorhabdus* bacteria based on our current data, which encounter predictable stages of host interactions.

Open symbols in the top row represent environments, closed symbols in the bottom row represent gene expression profiles. The color scheme represents traits being expressed in response to the current environment that benefit the fitness in the future (adaptive prediction). We hypothesize that the Lrp-dependent phenotypic switch in *X. nematophila* plays a role in such (pre)-adaptive behavior of the symbiotic bacteria in alternating host environments.